NASA Contractor Report 3327

Preliminary Development of Digital Signal Processing in Microwave Radiometers

William D. Stanley

CONTRACT NAS1-15676
SEPTEMBER 1980

NASA

NASA Contractor Report 3327

Preliminary Development of Digital Signal Processing in Microwave Radiometers

William D. Stanley
Old Dominion University
Norfolk, Virginia

Prepared for
Langley Research Center
under Contract NAS1-15676

National Aeronautics
and Space Administration

**Scientific and Technical
Information Branch**

1980

INTRODUCTION

The contract covered by this report involved a number of separate but closely related activities related to the field of microwave radiometry. These activities included the following specific tasks:

(1) The development of several control loop and dynamic noise model computer programs for simulating microwave radiometer measurements has been essentially completed. This effort was initiated under an earlier task order contract, and the results of this development have been published (refs. 1 and 2).

(2) Computer modeling of an existing stepped frequency radiometer has been done in an effort to determine its optimum operational characteristics.

(3) The classical second-order analog control loop has been investigated to determine its relative and possible optimum performance in reducing the error of the estimate in a microwave radiometer based on noise bandwidth and settling time criteria. Such results were not found anywhere in the literature.

(4) Several designs of digital signal-processing units for a microwave radiometer have been investigated extensively. One particular design has been identified as the most promising, and its behavior has been simulated extensively by means of the digital simulation programs mentioned in (1).

(5) Efforts have been initiated for developing the hardware and software required in the implementation of the digital signal-processing unit.

(6) Some of the general characteristics and peculiarities of digital processing of noiselike microwave radiometer signals have been investigated.

(7) Technical support has been provided in the form of computer data reduction of results obtained in actual ice missions.

During the period of performance, the following specific persons were involved at different times (all on a part-time basis): William D. Stanley (principal investigator, ODU), Roland W. Lawrence (graduate research

assistant, ODU), Sally E. Kerpelman (undergraduate research assistant, ODU), John M. Jeffords (graduate research assistant, ODU), and William H. Thornton (faculty consultant, ODU).

Dr. Stanley was directly involved in all tasks except (7), and Lawrence participated in all but (3) and (7). Jeffords performed most of the work in (3), and the appendix of this report was authored by him. Prof. Thornton provided consultative assistance in tasks (4) and (5). Kerpelman provided virtually all the assistance required in task (7).

This report provides a documentation of the efforts of tasks (2), (3), (4), (5), and (6). An attempt has been made to divide the report into logical units commensurate with the specific concepts investigated. However, due to a significant amount of overlap in some of these areas, the report does not necessarily proceed in an exact chronological format.

Use of trade names or names of manufacturers in this report does not constitute an official endorsement of such products or manufacturers, either expressed or implied, by the National Aeronautics and Space Administration.

CONTROL ANALYSIS OF FEEDBACK RADIOMETER

As a prelude to the modeling, analysis, and design of a Dicke noise-injection feedback radiometer, it is desirable to delineate the particular manner in which the control mechanism functions. A simplified block diagram of the important parameters of the closed-loop system is shown in figure 1. The signals appearing on the figure represent only the "dc-like" control levels expressed in terms of the effective temperature values at different points in the system. The fluctuation components of the signals do not appear in this model. The model shown in figure 1 will hereafter be designated as a "control model." The more elaborate statistical model will be referred to as a "dynamic noise model."

This simplified control model only shows one Dicke switch since it assumes that all frequency variations between the first Dicke switch and the correlation switch are sufficiently high that they can be neglected for control-loop analysis. The gain between the two Dicke switches has been momentarily lumped with the transfer function G(s). The frequency variation associated with G(s) is primarily that of the integrator and loop filter which constitute the estimation circuit portion of the system.

Analysis of the loop will now be made. The input temperature T_A undergoes a very slight attenuation due to the transmission coefficient $1 - K_{DC}$ of the directional coupler (typically 0.99). The injected noise is weighted by the coupling coefficient K_{DC} of the directional coupler (typically 0.01) and added to the antenna temperature. The effect of the Dicke switch is to introduce an additional 1/2 factor so that T_E on figure 1 can be expressed as

$$T_E = \frac{1}{2} (T_1 - T_B) \tag{1}$$

where T_1 is the effective output temperature of the directional coupler and T_B is the ambient temperature of the constant temperature enclosure.

Effective output temperature T_1 in turn can be expressed as

$$T_1 = \left(1 - K_{DC}\right) T_A + K_{DC} \left(T_B + T'_N\right) \tag{2}$$

where T'_N is the injected excess noise appearing at the attenuator output. In turn, T'_N can be expressed as

$$T'_N = K_{ATT}\ T_{EX}\ \tau\ K_1\ V_o \tag{3}$$

where K_{ATT} is the attenuator constant, T_{EX} is the excess temperature of the noise diode, τ is the pulse width of injected noise pulses, and K_1 is a constant relating output voltage V_o to pulse frequency F_o. The output voltage transform $V_o(s)$ can be expressed as the product of the transfer function $G(s)$ and the error temperature transform $T_E(s)$. For convenience, the s-domain notation will be omitted in most of the subsequent calculations. Thus,

$$V_o = -G\ T_E \tag{4}$$

Equations (1), (2), (3), and (4) may be solved simultaneously to yield a composite expression for the output voltage as a function of the input and reference temperatures. After some manipulation, the result is obtained as

$$V_o = \left(1 - K_{DC}\right) \left[\frac{G/2}{1 + G\ \beta/2}\right] \left(T_B - T_A\right) \tag{5}$$

where, for convenience, β has been defined as

$$\beta = K_{DC}\ K_{ATT}\ T_{EX}\ \tau\ K_1 \tag{6}$$

The output pulse frequency F_o is related to the input and reference temperatures by

$$F_o = \left(1 - K_{DC}\right) \left[\frac{G\ K_1/2}{1 + G\ \beta/2}\right] \left(T_B - T_A\right) \tag{7}$$

One other possible quantity of interest is the "error" temperature T_E, degined in terms of a hypothetical point following the addition of the noise-injection temperature, but after the 1/2 factor of the Dicke switch. This function is

$$T_E = \frac{1}{2} \frac{\left(1 - K_{DC}\right)\left(T_A - T_B\right)}{1 + G\,\beta/2} \tag{8}$$

As far as the control mechanism is concerned, the significant frequency dependency of the loop is contained in the G(s) transfer function. A typical arrangement involves a near-perfect integrator and a loop filter such as

$$G(s) = \frac{K_o}{s(1 + sT)} \tag{9}$$

The presence of this particular function results in a type 1 control loop. The resulting steady-state error due to a step function change in temperature at the input is zero on a deterministic basis. On the other hand, the presence of the noise fluctuations and a finite input bandwidth prevent the statistical error from ever reaching a zero value.

MODEL OF ANALOG RADIOMETER SYSTEM

The particular radiometer used as the reference for virtually all the analysis and design work involved in this study was the 4.5 to 7.2 GHz stepped frequency system developed by Harrington et al. (ref. 3). A simplified block diagram of the system is shown in figure 2. This particular radiometer is a Dicke square-wave correlated type employing closed-loop noise-injection feedback to reduce the effects of gain fluctuations. Many of the salient operational features of the system have been adequately described (ref. 3) and will not be discussed here. The emphasis in this development will be directed toward the establishment and utilization of certain mathematical models for describing various aspects of system operation.

While much of the emphasis in this overall study was devoted to the development of potential digital signal-processing schemes for radiometers, it was apparent at the very outset that the operation and limitations of the analog system had to be fully investigated first. Consequently, considerable effort was expended in obtaining various transfer functions and operational parameters for components within the analog system. Each of several sections will be discussed individually.

RF Subsystem

The RF subsystem will be defined as that portion of the radiometer from the output of the directional coupler to the input of the square-law detector. For the dc control model, all frequencies are sufficiently high that the net effect of this entire portion of the system may be represented by a single constant gain factor. On the other hand, for the dynamic random model, it is necessary to utilize an appropriate transfer function to represent the effect of the wideband filter preceding the square-law detector.

An approximate gain constant for the RF subsystem is determined by the procedure that follows. During the time that early testing on the

radiometer was performed, R. F. Harrington of NASA/LaRC accumulated a significant amount of data relative to signal and noise levels used in the evaluation. Based on a specified noise figure of 5 dB, Harrington estimated that the effective receiver temperature was about T_R = 627 K at some nominal frequency in the operating range. The Dicke reference temperature was established as T_B = 308 K. With the reference temperature applied continuously to the RF subsystem, the signal level at the input to the square-law detector was measured at approximately -33 dBm. The input power density producing this output is estimated to be $k(T_B + T_R) = 1.38 \times 10^{-23} \times (308 + 627) = 1.29 \times 10^{-20}$ W/Hz or -168.89 dBm/Hz. The corresponding gain × bandwidth factor is then estimated to be -33 dBm - (-168.89 dBm/Hz) = 135.89 dB-Hz. This corresponds to an absolute power gain × bandwidth of 3.884×10^{13} Hz. As it turns out, an early calculation based only on T_R employed an input power density of -170.63 dBm/Hz, which resulted in a gain bandwidth factor of 137.63 dB-Hz or about 5.792×10^{13} Hz. This value was rounded to 5.8×10^{13} Hz and used in many of the system simulations. This difference of about two dB is within the uncertainty range of the actual gain factors of the various components in the forward part of the loop as well as the frequency dependency range, and is believed to be insignificant in view of the general uncertainty concerning overall forward gain system parameters. This point of view is further reinforced by the fact that the gain involved is in the forward loop and has a relatively small effect on the closed-loop steady-state accuracy of the measurement within reasonable limits.

Diode Detector

The diode detector employed is an HP 5082-2350 Schottky diode which is biased in a square-law region of operation over the entire operating range of the radiometer. Within this region, the output dc voltage is then a linear function of the input power. Measurements by Harrington indicated a 200-μV output when the input was about -33 dBm (or 0.5 μW). The corresponding gain constant is thus $200 \times 10^{-6}/0.5 \times 10^{-6} = 400$ V/W.

Video Amplifier

The video amplifier is that section of the radiometer between the square-law detector and the output loop filter. This amplifier is basically a low-pass amplifier, but it need not pass dc since the mean temperature estimate being measured appears as a modulated component on the Dicke frequency. However, for square-wave correlation, it is necessary that a relatively large number of components of the square-wave be transmitted by the video amplifier with minimum attenuation and phase shift. Furthermore, noise injection with short pulses mandates that the amplifier have a large bandwidth compared with the reciprocal of the injection pulse width. (This point is pursued further later in this report.)

The actual circuits used in the video amplifier will now be considered. The first two stages, designated as IC1 and IC2, are identical, and each has the form shown in (a) of figure 3. The transfer function is determined to be

$$G_a(s) = \frac{sR_2C_2\left[1 + sC_1(R_0 + R_1)\right]}{(1 + sR_1C_1)\ (1 + sR_2C_2)} \tag{10}$$

With the element values shown on the figure, the function is

$$G_a(s) = \frac{66 \times 10^{-3}s(1 + 2.3892s)}{(1 + 66 \times 10^{-3}s)\ (1 + 79.2 \times 10^{-3}s)} \tag{11a}$$

$$= \frac{66 \times 10^{-3}s\ \left[1 + s/(2\pi \times 0.0666)\right]}{\left[1 + s/(2\pi \times 2.41)\right]\ \left[1 + s/(2\pi \times 2.0095)\right]} \tag{11b}$$

The corresponding Bode plot for IC1 and IC2 is shown in (b) of figure 3.

The circuit diagram for stage IC3 is illustrated in (a) of figure 4. The resulting transfer function $G_b(s)$ can be determined as

$$G_b(s) = \frac{sR_2C_1(1 + R_4/R_3)}{1 + s(R_1C_1 + R_2C_2 + R_2C_1) + s^2R_1R_2C_1C_2} \tag{12}$$

With the element values shown on the figure and the variable resistor adjusted for maximum gain, the function is

$$G_b(s) = \frac{10.5s}{(1 + 0.53047s)\ (1 + 28.2767 \times 10^{-6}s)} \tag{13a}$$

$$= \frac{10.5s}{\left[1 + s/(2\pi \times 0.3)\right]\ \left[1 + s/(2\pi \times 5.63 \times 10^3)\right]} \tag{13b}$$

The corresponding Bode plot is shown in (b) of figure 4.

Combining the effects of two sections of IC1 and one section of IC2, the complete Bode plot of the original video amplifier is shown in figure 5. Observe that a zero of transmission occurs at dc and that a low-frequency rolloff of 18 dB/octave appears. Furthermore, the response is relatively flat from above a few hertz to about 5 or 6 KHz. However, it was later discovered that the bandwidth should be broadened considerably to accommodate the relatively narrow noise-injection pulses.

DC Estimating Circuit

Following the correlation switch, the signal is processed by an estimating circuit. The estimating network originally consisted of an analog integrator and a loop filter, which was a lag-lead network. The lag-lead network was later redesigned as a straight lag network, and this process will be discussed in a later section.

The circuit diagram of the integrator is shown in figure 6, and the circuit diagram of the original loop filter is shown in figure 7. The integrator has a transfer function given by

$$G_i(s) = -\frac{1}{RCs} = \frac{-17.857}{s} \tag{14}$$

for the element values shown.

The transfer function of the lag-lead network is

$$G_{\ell\ell}(s) = \left(\frac{R_1 + R_0}{R_1}\right) \frac{\left(1 + \frac{sR_0R_1C}{R_0 + R_1}\right)}{\left(1 + sR_0C\right)} \tag{15}$$

For the particular element values shown on the figure, the transfer function is determined to be

$$G_{\ell\ell}(s) = \frac{11\ (1 + 2.545 \times 10^{-3}s)}{(1 + 28 \times 10^{-3}s)} \tag{16a}$$

$$= \frac{11\ \left[1 + s/(2\pi \times 62.525)\right]}{\left[1 + s/(2\pi \times 5.684)\right]} \tag{16b}$$

The Bode plot of the lag-lead network is shown in (b) of figure 7. A Bode plot representing the combined effects of the integrator and lag-lead network is shown in figure 8.

Noise-Injection Scheme

The noise-injection process in the closed-loop system is achieved by the use of a voltage-to-frequency (V/F) converter, which produces constant width pulses whose frequency is directly proportional to the loop output voltage. The pulses are applied to a PIN diode driver circuit which is used as a gate for an avalanche noise diode. When the pulses are on, the

noise diode output is directly applied through an attenuator to the auxiliary coupling port of a directional coupler. Conversively, when the pulses are off, no injection noise is applied, and only the ambient temperature T_B appears as an input from the feedback path. Under stable ideal closed-loop conditions, the injection noise plus the input antenna noise is just sufficient to balance the reference noise, and the effects of fluctuations in the forward path are eliminated. If the parameters of the feedback path are known accurately, the antenna temperature may be measured by determining the number of pulses used per unit time to establish the balance.

Data on the noise diode indicates that the excess noise temperature is about 31 dB above 290 K, corresponding to an excess temperature of approximately 365,000 K. The V/F converter is a Datel System VFV-10K, which has a sensitivity of about 863 pulses/s/V. Each pulse has a width of 70 μs so that the constant relating duty cycle to output loop voltage is about $863 \times 70 \times 10^{-6} = 0.0604$. The injected noise encounters a 6-dB fixed attenuator corresponding to a power gain constant of 0.25. The injected noise temperature adds to the ambient temperature of 308 K at the attenuator output. The resulting signal temperature then adds to the antenna temperature through the directional coupler coupling coefficient of -20 dB, corresponding to a power coupling constant of 0.01.

The manner in which the various constants contribute to the feedback noise is illustrated in figure 9. The possible input antenna temperature range is assumed to be from 0 to 300 K. The corresponding ranges of different temperatures are illustrated on the figure. The duty cycle ranges from about 0.334 to 0.00868, and the corresponding pulse rate ranges from 4774 pulses/s to about 124 pulses/s. Finally, the output voltage range is from about 5.532 V to 0.143 V. The injected noise has a sensitivity of about 25.55 K/pulse at the diode itself or about 0.0639 K/pulse at the point of injection. This corresponds to a sensitivity of about 22,050 K/V at the diode or about 55.124 K/V at the injection point.

The manner in which the pulses add to the unsymmetrical open-loop signal in order to balance out the net temperature is illustrated in figure 10. The waveform in (a) depicts the initial situation in which the reference temperature plus the receiver temperature is greater than the input brightness temperature plus the receiver temperature. However, the effect of added noise-injection pulses brings about a net balance of energy as illustrated in (b) before filtering and smoothing occurs. The levels in the tables are the typical values appearing at the input to the estimation circuit; and of course, the results are smoothed by that portion of the system. The fluctuations about the mean levels are not shown in these illustrations; i.e., these are the "dc-like" levels.

Other components in the system whose effects have been considered as constant for the purpose at hand include a tunnel diode amplifier manufactured by AERTECH having a noise figure of 6 dB and a gain of 26 dB ± 1 dB, a mixer and preamplifier stage produced by RHG having a noise figure of 7.5 dB ± 0.5 dB and a gain of 47 dB, and bandpass filters produced by CIR-Q-TEL having an insertion loss of less than 1 dB in the passband.

Combining all the constants discussed in this section, a control loop model for the stepped frequency radiometer is shown in figure 11 based on maximum gain for the variable gain stage. After several steps of manipulation, the closed-loop transfer function for this system is obtained from standard control loop analysis as

$$G_{CL}(s) = \frac{V_o(s)}{T_B(s) - T_A(s)} = \frac{20.214(1 + 2.545 \times 10^{-3}s)}{s^2 + 38.5496s + 1114.1} \qquad (17)$$

The poles of the transfer function are readily determined to be $s = -19.27 \pm j\ 27.25$. This means that the damping factor is $\alpha = 19.27$ and the damped radian frequency is $\omega_d = 27.25$ rad/s or $f_d = \omega_d/2\pi = 4.34$ Hz.

The undamped natural radian frequency is $\omega_o = 33.38$ rad/s and $f_o = \omega_o/2\pi = 5.31$ Hz. The damping ratio is $\zeta = \alpha/\omega_o = 0.577$.

It can be shown that the equivalent one-sided noise bandwidth B_N for this transfer function is given by

$$B_N = \left[\frac{1 + (\omega_o T_2)^2}{8\zeta}\right]\omega_o \tag{18}$$

where T_2 is the numerator time constant in the lag-lead network (2.545 ms in this case). The value $B_N = 7.28$ Hz was calculated for the parameters just considered.

The sensitivity ΔT of the closed loop feedback radiometer can be determined from the relationship

$$\Delta T = 2(T_B + T_R)\sqrt{\frac{2\,B_{NO}}{B_{SI}}} \tag{19}$$

where B_{NO} is the equivalent output noise bandwidth of the loop and B_{SI} is the equivalent statistical bandwidth of the input wideband filter. Using values obtained from the system, the values of ΔT for the four possible input bandwidths are summarized as follows:

B_{SI}	20 MHz	100 MHz	500 MHz	2 GHz
ΔT	1.60 K	0.71 K	0.32 K	0.16 K

These values represent sensitivities based only on the noise-reduction filtering and do not include variations in coupling factor, stability of the noise diode temperature, or Dicke ripple, which will be discussed later.

REDESIGN OF THE ANALOG LOOP

Although a primary objective of this study was the development of techniques for digital processing of radiometer signals, certain immediate operational objectives suggested that some design modifications of the existing stepped frequency analog radiometer would be worthwhile. The first area of concern was that of the loop filter following the integrator in the estimation circuit. Prior to this study, the circuit used for this purpose was the combination of circuits shown in figures 6 and 7. This circuit is a lag-lead network whose transfer function was given in equation (16).

The lag-lead network, in contrast to the lag network, has a larger equivalent noise bandwidth for a given damping ratio and thus does not, in general, smooth the fluctuations as effectively. (Although, for the values initially used in this system, the difference was not appreciable). A separate study was made by a graduate student, John M. Jeffords, to determine various tradeoffs and possible optimum strategies for designing a second-order loop in a feedback radiometer. While much standard information concerning the usual control design of a second-order loop is widely available, peculiar aspects of the radiometer design necessitated a separate study for this purpose. The results of Jeffords' study are given in the Appendix.

Jeffords used the equivalent noise bandwidth times the settling time as a criterion for optimization. This quantity will hereafter be referred to as the $B_N t_s$ product. Jeffords found that the absolute minimum $B_N t_s$ product did result from the simple lag network, and this occurred for $\zeta \approx 0.95$. When a numerator lead time constant (denoted as T_2) is used, the $B_N t_s$ constant increases rapidly. Simultaneously, the value of ζ which results in minimum $B_N t_s$ also increases.

An immediate reaction to this result might be to set $T_2 = 0$ corresponding to the lag network. However, other criteria must be considered before this conclusion is completely obvious, such as the sensitivities of ζ

and the steady-state error to changes in loop parameters. After all, the loop parameters, particularly forward loop parameters, are subject to fluctuations, so the stability of the error to changes in parameters should be considered.

Jeffords found that the sensitivity of the damping factor as a function of gain variations is a minimum in the vicinity of $\zeta = 1$ for $\omega_o T_2 = 1$. It was further found that the sensitivity of the error to changes in loop gain is smaller over a wide range of time for $\omega_o T_2$ products of 1 to 1.5 or so. The result of these last two findings could suggest the use of a lead network for certain applications in which a wide variation of gain fluctuations is expected. The results of Jeffords' study are developed in depth in the appendix.

As it turns out, the variation in gain parameters for a typical radiometer is not expected to be excessive. Furthermore, if some additional time above the minimum settling time is provided, the increase in error is not expected to be significant even though the sensitivity is high. Typical calculations suggest that this conclusion is correct.

After considering various aspects of the loop properties and the results of the study, a decision was made to select a value of ζ in the vicinity of unity (i.e., a critically damped loop) using a lag network only. The critically damped loop has certain design advantages, and it is sufficiently close in behavior to the optimum value that most of the properties are essentially identical. The $B_N t_s$ product for the critically damped loop is approximately 1.5. However, an additional time should be allowed for the loop to fully settle because of the higher sensitivity of the error to parameter changes in the case of the lag network.

The redesign of the loop based on a critically damped response was then formulated as follows: If the lag-lead network is replaced with a simple lag network, its transfer function $G_\ell(s)$ is

$$G_\ell(s) = \frac{K_\ell}{1 + sT_1} \tag{20}$$

The closed-loop transfer function is then determined to be of the form

$$\frac{V_o(s)}{T_B(s) - T_A(s)} = \frac{K_1}{s^2 + \frac{s}{T_1} + \frac{K_{LOOP}}{T_1}} \tag{21}$$

where K_1 is the forward gain constant and K_{LOOP} is the loop gain constant.

Following a review of the settling time specifications, it was decided to design around a damping constant $\alpha = 50$, thus producing a transfer function of the form

$$\frac{V_o(s)}{T_B(s) - T_A(s)} = \frac{K_1}{(s + 50)^2} \tag{22}$$

Comparing equations (21) and (22), it can be deduced that $T_1 = 0.01$ s and $K_\ell = 8.82$. The circuit form used to realize the appropriate lag network is shown in figure 12. This circuit replaces the original lag-lead network.

In order to properly study the effects on the actual radiometer of the lag-lead and lag networks, the test circuit of figure 13 was connected in the system, and the parameters adjusted to visually determine what appeared to be an optimum response. The results compared favorably with those obtained from the mathematical analysis.

One other design consideration for the loop will now be discussed. The injected noise pulses appearing at the radiometer input are relatively narrow, i.e., they are 70-μs wide. In the Dicke correlation process, it is necessary that all noise injected into the first half-cycle actually appear in the first half-cycle at the output switch. Any energy that

"spills over" due to bandwidth limitations will result in some error in the measurement process. Because of the short pulse widths, it was discovered that the bandwidth of the video amplifier was insufficient to process the noise-injection pulses without some distortions. Consequently, a degradation in the calibration factor as a function of the noise level was observed.

As a first step, the capacitor was removed. When the problem was still observed, it was noted that the particular operational amplifier used had an insufficient bandwidth. Consequently, it was replaced with an operational amplifier having a much higher bandwidth and slew rate, and the problem was thus resolved.

DICKE RIPPLE ANALYSIS

Along with the noise fluctuations present in the output of a Dicke radiometer, the ripple corresponding to the Dicke switching frequency and its harmonics must be considered. This ripple is present due to the modulation and demodulation processes of the switched signal. While these components may be kept to a sufficiently low level, they are often ignored in the design process, and this can lead to troublesome operation. Judging from an extensive survey of the literature, it appears that many investigators are not particularly concerned with their presence since virtually no discussion of their effects has been found by this investigator.

For the purpose of the ripple analysis, consider the block diagram shown in (a) of figure 14. It is assumed that steady-state conditions exist, in which case the square-ware is perfectly balanced with a sufficient amount of noise injection at the input. The constant K_1 represents all gain up to the point of the Dicke correlator, and this gain is assumed to be frequency independent as far as the frequency range of the Dicke switch and its harmonics are concerned. Note that this constant does not include the 0.5 Dicke constant shown in figure 11, since that constant arises in the switching process and does not appear explicitly in the figure.

The function $G(s)$ represents the net transfer function of the estimation circuit, which includes the integrator and the lag-lead or lag network. All of the significant frequency dependency in the loop is contained in this block.

The constant K_2 represents the feedback constant. As in the case of K_1, no significant frequency-dependent effects are assumed in this block.

The signal $v_i(t)$ appearing at correlator output is shown in (b) of figure 14 under balanced conditions. Fluctuations about the positive and negative mean levels are not shown. Since the function shown is a simple square-wave, the harmonic components may be readily determined.

The fundamental sine or cosine component of a symmetrical square-wave such as this is $4/\Pi$ times the peak amplitude. This component is then weighted by the transfer function evaluated at $s = j\omega_d$, where $\omega_d = 2\pi f_d$ and f_d is the Dicke switching frequency. Letting V_1 represent the peak output component at the Dicke frequency, this value is

$$V_1 = \frac{4}{\Pi} K_1 (T_B + T_R) |G_2(j\omega_d)| (1 - K_{DC}) \tag{23}$$

While the actual magnitude of the fundamental component is certainly important, a more meaningful measure is the relative level of the fundamental compared with the dc level. The dc level V_o in the steady state is

$$V_o = \frac{(T_B - T_A)}{K_2} (1 - K_{DC}) \tag{24}$$

Let $\alpha_1 = V_1/V_o$ represent the ratio of the fundamental ripple level to the dc component. This quantity is determined from equations (23) and (24) as

$$\alpha_1 = \frac{V_1}{V_o} = \frac{4}{\Pi} \frac{(T_B + T_R)}{(T_B - T_A)} K_1 |G_2(j\omega_d)| K_2 \tag{25}$$

The quantity $K_1 |G_2(j\omega_d)| K_2$ in equation (25) represents the net loop gain for that particular frequency without the 0.5 Dicke switching factor. In the dc control loop analysis, it was convenient and proper to include the 0.5 factor in the definition of the loop gain. In order to make this analysis consistent with the control model, the 0.5 factor is absorbed in the loop gain definition, and an additional factor of 2 is put in front to compensate. Thus, the ripple factor α_1 can be expressed as

$$\alpha_1 = \frac{8}{\Pi} \frac{(T_B + T_R)}{(T_B - T_A)} | G_L(j\omega_d) | \tag{26}$$

where $|G_L(j\omega_d)|$ is the magnitude of the loop gain transfer function evaluated at the Dicke frequency with the 0.5 factor included.

A symmetrical square-wave of the form shown in (b) of figure 14 has only odd harmonics. The ratio of the nth harmonic magnitude V_n to the dc component V_o will be denoted as α_n. This function can be determined as

$$\alpha_n = \frac{8}{n\pi} \frac{(T_B + T_R)}{(T_B - T_A)} |G_L(jn\omega_d)| \tag{27}$$

For a typical loop gain function, the fundamental component V_1 is usually much larger than any of the other components. Consequently, the assumption that the total harmonic level is approximately the same as α_1 is usually valid. This assumption will be made in the analysis that follows. In the existing radiometer, the Dicke frequency f_d is approximately 120 Hz.

For the original loop design, the ripple level of the fundamental can be determined as

$$\alpha_1 = \frac{8}{\pi} \frac{(T_B + T_R)}{(T_B - T_A)} \left| \frac{31.195\ (1 + 2.545 \times 10^{-3} j\omega)}{j\omega(1 + 28 \times 10^{-3} j\omega)} \right| \times 100\% \tag{28}$$

For the modified design, the corresponding function is

$$\alpha_1 = \frac{8}{\pi} \frac{(T_B + T_R)}{(T_B - T_A)} \left| \frac{25}{j\omega(1 + 0.01 j\omega)} \right| \times 100\% \tag{29}$$

As it turns out, the ripple levels for these two functions are almost the same, so only one will be shown graphically. The output peak ripple level expressed as a percentage of the output signal reading is shown in figure 15. This does not include the effect of post-loop filtering, which further reduces the ripple level.

From this curve, it is readily observed that the ripple level increases markedly with increasing input temperature and could be most troublesome if not properly eliminated. Computer simulation of the two systems did indeed verify that the ripple level was (a) dominated by the fundamental component, and (b) equal to the value predicted by the mathematical model.

One way in which the ripple level could be reduced significantly in the analog system is by means of additional loop filtering. In order not to disturb the control mechanism of the loop, which is dominated by two very low frequency poles, it is necessary that the loop filter have a cutoff or filtering range well above a few hertz (the range of the dominant poles), but at the same time it must have a high attenuation at f_d = 120 Hz.

Several possible analog filters were investigated for this purpose and simulated with the available computer programs. Some three-pole Butterworth filter designs with cutoff frequencies below 100 Hz were used, and the simulations verified that they would be quite effective in reducing this ripple.

One particular filter of interest for this purpose was an analog notch filter whose notch was placed at the Dicke frequency. The particular filter used had the transfer function $G_N(s)$ given by

$$G_N(s) = \frac{(1 + 1.7591 \times 10^{-6}s^2)}{1 + 2.5678 \times 10^{-3}s + 5.0555 \times 10^{-6}s^2 + 4.375 \times 10^{-9}s^3} \tag{30}$$

or

$$G_N(s) = \frac{402.124(s^2 + 568.49 \times 10^3)}{s^3 + 1.1557 \times 10^3 s^2 + 587.01 \times 10^3 s + 228.60 \times 10^6} \tag{31}$$

The amplitude response of this filter is shown in figure 16. This filter was found to to quite effective since it completely eliminates the fundamental component. However, there is a small effect due to the higher harmonics which are not attenuated by the notch filter.

GENERAL DIGITAL CONSIDERATIONS

In this section several general considerations concerning digital processing of radiometer data will be investigated. Most of these considerations are general in that they apply to systems other than the radiometer, but it was necessary to review their significance in the context of the radiometer analysis. Some of these factors arise because of conversion between the analog signal and the digital signal and the reverse process.

First, consider the analog system shown in figure 17 with an input $x(t)$, an output $y(t)$, and a transfer function $G(s)$, where $G(s) = Y(s)/X(s)$. Assume now that the input $x(t)$ is chosen to be a wideband noise source; i.e. $x(t) = n_x(t)$. Assume that the "power" spectral density of $n_x(t)$ is uniform and given by $G_{nx}(f) = \eta_x$ V^2/Hz (or W/Hz) on a one-sided basis, and assume that $\overline{n_x(t)} = 0$. The variance of the output $\sigma_y^2 = E\left[y^2(t)\right]$ can be expressed as

$$\overline{y^2(t)} = E\left[y^2(t)\right] = \int_0^\infty |G(j\omega)|^2 \eta_x \, df \tag{32}$$

This result can be expressed in countour integral form as

$$\overline{y^2(t)} = \frac{1}{2\pi j} \int_C \frac{\eta_x}{2} G(s)G(-s) \, ds \tag{33}$$

where C is a contour encompassing the $j\omega$-axis and an infinite semi-circle in the left-hand half-plane. It is further assumed that all poles of $G(s)$ are located in the left-hand half-plane and that the high-frequency rolloff rate of $|G(jw)|$ is no less than 6 dB/octave.

Now assume that a sampled-data version of $x(t)$ is formed, and let $x(n)$ denote this quantity. Assume that all the samples of $x(n)$ are statistically independent. (More will be said about this assumption in a later section.) Assume also that a discrete transfer function $H(z)$

corresponding in some sense to $G(s)$ is formed, and let $y(n)$ represent the discrete output. From the properties of z-transforms, $Y(z) = H(z)X(z)$. However, before involving some of the properties of the discrete-time signal, consider the process of transforming the s-plane contour integral of equation (34) into the z-plane in a direct correspondence sense, assuming of course that $H(z)$ corresponds closely to $G(s)$. Since $z = \epsilon^{sT}$ is the relationship between the z and s variables, $dz = T\epsilon^{sT}ds = Tzds$ and $ds = dz/Tz$. Substituting this expression in equation (33), and replacing $G(s)$ by $H(z)$ and $G(-s)$ by $H(z^{-1})$, the following form of the contour integral results:

$$\overline{y^2(n)} = \frac{1}{2\pi j}\left[\frac{\eta_x}{2T}\int_{C_1}\frac{H(z)H(z^{-1})}{z}\,dz\right] \tag{34}$$

where $\overline{y^2(n)}$ is the output variance of the sampled signal and C_1 is the corresponding contour in the z-plane.

A result from discrete transfer function theory is the relationship

$$\overline{y^2(n)} = \frac{1}{2\pi j}\left[\int_C \frac{H(z)H(z^{-1})}{z}\,dz\right]\overline{x^2(n)} \tag{35}$$

for the case where all samples of $x(n)$ are <u>statistically independent</u>.

From the preceding results, it can be deduced that the quantity η_x represents a power spectral density in V^2/Hz for a <u>continuous analog signal</u>. However, $\eta_x/2T = (\eta_x/2)f_s$ represents a <u>total</u> variance in V^2 for a sampled-data version of an analog signal, and this corresponds directly to $\overline{x^2(n)}$. Thus, the relationships correspond to each other with power density (or voltage-squared density) being the input for the analog case and total variance being the input for the discrete case. In both cases, the output variance is the total variance in volts-squared. Looking

at it from a different point of view, the total input in V^2 is divided over the range $f_s = 1/T$ for the discrete-time signal case. In systems involving A/D and D/A conversions, it is necessary to convert back and forth through these relationships to envision the manner in which the signal forms change.

The point of this discussion is that the discrete-time and continuous-time forms produce identical results when viewed from the proper perspective. When continuous-time systems are considered, it is more convenient to work with power (or voltage-squared) spectral density and to consider the power divided over the frequency range of the sampling frequency (or half the sampling frequency). On the other hand, when discrete-time systems are analyzed, it is often more convenient to express variance in terms of the total mean-square value. The two points of view are equivalent provided that the sampling frequency $f_s = 1/T$ is used for dividing up the power on a two-sided basis. Alternately, the folding frequency $f_o = f_s/2$ could be used on a one-sided basis.

Consider now the process of representing a finite set of samples taken with an A/D converter by an ideal train of inpulses. In the frequency domain, the spectrum of an impulse train $\delta_T(t)$ is expressed as

$$F\left[\delta_T(t)\right] = \frac{1}{T} \sum_{-\infty}^{\infty} \delta(f - nf_s) \tag{36}$$

However, an actual train of nonzero width pulses would have a spectrum weighted by $d = t_1/T$, which would approach zero as $t_1 \to 0$. Consequently, the impulse spectrum has been effectively weighted by $1/t_1$ by using the ideal impulse approximation. On the other hand, when the sampled signal is converted back to a continuous-time signal, it can be thought of as being held by a zero-order holding circuit whose magnitude is unity. The transfer function for this device can be expressed as

t_1 sine ft_1 so that the spectrum is weighted by t_1, the net effect is $t_1 x (1/t_1) = 1$, and the level of the signal is preserved.

SAMPLING EFFECTS OF NOISE SPECTRUM

A major objective of this study was to identify possible schemes by which the processing and reduction of radiometer data could be achieved by digital signal-processing techniques. While the general field of digital signal processing is quite mature, there has been relatively little work reported in the literature on its application to radiometer type signals and systems. There are some peculiar aspects of the radiometer process that result in difficulty in applying standard signal-processing techniques directly to the signal. A significant portion of this study was devoted to investigating the nature of the signal and possible ways of circumventing these difficulties.

The "signal" at the front end of a microwave radiometer is actually wideband noise having a Gaussian amplitude distribution with zero mean. The wideband input filter establishes the bandwidth over which the measurement is performed, which typically ranges from 20 MHz to 2GHz. The square-law detector changes the form of the signal to one with a chi-square distribution with one degree of freedom. The mean of this signal is proportional to the total power in the input signal. Along with the mean value, which represents the quantity to be estimated, is a large background noise signal which must be smoothed to obtain the value of the true estimate. This undesired background signal has a triangular power spectrum. Subsequent processing of the detector output reduces significantly the level of the background while providing an estimate of the true mean.

In a Dicke radiometer, correlation of the signal in order to cancel out the effective receiver temperature noise is also achieved in the postdetector processing. In the case of a noise-injection feedback radiometer, an additional objective that must be performed is the development of a low-frequency control signal to provide a proper feedback mechanism for the loop.

One of the earliest questions of interest in investigating possible digital signal-processing schemes is to determine an appropriate point for sampling the analog signal. At first glance, one might conclude that there would be no hope of sampling the analog signal prior to the square-law detector since the bandwidths there could be as high as 2 GHz and hence result in a required sampling rate of 4 GHz using the conventional sampling rate interpretation. On the other hand, one might argue that since the mean value, not signal reproduction, is the only quantity of real concern, perhaps an undersampled signal could be usable. After all, the Dicke process itself as utilized in the front end of the radiometer is a form of sampling and its rate is far below the required Nyquist rate.

As a result of these questions, an analytical investigation was made to determine the possible implications of undersampling a wideband noiselike signal. Certain simplifying assumptions were made in order to keep the analysis to a manageable level that would provide some useful practical interpretations.

Assume a very wideband noise source $n_i(t)$ whose power spectrum is $G_{ni}(f) = \eta/2$ on a two-sided basis as shown in figure 18(a). Assume first that the signal is filtered directly by a low-pass filter with an equivalent one-sided noise bandwidth B_N, as shown in (b). The instantaneous output noise of this filter is $n_{01}(t)$, and the total variance associated with this noise is N_{01}. From the basic definition of noise bandwidth, this variance is simply

$$N_{01} = 2B_N \frac{\eta}{2} = \eta B_N \tag{37}$$

Now consider the system shown in (c) of figure 18. The signal is first sampled (or modulated) by a pulse signal $p(t)$ whose form is shown in (d). Consequently, $n_s(t)$ can be expressed as

$$n_s(t) = n_i(t)\ p(t) \tag{38}$$

Since $p(t)$ is periodic, it can be expressed as a Fourier series of the form

$$p(t) = \sum_{-\infty}^{\infty} c_n \varepsilon^{jn\omega_s t} \tag{39}$$

where $f_s = \omega_s/2\Pi = 1/T$ is the sampling rate and T is the time between successive samples. For the pulse train $p(t)$ with unity pulse amplitude as shown, the coefficient c_n is given by

$$c_n = d \text{ sinc } nd \tag{40}$$

where $d = t_1/T$ is the duty cycle of the pulse train. Substitution of equation (39) in equation (38) yields

$$n_s(t) = n_i(t)\left[\sum_{-\infty}^{\infty} c_n \varepsilon^{jn\omega_s t}\right] \tag{41a}$$

$$= \sum_{-\infty}^{\infty} c_n \, n_i(t) \varepsilon^{jn\omega_s t} \tag{41b}$$

The autocorrelation function $R_{ns}(\tau)$ corresponding to $n_s(t)$ is

$$R_{ns}(\tau) = E\left[n_s(t + \mu)\, n_s^*(t + \mu - \tau)\right] \tag{42}$$

where μ is uniformly distributed over the range $0 \leq \mu \leq T$ and is a variable introduced as a more rigorous means for establishing stationarity of the process. $R_{ns}(\tau)$ is expanded as follows:

$$R_{ns}(\tau) = E\left\{\left[n_i(t+\mu)\sum_{-\infty}^{\infty} c_n \varepsilon^{jn\omega_s(t+\mu)}\right]\right.$$

$$\left.\cdot\left[n_i(t+\mu-\tau)\sum_{-\infty}^{\infty} c_n^* \varepsilon^{-jn\omega_s(t+\mu-\tau)}\right]\right\} \tag{43}$$

Interchanging the order of the averages results in

$$R_{ns}(\tau) = \overline{\left[n_i(t+\mu)\, n_i(t+\mu-\tau)\right]} \cdot \overline{\left[\left(\sum_{-\infty}^{\infty} c_n \varepsilon^{jn\omega_s(t+\mu)}\right)\right.}$$

$$\left.\times\overline{\left(\sum_{-\infty}^{\infty} c_n^* \varepsilon^{-jn\omega_s(t+\mu-\tau)}\right)}\right]$$

$$= R_{ni}(\tau)\left[\sum_{-\infty}^{\infty} |c_n|^2 \varepsilon^{jn\omega_s\tau}\right] \tag{44}$$

The power spectrum $G_{ns}(f)$ of the sampled signal is determined by computing the Fourier transform of equation (44).

$$G_{ns}(f) = \sum_{-\infty}^{\infty} |c_n|^2 \, G_{ni}(f - nf_s) \tag{45a}$$

$$= \sum_{-\infty}^{\infty} |c_n|^2 \, \frac{\eta}{2} \tag{45b}$$

$$= \frac{\eta}{2} \sum_{-\infty}^{\infty} |c_n|^2 = \frac{\eta}{2} C \tag{45c}$$

where C is the summation. In comparison with the unsampled signal, the power spectrum of the sampled signal is multiplied by the infinite summation shown.

The nature of this summation will now be investigated. It can be manipulated as follows:

$$C = \sum_{-\infty}^{\infty} |c_n|^2 = \sum_{-\infty}^{\infty} d^2 \, \mathrm{sinc}^2 nd$$

$$= \sum_{-\infty}^{\infty} d^2 \left(\frac{\sin n\pi d}{n\pi d} \right)^2 = \frac{d}{\pi} \sum_{-\infty}^{\infty} \left(\frac{\sin n\pi d}{n\pi d} \right)^2 \pi d \tag{46}$$

The summation in equation (46) converges to a value of π. Using this result, equation (46) may be expressed as

$$C = \frac{d}{\pi} \times \pi = d \tag{47}$$

Finally, the output noise power N_{02} under this condition becomes

$$N_{02} = d \, \frac{\eta}{2} \, (2B_N) = d\eta B_N \tag{48}$$

Comparing equation (48) with equation (37), it is seen that the output noise fluctuation power is d times the value that would be obtained without sampling. At first glance, this sounds appealing, since the total fluctuation power is apparently reduced by the sampling process. However, to truly evaluate this approach, it is necessary to consider the existence of a signal component as well. If such a signal component is present, it appears as a frequency domain impulse at dc. Let $\overline{V}_1$ represent the value of the signal component (mean value to be estimated). The signal power S_{01} of the mean value for the continuous nonsampled case is simply

$$S_{01} = (\overline{V}_1)^2 \tag{49}$$

With sampling, it is easy to show that the dc component $\overline{V}_2$ is simply

$$V_2 = d\overline{V}_1 \tag{50}$$

The signal power S_{02} with sampling is then

$$S_{02} = d^2(\overline{V}_1)^2 = d^2 S_{01} \tag{51}$$

The ratio of the signal-to-noise ratio after sampling to the signal-to-noise ratio before sampling is determined by

$$\frac{S_{02}/N_{02}}{S_{01}/N_{01}} = \frac{S_{02}}{S_{01}} \frac{N_{01}}{N_{02}} = d^2 \cdot \frac{1}{d} = d \tag{52}$$

Thus, the signal-to-noise ratio is degraded by a factor of d when the wideband noise signal is undersampled.

A further explanation of this process will be made. The noise components are uncorrelated; therefore, the fluctuation power reduces in direction proportion to the time of observation. On the other hand, the signal (mean value) is a coherent component and its voltage level reduces in direction proportion to the time of observation, meaning that its power reduces in proportion to the square of the time of observation. Thus, the signal power decreases at a much faster rate than the noise power.

The preceding development has been idealized somewhat in order to illuminate the concept fully. The noise was considered separately from the signal to simplify the derivation. When both the mean value (signal) and fluctuation noise appear together, an additional term appears in equation (44), which is the square of the mean value multiplied times the quantity in the brackets. The corresponding spectrum of equation (45c) then contains an infinite number of line components at integer multiples of the sampling frequency. Depending on the manner in which the result is filtered in order to enhance the signal with respect to the noise, these line components may or may not affect the net overall fluctuation level. The exact ratio given by equation (52) applies only when these line components are eliminated. However, the signal-to-noise ratio is degraded by the process of viewing the signal for a portion of the time when the signal is undersampled.

When the sampling rate is sufficiently high that no aliasing occurs, only the c_o term in equation (45c) contributes to the noise at low frequencies. In this case, the noise power, like the signal power, is proportional to d^2 and both quantities decrease at the same rate. With proper filtering in this case, it is possible to avoid any degradation of the signal-to-noise ratio.

An interesting inference from this development is that the basic Dicke radiometer fits the aliasing result as a special case. With the Dicke radiometer, the signal is effectively sampled for a half-cycle, and thus $d = 0.5$. Under optimum conditions of estimation, the noise fluctuation power-to-signal power has an additional factor of two, which agrees with the preceding results.

From the preceding development, it can be deduced that undersampling a noise spectrum is not, in general, an advisable procedure in digital processing except when special objectives are sought, such as in the Dicke radiometer.

OPTIMUM SAMPLING RATE

Analysis of sampled-data signal fluctuations can be approached from two separate points of view: (1) a frequency domain approach based on filtering of the signal and (2) a purely statistical point of view based on a reduction of the variance. Both points of view are correct if properly interpreted. Furthermore, it appears that the frequency domain point of view is most amenable to interpretation when the signal is oversampled, while the statistical point of view is more convenient when the signal is undersampled. The approaches are about equal in complexity when the signal is sampled exactly at the minimum Nyquist rate.

The development that follows should lead to some interesting and useful interpretations for these concepts. Consider a signal whose two-sided power spectral density $G_i(f)$ is of a rectangular form as shown in (a) of figure 19. This function is then described by

$$G_i(f) = \frac{\eta}{2} \qquad -B_i < f < B_i \tag{53}$$

$$= 0 \quad \text{otherwise}$$

The total variance σ_i^2 of the signal is

$$\sigma_i^2 = 2B_i \frac{\eta}{2} = B_i \eta \tag{54}$$

Now assume that the signal is sampled by an ideal impulse sampler with sampling rate f_s. For convenience the impulse sampler will be assumed to have a relative weight $T = 1/f_s$ so that the impulse train $\delta_T(t)$ can be expressed as

$$\delta_T(t) = T \sum_{-\infty}^{\infty} \delta(t - \eta T) \tag{55}$$

The reason for this assumption is to cancel out the 1/T factor that appears as a multiplier for the spectral components of the sampled spectrum of an ideal impulse train, which would create an additional "confusion factor" in interpreting some of the results that follow. This factor actually does not affect the final results anyway, since the holding/reconstruction circuit effectively cancels the 1/T factor, but by putting in the T factor as assumed, the levels of the spectral components can be better interpreted.

After the signals are sampled, a sum-and-dump algorithm will be applied to the set of discrete numbers involved. This algorithm reads

$$y = \frac{1}{N}\sum_{n=1}^{N} X_n \tag{56}$$

where X_n represents the set of N discrete output values of the sampler, and y represents the estimate obtained from application of the algorithm. The average is performed over an interval of τ seconds, where

$$\tau = NT \tag{57}$$

Three possibilities will now be considered: (1) Nyquist rate sampling, (2) undersampling, and (3) oversampling.

Nyquist Rate Sampling

For this first case, the sampling rate will be assumed as

$$f_s = 2B_i \tag{58}$$

The form of the sampled spectrum $G_0^{(1)}(f)$ is shown in (b) of figure 19. Observe that there is neither aliasing nor spectral gaps. The spectrum has exactly filled in the gaps without any "overcrowding."

From a frequency domain point of view, the effect of the sum-and-dump algorithm can be represented by an equivalent noise bandwidth B_N,

which on a two-sided basis can be shown to be

$$B_N = \frac{1}{\tau} = \frac{1}{NT} \tag{59}$$

The variance σ_y^2 of the estimate y can then be expressed as

$$\sigma_y^2 = \frac{\eta}{2} B_N = \frac{\eta}{2\tau} = \frac{\eta}{2NT} = \frac{\eta f_s}{2N} \tag{60}$$

The several forms listed provide different interpretations, but they are essentially frequency domain in form. These results relate directly to the traditional continuous integrate-and-dump circuit in which the output variance is determined by a similar form.

A different interpretation of equation (60) is obtained by noting that

$$\frac{\eta}{2} f_s = \eta B_i = \sigma_i^2 \tag{61}$$

Substituting of equation (61) in equation (60) results in

$$\sigma_y^2 = \frac{\sigma_i^2}{N} \tag{62}$$

This form is the familiar statistical result concerned with the sample mean concept. The variance of the sample mean is the variance of the process sampled divided by the number of samples, provided that the samples are all statistically independent. It is seen that this concept agrees exactly with the frequency domain point of view when the signal is sampled at the Nyquist rate. However, results when the signal is either undersampled or oversampled will be considered next.

Undersampling ($f_s < 2B_i$)

Although the results that will be developed generally apply to any degree of undersampling, it is convenient to assume that the bandwidth

B_i is an integer multiple of the folding frequency. Thus, let

$$B_i = \frac{M_u}{2} f_s \tag{63}$$

where M_u is an "undersampling" integer factor. For $M_u = 1$, this case reduces to the Nyquist sampling case. However, the case of interest involves $M_u > 1$.

Because the signal is undersampled, aliasing of the spectrum will occur. The resulting sampled spectrum $G_0^{(2)}(f)$ will be of the form shown in figure 20. (This case corresponds to $M_u = 4$.) The aliasing results in exactly M_u components adding together in the low frequency range. Since these components add incoherently, the fluctuation power in the low-frequency range is exactly M_u times the value of the unsampled signal.

From a frequency domain point of view, the variance σ_y^2 is now

$$\sigma_y^2 = \frac{\eta M_u}{2} B_N = \frac{\eta M_u}{2\tau} = \frac{\eta M_u}{2NT} = \frac{\eta M_u f_s}{2N} \tag{64}$$

Comparing equation (64) with equation (60), it initially appears that the variance has been increased by a factor M_u over the case of Nyquist sampling, and this result is correct if all the other factors in the expression are the same as before. However, the input spectral density η is in a sense now divided over a greater bandwidth for a given input variance. The input variance is

$$\eta = \frac{\sigma_i^2}{B_i} \tag{65}$$

Substitution of equation (65) in equation (64) results in

$$\sigma_y^2 = \frac{\sigma_i^2 M_u f_s}{2B_i N} = \frac{\sigma_i^2}{N} \tag{66}$$

where the assumption of equation (63) is utilized.

Hence this result is exactly the same as equation (62) for the case of Nyquist sampling because of the fact that all samples are statistically independent. Thus, the question of whether the output variance is greater or not with undersampling depends on the point of view. From a purely statistical point of view, the output variance is 1/N times the input variance and the reduction effect is the same whether Nyquist sampling or undersampling is used for the given number of points. However, from a frequency domain point of view, the fluctuations appear to be greater; but, for a given input variance, the power density is smaller, representing the fact that noise power is spread over a wider bandwidth than before. The fact is, however, that undersampling is not optimum in the sense that a greater reduction of variance could have been achieved in the same time by employing more samples. In other words, undersampling results in the variance being reduced as much as can be expected for the number of points involved, but it could be reduced more in the same amount of time by using more samples.

Oversampling ($f_s > 2B_i$)

As in the case of undersampling, an integer relationship between the bandwidth and the sampling rate will be conveniently chosen. In this case, the following form will be assumed:

$$f_s = M_o(2B_i) \tag{67}$$

where M_o is an "oversampling" factor and is the ratio of the actual sampling rate to the Nyquist rate. The resulting sampled spectrum will be of the form shown in figure 21. (This case corresponds to $M_o = 2$). Note in this case that there are "holes" in the resulting spectrum.

The output variance σ_y^2 in this case is

$$\sigma_y^2 = \frac{\eta}{2}B_N = \frac{\eta}{2\tau} = \frac{\eta}{2NT} = \frac{\eta f_s}{2N} \tag{68}$$

A statistical intepretation of this result is obtained by substituting f_s from equation (67) in equation (68) and utilizing the fact that

$$\eta = \frac{\sigma_i^2}{B_i} \tag{69}$$

The result is

$$\sigma_y^2 = \frac{M_o}{N} \sigma_i^2 \tag{70}$$

In this case, it appears that the output variance is increased by a factor of M_o over that of the Nyquist sampled case, and this point of view would be correct if σ_i^2 were the same as for the Nyquist sampled case. However, the input fluctuations are now confined to a narrower bandwidth for a given input power spectrum. From the frequency domain point of view, the variance has been reduced as much as can be expected for the given integration time. In this case, the frequency domain point of view seems to be easier to interpret due to the lack of aliasing in the spectrum.

To summarize this case, oversampling results in the variance being reduced as much as can be expected for the particular time involved, but it could be reduced more by letting the same number of points extend over a longer period of time. In other words, the samples are too close together to be completely statistically independent, and increasing the time between samples will result in a greater reduction of the variance for the same number of points.

From the preceding developments, it can be concluded that the Nyquist rate is an optimum rate for the reduction of variance in a sampled-data signal with rectangular power spectrum both from the frequency domain point of view and from the statistical point of view. At that rate, both the filtering and the statistical independency properties are "doing their best."

The optimum rate for this purpose should not be confused with the signal reconstruction objective in other applications where a rate exceeding the Nyquist rate is always used. As a matter of fact, the assumption of a flat spectrum has been made thus far, so it is logical to ask what modification is necessary when the power spectrum rolls off more gradually, as it typically does.

Consider, for example, the gradual spectral rolloff shown in (a) of figure 22. In order to make the aliasing error vanishingly small, the sampling rate f_{s_1} is selected to be as shown in (b). While the resulting increase in the aliasing power contained up to the folding frequency is negligible, the variance reduction is suboptimal in that it is less than the 1/N factor. Specifically, the output variance σ_o^2 resulting from a sample mean definition can be most directly calculated from a frequency domain point of view and is

$$\sigma_o^2 = \int_{-0.5f_s}^{0.5f_s} G_1(f)\left(\frac{\sin\frac{N\omega T}{2}}{N\sin\frac{\omega T}{2}}\right)^2 df \tag{71}$$

An alternate strategy with such a rolloff as this is to undersample somewhat so as to "conserve the sampling rate" with the philosophy that the variance won't increase much in the process. The results of this assumption are shown in (c) of figure 22. The output variance in this case is

$$\sigma_o^2 = \int_{-0.5f_s}^{0.5f_s} G_2(f)\left(\frac{\sin\frac{N\omega T}{2}}{N\sin\frac{\omega T}{2}}\right)^2 df \tag{72}$$

where $G_2(f)$ is the modified spectrum with aliasing.

The case where aliasing is present (fig. 22c) results in an increase in the output fluctuations as compared to the case of figure 22(b), but the decrease is more "efficient" for the same number of points. The tradeoff of interest is whether or not the reduction in the required sampling rate is worth the cost of the increased variance. Each case would have to be considered on its own merits. If the data rate is rather slow and the digital circuitry is capable of operating at a high rate anyway, the optimum choice will likely be to sample at a high enough rate to eliminate all aliasing error.

SECOND-ORDER DIGITAL LOOP DESIGNS

Early in the course of this study, several second-order control loop designs were investigated and successfully simulated. The choice of a second-order loop was made at that time because the current analog system utilized a second-order loop. As will be shown later, a first-order loop followed by post-loop sum-and-dump filtering was finally selected for the prototype implementation. Nevertheless, there are still some worthwhile features of the second-order loop that could make it a viable candidate for some applications. Consequently, some of the intrinsic features of a second-order digital loop will be discussed in this section, and some representative designs will be shown.

The concept of utilizing the second-order loop was based on performing virtually all the data smoothing in the loop itself and considering little or no post-loop filtering. It was also decided to employ coefficients in this design that could be realized exactly by a rather limited number of bits. In this case exact coefficients were known, making the equivalent smoothing bandwidths more readily predicted.

In establishing equivalence, or at least correspondence, between a digital loop and an analog loop, several approaches are possible. None of these are "exact" in one sense since the discrete-time system is different from the continuous-time system, and the best that can be done is to establish a correspondence with respect to some particular criterion. For that reason, a comparison with respect to more than one criterion will be made in some of the developments that follow.

One criterion is the direct z-transform correspondence $z = \varepsilon^{sT}$ or, equivalently, $s = (1/T)\ \ell n\ z$. This relationship computes the values of s and z that correspond to each other through the z-transform definition, and in this sense is exact.

A second criterion is a correspondence through the bilinear transformation. A popular and convenient means for designing digital

filters is to employ a prototype continuous system variable p, obtain a continuous transfer function approximating the desired behavior, and then to replace p by

$$p = \frac{K(1 - z^{-1})}{1 + z^{-1}} \tag{73}$$

where K is a mapping constant. For very low frequency correspondence between the prototype analog frequency and the final digital frequency, it can be shown that an optimum choice of K is

$$K = \frac{2}{T} = 2f_s \tag{74}$$

The actual second-order functions chosen for the loop were based on a *modified bilinear transformation criterion. Consider momentarily a* first-order analog function of the form

$$G(p) = \frac{\alpha}{p + \alpha} \tag{75}$$

When the bilinear transformation is applied to equation (75), the corresponding H(z) is determined as

$$H_d(z) = \frac{\alpha}{K + \alpha} \frac{(1 + z^{-1})}{1 - Bz^{-1}} \tag{76}$$

where

$$B = \frac{K - \alpha}{K + \alpha} \tag{77}$$

Consequently, if B is selected as a convenient value in the digital filter, the corresponding α in the analog sense can be determined as

$$\alpha = \frac{K(1 - B)}{1 + B} \tag{78}$$

The first design of a digital estimating circuit considered is shown in figure 23. The particular structure shown in the figure represents only the digital processor portion starting from the A/D converter and continuing to the point at which the output estimate is determined. The feedback noise-injection scheme is not shown in the figure. The difference equations describing this system are as follows:

$$u(n) = x(n) + x(n - 1) + u(n - 1) \tag{79}$$

$$v(n) = 2^{-3}\, u(n) \tag{80}$$

$$w(n) = v(n) + v(n - 1) + 0.875\, w(n - 1) \tag{81}$$

$$y(n) = 2^{-3}\, w(n) \tag{82}$$

The corresponding transfer functions are

$$\frac{U(z)}{X(z)} = \frac{1 + z^{-1}}{1 - z^{-1}} \tag{83}$$

$$\frac{V(z)}{U(z)} = 2^{-3} \tag{84}$$

$$\frac{W(z)}{V(z)} = \frac{1 + z^{-1}}{1 - 0.875z^{-1}} \tag{85}$$

$$\frac{Y(z)}{W(z)} = 2^{-3} \tag{86}$$

The composite transfer function is

$$H(z) = \frac{Y(z)}{X(z)} = \frac{2^{-6}(1 + z^{-1})^2}{(1 - z^{-1})(1 - 0.875z^{-1})} \tag{87}$$

The low-frequency behavior of $H(z)$ may be determined by substituting $z = \varepsilon^{sT}$ and letting s become very small. The function $H(\varepsilon^{sT})$ then asymptotically approaches

$$H(\varepsilon^{sT}) \approx \frac{2^{-6}(2)^2}{sT(0.125)} = \frac{0.5}{sT} \quad \text{(for small s)} \tag{88}$$

For this particular design, with the sampling rate selected as $f_s = 750$ Hz, the function approximates 375/s.

Based on the constant $B = 0.875$ in equation (76), the corresponding analog α may be approximated by either setting $\varepsilon^{-\alpha T} = 0.875$ or by using the bilinear transformation. In the first approach, $\alpha = 100.15$ rad/s. In the second approach, $\alpha = 100$ rad/s based on equation (78). The two values are in close agreement, and correspond very closely to the optimum analog value selected in an earlier redesign effort.

The actual analog transfer function $G(s)$ of the estimation circuit was earlier selected as

$$G(s) \equiv \frac{17.857 \times 8.82}{s(1 + 0.01s)} \tag{89}$$

For small values of s, this function approximates

$$G(s) \approx \frac{157.5}{s} \tag{90}$$

The corresponding digital function has more than twice the gain required, so the signal should be attenuated by a factor of 157.5/375 = 0.42 before processing.

The second approach considered in second-order loop designs was one in which two separate modes could be employed. The first mode, designated mode A, is the lower resolution, faster response mode. On the other

hand, mode B provides a greater resolution at the expense of a longer integration time. For this particular design, an Intel 8086 microprocessor development unit had been identified for prototype development work. Consequently, its clock frequency of 4.9 MHz was selected for timing, and the sampling rate was chosen as

$$f_s = 4.9 \times 10^6/2^{13} = 598.14 \text{ Hz}$$

The discrete transfer function of the lag-lead digital filter was selected in the form

$$H_\ell(z) = \frac{K_d}{1 - Bz^{-1}} \tag{91}$$

The value of B for mode A was selected as

$$B = 0.1101_2 = 0.8125_{10} \tag{92}$$

where the subscripts 2 and 10 represent the binary and decimal bases, respectively. The corresponding value of α in the analog representation is determined from the direct z-transform definition as

$$\alpha = -(1/T)\ \ell n\ 0.8125 = 124.20 \text{ rad/s}$$

and from the bilinear transformation as

$$\alpha = 2 \times 598.14 \times (1 - 0.8125)/(1 + 0.8125) = 123.75 \text{ rad/s}$$

To simplify further references, the value $\alpha = 124$ rad/s for mode A will be assumed in subsequent discussions.

The layout of mode A is shown in figure 24. The various difference equations are tabulated as follows:

$$u(n) = x(n) + x(n - 1) + u(n - 1) \tag{93}$$

$$v(n) = 2^{-4}u(n) \tag{94}$$

$$w(n) = v(n) + v(n - 1) + 0.8125\ w(n - 1) \tag{95}$$

$$y(n) = 2^{-2}\ w(n) \tag{96}$$

The corresponding transfer functions are

$$\frac{U(z)}{X(z)} = \frac{1 + z^{-1}}{1 - z^{-1}} \tag{97}$$

$$\frac{V(z)}{U(z)} = 2^{-4} \tag{98}$$

$$\frac{W(z)}{V(z)} = \frac{1 + z^{-1}}{1 - 0.8125z^{-1}} \tag{99}$$

$$\frac{Y(z)}{W(z)} = 2^{-2} \tag{100}$$

The composite transfer function is

$$\frac{Y(z)}{X(z)} = \frac{2^{-6}(1 + z^{-1})^2}{(1 - z^{-1})(1 - 0.8125z^{-1})} \tag{101}$$

As observed in equation (90), the analog estimating circuit approximates 157.5/s for small s. The function of equation (101) approximates $2^{-6}(2)^2/sT(0.1875) = 199.38/s$. Thus, a small attenuation of the analog signal before sampling should result in nearly equal behavior of the digital system as compared with the analog system.

The value of B for mode B was selected as

$$B = 0.111101_2 = 0.953125_{10} \tag{102}$$

The corresponding value of α from the direct z-transform was computed as $\alpha = -(1/T)\ \ell n\ 0.953125 = -28.716$ rad/s and from the bilinear transformation as $\alpha = 2 \times 598.14(1 - 0.953125)/(1 + 0.953125) = 28.71$. The latter value will be selected for subsequent references.

The layout for mode B is shown in figure 25. The various difference equations are tabulated as follows:

$$u(n) = x(n) + x(n - 1) + u(n - 1) \tag{103}$$

$$v(n) = 2^{-5}x(n) \tag{104}$$

$$w(n) = v(n) + v(n - 1) + 0.953125\ w(n - 1) \tag{105}$$

$$y(n) = 2^{-5}\ w(n) \tag{106}$$

The corresponding transfer functions are

$$\frac{U(z)}{X(z)} = \frac{1 + z^{-1}}{1 - z^{-1}} \tag{107}$$

$$\frac{V(z)}{X(z)} = 2^{-5} \tag{108}$$

$$\frac{W(z)}{V(z)} = \frac{1 + z^{-1}}{1 - 0.953125z^{-1}} \tag{109}$$

$$\frac{Y(z)}{W(z)} = 2^{-5} \tag{110}$$

The composite transfer function is

$$\frac{Y(z)}{X(z)} = \frac{2^{-10}(1 + z^{-1})^2}{(1 - z^{-1})(1 - 0.953125z^{-1})} \qquad (111)$$

The function of equation (111) approximates $2^{-10}(2)^2/sT(0.046875) = 49.845/s$ for small s. The corresponding analog filter transfer function was quite close when redesigned for this higher accuracy mode. Note that the present analog system does not operate in a higher resolution mode such as this. Instead, higher resolution is achieved by post-loop processing of the data obtained from the lower resolution operating mode.

CANCELLATION OF DICKE RIPPLE

A troublesome problem in an analog Dicke radiometer system is the presence of the Dicke ripple component in the data output. Because of the periodic switching in such a radiometer, an undesired disturbance at the switching frequency appears in the signal output. This disturbance consists of a fundamental component at the switching frequency plus components at odd integer multiples of the switching frequency if symmetrical switching is employed. Due to the normal low-pass nature of the forward transfer function, the most troublesome component is the fundamental, and its magnitude is a close approximation to the total ripple level in most cases.

While it is possible to set the loop parameters to adjust this ripple to a tolerable level by careful design, an interesting concept came to light in investigating possible digital-processing schemes. Consider the discrete transfer function $H(z)$ of the trapezoidal integration approximation as given by

$$H(z) = \frac{K(1 + z^{-1})}{1 - z^{-1}} \tag{112}$$

The steady-state transfer function $H(\varepsilon^{j\omega T})$ corresponding to this function is readily shown to be

$$H(\varepsilon^{j\omega T}) = \frac{K \cos \frac{\omega T}{2}}{\sin \frac{\omega T}{2}} = K \cot \pi f T \tag{113}$$

The form of the magnitude response $|H(\varepsilon^{j\omega T})|$ corresponding to equation (113) is shown in figure 26. The frequency response approximates that of an ideal integrator in the very low frequency range, i.e., for $f << 1/2T$. However, for $f = 1/2T$, the steady-state transmission is identically zero.

Assume now that the sampling frequency $f_s = 1/T$ is chosen to be twice the Dicke frequency f_d, i.e., $f_s = 2f_d$. This results in a zero or null of transmission at the Dicke frequency and at odd integer multiples of the Dicke frequency. Thus, as long as the switched signal satisfies the half-wave symmetry conditions of Fourier theory, all undesired components in the ripple disturbance will be completely eliminated.

As it turns out, the proposed feedback schemes utilize a pulse-injection process which disturbs the half-wave symmetry of the switched signal. The resulting signal in this case does contain even harmonics which are not eliminated by this process. However, such components are easier to handle since they are higher in frequency and smaller in magnitude. The major point of interest is that a significant reduction, or possibly an elimination, of the switching ripple can be achieved directly through a digital algorithm.

PROPOSED CONTROL LOOP

After investigating in some detail the several second-order loop designs previously discussed, attention was directed toward the concept of a first-order loop followed by post-loop sum-and-dump filtering. Because of the presence of the post-loop filtering, the system was actually of higher order, but for subsequent references the term "first-order processor" or simply "first-order loop" will be used.

Some of the advantages of the first-order loop determined from this investigation are (1) the form of the response is less sensitive to parameter deviations than the second-order loop. Small variations in gain parameters can sometimes adversely change the damping ratio of a second-order loop. (2) The loop can be made to respond faster, thereby allowing a greater reduction of fluctuations by the sum-and-dump post-loop filter. (3) It is easier to take advantage of the Dicke cancellation scheme previously discussed when the loop is a first-order design.

The basic design of the first-order estimation loop filter is shown in figure 27. The difference equations for this system are

$$w(n) = x(n) + x(n - 1) + w(n - 1) \tag{114}$$

$$y(n) = 0.25\ w(n) \tag{115}$$

The corresponding transfer function $H(z)$ for the filter is

$$H(z) = \frac{Y(z)}{X(z)} = \frac{0.25(1 + z^{-1})}{1 - z^{-1}} \tag{116}$$

The design of the loop estimation and feedback system is shown in figure 28. The timing references for this system are derived from the 4.9 MHz and the 2.45 MHz signals available in the microprocessor unit.

The sampling rate for the analog signal is f_s = 2.45 MHz/2^{12} = 598.14 Hz. The A/D converter is an Analog Devices type AD-572 12-bit successive approximation unit. The drive for the Dicke frequency f_d is obtained by dividing f_s by 2, thus giving f_d = 299.07 Hz. This results in zeros of transmission at odd integer multiples of the Dicke frequency as previously discussed.

The analog aliasing filter is a cascade of 3 simple one-pole filters, each having a 3-dB break frequency at 100 Hz. An investigation was made to determine the need for more sophisticated aliasing filter designs having complex poles, inasmuch as this particular filter has a rather pronounced amplitude "droop" in its passband. However, since the only component of primary interest is the dc component, and since the actual passband shape is relatively unimportant, this filter was found to be perfectly adequate, and it simplifies the overall design. There is a small aliasing error, but its level is insignificant in view of other error contributions.

The noise-injection scheme proposed for this design differs considerably from the original design in that it will be injected continuously during a portion of the Dicke cycle. In this manner, the bandwidth requirements of the broadband amplifier preceding the Dicke correlator are eased considerably. The noise is injected once per cycle as illustrated by figure 29. (Actually, it is injected on both half-cycles, but since the Dicke switch only sees it once per cycle, the extra injection does not appear on the figure). The length of time that the noise-injection pulse is on is determined by the value of the digital word at the output of the loop digital filter. A word is loaded in the down-counter once per sample time T. The noise diode is gated on through the PIN switch at the beginning of this interval. When the down-counter reaches zero, the "status" signal turns off the switch, thereby reducing the noise injection to zero.

The maximum duty cycle corresponds to minimum input temperature, which results in maximum feedback temperature injection. Based on a reference temperature of 308 K, a directional coupler coefficient of

-20 dB, an excess noise temperature of 365,000 K, an additional attenuation of 10 dB in the feedback loop, and an input temperature of 0 K, the maximum duty cycle was found to be 0.835. Conversely, the minimum duty cycle corresponding to 300 K input was found to be 0.0217. The range of temperatures and duty cycle are illustrated on figure 30. Operation near minimum duty cycle poses the same sort of problems as the current analog system since the resolution is degraded seriously in that range.

It was decided not to operate at a duty cycle of unity due to "spillover" resulting from finite bandwidth limitations. Consequently, the duty cycle of 0.835 was judged to be a good choice for the maximum value of the duty cycle.

While odd harmonics of the Dicke frequency are eliminated by the digital filter, even harmonics will appear due to the asymmetrical noise injection. Referring to figure 29, an analysis of the levels of even harmonics present may be made from a combination of the energy balance and Fourier theory. At a condition of zero steady-state error, the area of the positive half-cycle must equal in magnitude the area of the negative half-cycle. This means that

$$C\,T_I t_1 + C(T_A + T_R)T = C(T_B + T_R)T \tag{117}$$

which results in

$$T_I t_1 = (T_B - T_A)T \tag{118}$$

or

$$T_I d = T_B - T_A \tag{119}$$

where $d = t_1/T$ is a duty cycle defined as the ratio of the "on" interval to half of the Dicke period. (Equivalently, it is the total on time,

including the superfluous extra injection, per Dicke period to the total period.). Full injection corresponds to d = 1.

The even harmonics that arise from the asymmetry may be considered to originate from a pulse train having a period 2T, a duty cycle d/2, and an amplitude CT_I. The magnitudes A_n of these components on a conventional sine-cosine basis can be expressed as

$$A_n = 2\left(\frac{d}{2}\right)CT_I \frac{\sin n\pi d/2}{n\pi d/2} = C(T_B - T_A) \sin \frac{n\pi d/2}{n\pi d/2} \tag{120}$$

Since the fundamental and odd harmonics are eliminated by the loop filter, the most significant component of concern is the second harmonic term. This value is

$$A_2 = CT_I \frac{\sin \pi d}{\pi} \tag{121}$$

As one would expect, $A_2 = 0$ for d = 1. Conversely, the maximum value of A_2 occurs for d = 0.5, meaning that noise is injected half of the time between successive analog samples. This maximum value $A_2 = CT_I/\pi$ occurs for an input temperature $T_A \approx 124$ K. This could be serious except for the fact that the 3-pole aliasing filter has an attenuation of about 47 dB at the sampling frequency, plus the rolloff of the loop itself provides an attenuation of about 37.5 dB. The overall level of the even harmonics was found to be negligible in all the simulations.

A simplified block diagram of the control model for the discrete-time system is shown in (a) of figure 31. The gain of 4.61×10^{-3} represents the net effect of the original gain of 2.88×10^{-3} times an additional gain of 1.6 that was later added to establish an optimum transient response. The second block is a "redefinition" gain established by the following procedure: The input range of the A/D converter is set at ±2.5 V, which was determined by simulation to be

the proper level. This means that the least significant bit at the input corresponds to $5V/2^{12} = 1.22$ mV. In passing through the processor, a 4 to 1 expansion of the signal level occurs, meaning that two additional bits are required. However, it is desired to "redefine" the signal on a normalized basis so that each digital word has a maximum value of unity. Considering the 2.5 V maximum at the input coupled with the 4 to 1 expansion, the output would really have a maximum of 10 V on an analog basis, so a "gain" factor of 0.1 is used to establish it at unity maximum level.

The forward gain function $H_1(z)$ is then

$$H_1(z) = 115.25 \times 10^{-6} \frac{(1 + z^{-1})}{1 - z^{-1}} \tag{122}$$

For very small s, this function behaves approximately like an analog gain function

$$G_1(s) \approx \frac{115.25 \times 10^{-6}(2)}{sT} = \frac{0.138}{s} \tag{123}$$

This equivalence is shown in (b) of figure 31, which clearly illustrates the nature of the corresponding first-order analog system.

The appropriate loop gain content is $0.138 \times 365 = 50.32$, which will be rounded off to 50 for subsequent calculations. The closed loop transfer function $G(s)$ will then be expressed as

$$G(s) = \frac{0.137}{s + 50} = \frac{2.74 \times 10^{-3}}{1 + \frac{s}{50}} \tag{124}$$

The overall proposed system is shown in figure 32.

POST-LOOP PROCESSOR

The digital filter contained in the loop was designed primarily to provide the necessary dynamic loop behavior for optimum control of the noise-injection process. In contrast, the primary objective of the post-loop filter was to provide a smoothed estimate of the brightness temperature in as short a time as possible commensurate with the sensitivity specifications.

The concept used to reduce the variance of the temperature estimate in the post-loop processor was the well-known sample mean algorithm. This process will hereafter be denoted as a "sum-and-dump" algorithm due to its close similarity to the integrate-and-dump circuit used in analog matched filter and estimation systems. Indeed, the mathematical behavior of the sum-and-dump algorithm on a discrete-time basis is virtually identical to the behavior of the integrate-and-dump filter on a continuous-time basis.

The integrate-and-dump analog filter is optimum in that the product of the equivalent noise bandwidth times the settling time is minimum for all analog lumped filters. The corresponding sum-and-dump algorithm possesses the same optimum property among the class of discrete-time filters.

The post-loop processing is actually a set of several similar sum-and-dump algorithms of different lengths as shown in figure 33. Each algorithm involves a scanning window that picks up all applicable loop samples over the duration of the loop. The number of points chosen in a window is always selected as an integer power of two. This simplifies the multiplication and division required by the microprocessor, and it simplifies the structure of the dependency between shorter and longer versions of the algorithm.

Let $y(n)$ represent the discrete values appearing at the output of the loop, and let $y_N(i)$ represent the smoothed discrete values appearing at the output of different length post-loop algorithms. The

integer N represents the number of points in the particular algorithm. Note that n is an integer changing at the loop sampling rate while i changes only once for every 16 values of n. Thus,

$$n = 16i \tag{125}$$

or

$$i = \text{integer part of } \left(\frac{n}{16}\right) \stackrel{\text{def}}{=} I\left(\frac{n}{16}\right) \tag{126}$$

The first value is simply $y_1(i)$, which is not actually a smoothed value but is the output of the loop as held for an interval of 16 periods at the sampling rate, i.e., T_o = 26.75 ms. Thus,

$$y_1(i) = y(i) \text{ for } i = I\left(\frac{n}{16}\right) \tag{127}$$

The remaining values at the outputs of different stages can all be expressed directly in terms of $y_1(i)$, or they can be expressed in terms of smoothed estimates of lower order. All estimates are updated every 16 loop samples even though the statistical dependency of subsequent samples increases with the order of the estimate.

A tabulation of the various estimates follows:

$$y_2(i) = \frac{y_1(i) + y_1(i - 1)}{2} \tag{128}$$

$$y_4(i) = \frac{y_1(i) + y_1(i - 1) + y_1(i - 2) + y_1(i - 3)}{4} \tag{129a}$$

$$= \frac{y_2(i) + y_2(i - 2)}{2} \tag{129b}$$

$$y_8(i) = \frac{1}{8}\sum_{I=0}^{7} y_1(i - I) \tag{130a}$$

$$= \frac{y_4(i) + y_4(i - 4)}{2} \tag{130b}$$

$$y_{16}(i) = \frac{1}{16}\sum_{I=0}^{15} y_1(i - I) \tag{131a}$$

$$= \frac{y_8(i) + y_8(i - 8)}{2} \tag{131b}$$

$$y_{32}(i) = \frac{1}{32}\sum_{I=0}^{31} y_1(i - I) \tag{132a}$$

$$= \frac{y_{16}(i) + y_{16}(i - 16)}{2} \tag{132b}$$

$$y_{64}(i) = \frac{1}{64}\sum_{I=0}^{63} y_1(i - I) \tag{133a}$$

$$= \frac{y_{32}(i) + y_{32}(i - 32)}{2} \tag{133b}$$

Additional representations of the sum-and-dump algorithms from a digital filter perspective and a z-transform point of view are shown in figures 34 and 35, respectively.

The variance reduction of the sum-and-dump algorithm will now be analyzed. First, the assumption of a uniform power spectrum will be made, and this will be modified later to include loop frequency dependency. Consider then the general form of the algorithm as given by

$$y_N(i) = \frac{1}{N} \sum_{I=0}^{N-1} y_1(i - I) \tag{134}$$

Let $Y_N(z)$ represent the z-transform of $y_N(i)$ and let $Y_1(z)$ represent the z-transform of $y_1(n)$. Transformation of both sides of equation (134) yields

$$Y_N(z) = \frac{1}{N} \sum_{I=0}^{N-1} Z^{-I}\, Y_1(z) \tag{135}$$

The transfer function $H_N(z)$ of the post-loop sum-and-dump algorithm can be expressed as

$$H_N(z) = \frac{Y_N(z)}{Y_1(z)} = \frac{1}{N} \sum_{I=0}^{N-1} z^{-I} \tag{136}$$

The steady-state frequency response will be denoted as $H_N'(f)$, and this quantity is determined by substituting $z = \epsilon^{j\omega T_o}$ in equation (136). (Note that T_o is the post-loop sample time, not the loop sample time, i.e., $T_o = 16T$.) The result initially is

$$H_N'(f) = \frac{1}{N} \sum_{I=0}^{N-1} \epsilon^{-j\omega T_o} \tag{137}$$

By means of the summation formula

$$\sum_{0}^{N-1} a^I = \frac{1 - a^N}{1 - a} \tag{138}$$

and the exponental definition of the sine function, equation (137), can be expressed as

$$H_N'(f) = \frac{\sin(N\omega T_o/2)}{N \sin(\omega T_o/2)} \varepsilon^{-j(N-1)\frac{\omega T_o}{2}} \tag{139}$$

The equivalent one-sided noise bandwidth B_N can be expressed as

$$B_N = \int_0^{0.5f_{os}} |H(f)|^2 df \tag{140a}$$

$$= \int_0^{0.5f_{os}} \left(\frac{\sin N\pi T_o f}{N \sin \pi T_o f}\right)^2 df \tag{140b}$$

where f_{os} is the post-loop sampling rate, i.e. $f_{os} = 1/T_o = f_o/16$.

For integration purposes, a change of variables was made by setting $x = T_o f$, and the integral then becomes

$$B_N = \frac{1}{T_o} \int_0^{0.5} \left(\frac{\sin N\pi x}{N \sin \pi x}\right)^2 dx \tag{141}$$

It can be shown that the value of this integral is given by

$$B_N = \frac{1}{T_o} 2^{-[\log_2 N + 1]} \tag{142a}$$

$$= \frac{1}{2NT_o} = \frac{0.5}{NT_o} \tag{142b}$$

Let $\tau = NT_o$ = total time interval for averaging. Substituting this value of τ in equation (142), the one-sided equivalent noise bandwidth is simply

$$B_N = \frac{0.5}{\tau} \tag{143}$$

This result is exactly the same as for the continuous-time integrate-and-dump filter with τ as the integration time. Thus, the sum-and-dump algorithm for a discrete time signal functions exactly the same as the integrate-and-dump filter for a continuous-time signal provided that the summation interval in the discrete-time case is equal to the integration interval in the continuous-time case. A further subtle assumption is that the power spectra for the two cases would have to be compared on the same basis. This would imply optimum sampling at the Nyquist rate for the discrete-time system as previously discussed.

Assume momentarily that the input $y_1(i)$ has a uniform power spectral density $G_{y_1}(f) = \eta$ on a one-sided basis over the frequency range from dc to 0.5 f_{so}. The output variance $\sigma_{y_N}^2$ is then given by

$$\sigma_{y_N}^2 = \frac{0.5\eta}{NT_o} = \frac{0.5\eta}{\tau} \tag{144}$$

The fact is, however, that the input noise power spectrum in the case of interest is not flat but has the shape of the power transfer function of the loop. The loop relative amplitude-squared response function $A_L^2(f)$ expressed as a function of steady-state frequency is dominated by a single pole and is of the form

$$A_L^2(f) = \frac{1}{1 + \left(\frac{f}{f_1}\right)^2} \tag{145}$$

where f_1 is the 3-dB loop frequency. As a close estimate of the anticipated design value, the damping constant of the loop is about $\alpha = 50$ corresponding to $f_1 = 50/2\pi = 7.96$ Hz, which was rounded to 8 Hz, giving

$$A_L^2(f) = \frac{1}{1 + \left(\frac{f}{8}\right)^2} \tag{146}$$

An equivalent noise bandwidth B_{NO} based on the combination of the loop response given by equation (146) and the sum-and-dump algorithm can now be derived. The form for the equivalent noise bandwidth is

$$B_{NO} = \int_0^{0.5f_s} \left(\frac{\sin N\pi T_o f}{N \sin \pi T_o f}\right)^2 \frac{df}{1 + \left(\frac{f}{8}\right)^2} \tag{147}$$

This function was modified for integration by substituting $x = T_o f$ as before. After some simplification, the result becomes

$$B_{NO} = \frac{1}{T_o} \int^{0.5} \left(\frac{\sin N\pi x}{N \sin \pi x}\right)^2 \frac{dx}{1 + \left(\frac{x}{0.214}\right)^2} \tag{148}$$

This integral was evaluated numerically for values of N ranging from 2 to 64 (in integer powers of 2). It is convenient to tabulate the integrals in the form $B_{NO}\tau = B_{NO}NT_o = \gamma$. These data are shown below plus the case for N = 1

N	1	2	4	8	16	32	64
$\gamma = B_{NO}\tau$	0.3362	0.3459	0.4177	0.4586	0.4793	0.4896	0.4948

Observe that as the number of points increases, γ approaches 0.5 or B_{NO} approaches $0.5/\tau$, which is the value without the additional loop filtering. In this limiting range, the post-loop algorithm reduces the spectrum at such a low frequency range that the effect of the loop filter is negligible.

SENSITIVITY OF PROPOSED DESIGN

In this section, an analysis of the sensitivity of the proposed loop design will be performed. Although the loop is a hybrid system in that it is partly a continuous-time system and partly a discrete-time system, the input-output relationships on a continuous-time basis will be maintained since it is from this point of view that the results must be interpreted and applied.

As previously shown, the transfer function of the control loop is dominated by a single pole and is approximately equivalent to a continuous-time system of the form

$$G(s) = \frac{Y}{T_B - T_A} = \frac{0.137}{s + 50} \tag{149}$$

where Y is the output loop estimate before post-loop filtering. The steady-state transfer function $G(jw)$ corresponding to equation (149) can be expressed as

$$G(j\omega) = \frac{0.137}{50 + j\omega} = \frac{2.74 \times 10^{-3}}{1 + j\frac{\omega}{50}} \approx \frac{2.74 \times 10^{-3}}{1 + j\frac{f}{8}} \tag{150}$$

where the 3-dB break frequency is rounded slightly to 8 Hz for convenience.

The digital words from the output of the loop are then processed through the post-loop filter. The equivalent noise bandwidth B_{NO} for the whole system is determined from the results of equation (148), which were tabulated in the last section.

The sensitivity ΔT of the closed-loop noise-injection feedback radiometer is determined from the equation

$$\Delta T = 2(T_B + T_R)\sqrt{\frac{2B_{NO}}{B_{SI}}} \tag{151}$$

where T_B is the reference temperature (308 K for this system), T_R is the input noise temperature of the receiver, B_{NO} is the equivalent noise bandwidth, and B_{SI} is the input statistical bandwidth. For this system B_{NO}, can be expressed as

$$B_{NO} = \frac{\gamma}{\tau} = \frac{\gamma}{NT_o} \tag{152}$$

where γ is the constant corresponding to the summation interval as given in the previous section.

Substitution of equation (152) in equation (151) along with present radiometer values yields

$$\Delta T = 1870 \sqrt{\frac{2\gamma}{B_{SI} N T_o}} = 16.1696 \times 10^3 \sqrt{\frac{\gamma}{B_{SI} N}} \tag{153}$$

where the value $T_o = 26.7496$ ms was used. For different values of N, the results of equation (153) are summarized below.

N = 2

$$\Delta T = \frac{6.725 \times 10^3}{\sqrt{B_{SI}}} \tag{154}$$

N = 4

$$\Delta T = \frac{5.225 \times 10^3}{\sqrt{B_{SI}}} \tag{155}$$

N = 8

$$\Delta T = \frac{3.871 \times 10^3}{\sqrt{B_{SI}}} \tag{156}$$

N = 16

$$\Delta T = \frac{2.799 \times 10^3}{\sqrt{B_{SI}}} \tag{157}$$

N = 32

$$\Delta T = \frac{2 \times 10^3}{\sqrt{B_{SI}}} \tag{158}$$

N = 64

$$\Delta T = \frac{1.422}{\sqrt{B_{SI}}} \tag{159}$$

The ΔT values for different bandwidths were computed and are listed in table 1. Along with the values of ΔT, it is also necessary to determine the length of time required for a measurement. The total measurement time τ_M can be represented as the sum of two components of the form:

$$\tau_M = \tau + \tau_s \tag{160}$$

The quantity τ represents the time required to perform the post-loop algorithm and is simply $\tau = NT_o$ as previously discussed. On the other hand, τ_s is the settling time of the loop, and its value depends on the exact criteria of final value closeness chosen for the loop.

The following arbitrary but reasonable criterion was employed for defining the settling time of the loop. The buildup of the output estimate of the loop on a continuous-time basis would be of the form

$$y(t) = C_1(T_B - T_A)\ (1 - \varepsilon^{-50t}) \tag{161}$$

where C_1 is a constant. The error Δy based on a finite settling time is

$$\Delta y = C_1(T_B - T_A)\varepsilon^{-50t} \tag{162}$$

A worst-case value of $T_B - T_A = 308$ was selected. The time τ_s was then calculated such that the error was no greater than $\Delta T/10$; i.e., the settling time error could be no greater than 10 percent of the fluctuation error. This criterion results in the following value for τ_s as a function of ΔT.

$$\tau_s = \frac{1}{50} \ln \frac{3080}{\Delta T} \tag{163}$$

These data are also tabulated in table 1 along with the calculated values of the total measurement time.

SIMULATION OF PROPOSED DESIGN

The proposed system was simulated on the digital computer using Advanced Continuous System Language (ACSL) and some special programs that were developed earlier under this and a previous contract. The actual programs have been described in some earlier publications (refs. 1 and 2).

Because it would consume far too much computer time to simulate the radiometer with the actual bandwidths employed in the real-life system, a decision was made use a simulated input statistical bandwidth of $1/(2)^8 = 1/256$ of the smallest RF bandwidth. The resulting simulation bandwidth is then 20 MHz/256 = 78.125 kHz. The reason for this seemingly odd choice will now be explained. Since the sensitivity of the measurement varies as $1/\sqrt{B_{SI}}$, the ΔT of the simulation is $\sqrt{256} = 16$ times the corresponding value of the actual design at the smallest bandwidth. A factor of 16 corresponds to 4 bits in a binary representation. While the actual system will employ 12-bit words, it was desired in the simulation to have quantization effects appear in the same relative level as they would in the final design. This could then be readily achieved by employing an 8-bit A/D converter and a 256-step down-counter for the noise-injection counter in the simulation. Thus, in the simulation, the relative quantization error as compared to the ΔT level would be in the same proportion as for the final design.

Even with the scaling employed, the computer simulations were quite expensive, and only a limited number were used. Nevertheless, the results obtained were quite good, and they verify the predicted behavior quite well.

The results of four separate runs with all post-loop outputs are tabulated in tables 2 through 7. In interpreting these results, bear in mind that the limited number of runs coupled with the dynamic nature

of the statistical parameters result in some high statistical variations from run to run. However, the general trends and averages here are most significant in establishing the validity of the concept.

In each of the tables, the following parameters are tabulated:

"time" = value of time at which averages are computed.

temperature estimates 1 - 4 = the tabulated results obtained at the times listed. The input temperature is T_A = 100 K. The output is scaled so as to read $0.99(T_B - T_A)$ = 205.92 K, which would be the ideal value.

$\bar{y}_N$ = estimate of mean value of process obtained by an ensemble average for the four runs

s_{y_N} = estimate of standard deviation of process

σ_{y_N} = theoretical predicted value of standard deviation obtained using results of preceding section

$\hat{\bar{y}}_N$ = mean value of estimated means

$\hat{s}_{y_N}$ = mean value of estimated standard deviations

Table 2 provides a tabulation of the various data for $y_2(n)$, i.e., the estimate based on two post-loop samples. Note that the mean of the standard deviations is 23.99 K, which compares favorably with the theoretical value of 24.06 K.

As N increases, the statistical dependency between averages performed at different values of time increases so that estimations of the values down the column decrease in effectiveness. In other words, the greater the resolution of the estimate itself, the less one is able to assess the accuracy of the resolution.

Table 3 provides a tabulation of the results for $y_4(n)$. The mean of the standard deviations is 17.75 K compared with a predicted value of 18.69 K. The values given in tables 4 through 7 provide similar results for $y_8(n)$, $y_{16}(n)$, $y_{32}(n)$, and $y_{64}(n)$ respectively.

The results are illustrated graphically in figure 36.

APPENDIX

ANALYSIS OF CLOSED LOOP NETWORK AND NOTCH FILTER

by

John M. Jeffords

Old Dominion University

Electrical Engineering Department

INTRODUCTION

Old Dominion University and NASA/Langley Research Center are involved in an effort to develop design techniques for improved microwave radiometers. This report documents part of the analysis performed on circuits used to model a portion of the radiometer system in support of the continuing design effort.

A microwave radiometer is a receiver used to estimate the mean value of a noise signal in the presence of background thermal noise. Although microwave radiometers exist in a variety of configurations with different complexities, sensitivities, and accuracies, the current interest of this effort is the noise-injection feedback system. In this configuration, the output of a controlled noise source is added to the input noise and the sum is compared to a stable reference noise. Feedback is used to adjust the controlled noise source so that a balance is achieved. The input noise is then the difference between the known reference noise and the output of the controlled noise source.

Although digital signal processing is contemplated for the microwave radiometers to be developed, a better understanding of the current analog systems was desired. The current system evolved through a combination of both analytical and empirical techniques. An analysis of this system provides a baseline upon which future design can be established.

Although the actual microwave radiometer involves the interaction of a number of random processes, the control mechanism of the feedback loop can be modeled by a simpler "deterministic" form which approximates the loop operation at very low frequencies.

STATEMENT OF PROBLEM

The specific objectives of this study were to:

1. Determine the optimum value of damping factor for the loop to minimize the product of noise bandwidth and settling time.

2. Extend the concept of settling time as usually given in books on control theory to include a more general criterion for precision-bounded measurements.

3. Determine the relative sensitivity of the loop to changes in the open-loop gain factor, particularly in regard to the error.

4. Investigate the use of a lead time constant as it affects error and sensitivity of the loop.

5. Evaluate the performance of a notch filter.

GENERAL APPROACH

Loop Analysis

Figure A-1 is the block diagram of the closed-loop, noise-injection, feedback deterministic radiometer model upon which this analysis is based (ref. 1). For analysis purposes, this block diagram was simplified to the block diagram of figure A-2 in which Boltzmann's constant, the square-law detector constant, the gains of the RF and AF amplifiers, the Dicke constant, and the gains of the integrator and the lead-lag network have all been combined into K_1, and the gains of the directional coupler and isolator and the conversion factors associated with the noise diode have been combined into K_2.

A basic measure of system performance used in the evaluation was the response of the system to a unit step input. If such an input is applied to the system of figure A-2, some steady-state output will eventually be reached as indicated in figure A-3. If we define settling time, t_s, as the time required for the output to reach and remain within some arbitrary percentage of the final value, settling time can be used as a measure of system performance. For this evaluation, the settling time was defined as the time after which the output would not deviate from the final value by more than 0.01 percent.

The noise-equivalent bandwidth, B_N, of a system with transfer function $H(f)$, is the bandwidth of an ideal filter with the same midband

gain, H_o, as H(f), and which passes the same average noise power as H(f) when white noise is applied as its input. The standard definition of B_N is

$$B_N = \frac{1}{H_o^2} \int_o^\infty |H(f)|^2 \, df \tag{A-1}$$

To determine the noise-equivalent bandwidth of the system of figure A-2, temporarily use p as the independent variable of the transfer function. Then, H(p) is given by

$$H(p) = \frac{\frac{1}{K_2}(1 + T_2 P)}{1 + \left(\frac{1 + K_1 K_2 T_2}{K_1 K_2}\right) p + \frac{T_1}{K_1 K_2} p^2}$$

$$= \frac{\frac{1}{K_2}\left(1 + \omega_o T_2 \frac{p}{\omega_o}\right)}{1 + \frac{2\zeta}{\omega_o} p + \left(\frac{p}{\omega_o}\right)^2} \tag{A-2}$$

where

$$\frac{2\zeta}{\omega_o} = \frac{1 + K_1 K_2 T_2}{K_1 K_2} \quad \text{and} \quad \omega_o^2 = \frac{K_1 K_2}{T_1}$$

Making the change of variable, $s = p/\omega_o$,

$$H(s) = \frac{\frac{1}{K_2}(1 + \omega_o T_2 s)}{1 + 2\zeta s + s^2} \tag{A-3}$$

Evaluating equation (A-1) for this transfer function,

$$B_N = \frac{1 + (\omega_o T_2)^2}{8\zeta} \tag{A-4}$$

where B_N is a measure of the average noise power that will be present in the output of the system when white noise is present at the input.

In general, as the parameters of the system of figure A-2 are varied, both B_N and t_s will change. Although optimum performance involves minimizing both B_N and t_s, parameter values which minimize B_N tend to make t_s large, and vice versa. Therefore the product of B_N and t_s was selected as a performance criterion.

The underdamped, critically damped, and overdamped responses to the system of figure A-2 to a unit step input are given by equations (A-5), (A-6) and (A-7) respectively. In these equations, the actual unit step response is $y_1(t)$ where $y(t) = K_2 y_1(t)$.

Underdamped response

$$y(t) = 1 - Ae^{-\zeta t} \sin\left(\sqrt{1 - \zeta^2}\, t + \Theta\right) \tag{A-5}$$

where

$$A = \sqrt{\frac{(\zeta - \omega_o T_2)^2}{1 - \zeta^2} + 1}$$

and

$$\Theta = \tan^{-1}\left(\frac{\sqrt{1 - \zeta^2}}{\zeta - \omega_o T_2}\right)$$

Critically damped response

$$y(t) = 1 - \left[(1 - \omega_o T_2)t + 1\right] e^{-t} \tag{A-6}$$

Overdamped response

$$y(t) = 1 - Be^{-\zeta t} \sinh\left(\sqrt{\zeta^2 - 1}\, t + \phi\right) \tag{A-7}$$

where

$$B = \sqrt{\frac{(\zeta - \omega_o T_2)^2}{\zeta^2 - 1}} - 1$$

and

$$\phi = \tanh^{-1}\left(\frac{\sqrt{\zeta^2 - 1}}{\zeta - \omega_o T_2}\right)$$

Figure A-4 indicates how the settling time was determined for the underdamped case where the overshoot exceeds the target percentage of deviation (figure A-4a), the underdamped case where the overshoot is less than the target percentage of deviation (figure A-4b), and the critically damped and overdamped cases (figure A-4c).

Since both B_N and t_s are functions of the damping factor, ζ, changes in the damping factor can be expected to change the $B_N t_s$ product. If the per unit sensitivity of damping factor to K_L is defined as

$$S^{\zeta}_{K_L} = \frac{\frac{\Delta\zeta}{\zeta}}{\frac{\Delta K_L}{K_L}} \approx \frac{\partial\zeta}{\partial K_L} \frac{K_L}{\zeta} \tag{A-8}$$

where $K_L = K_1K_2$, the sensitivity of damping factor to changes in loop gain for the system of figure A-2 is

$$S_{K_L}^{\zeta} \approx -\frac{1}{2} \quad \frac{1 - K_L T_2}{1 + K_L T_2} \tag{A-9}$$

which can be expressed as

$$S_{K_L}^{\zeta} \approx -\frac{1}{2} \quad \frac{\zeta - \omega_o T_2}{\zeta} \tag{A-10}$$

Maximum overshoot and the time at which it occurs for the underdamped case were evaluated by setting the partial derivative of $y(t)$ with respect to t equal to zero and solving the resulting equation for t. The result is equation (A-11). This value of t is substituted into the expression for $1-y(t)$ to obtain the maximum overshoot of equation (A-17).

$$t_{max} = \frac{1}{\sqrt{1 - \zeta^2}} \left[\tan^{-1} \left(\frac{\sqrt{1 - p^2}\ \omega_o T_2}{\zeta \omega_o T_2 - 1} \right) + n\pi \right] \tag{A-11}$$

$$n = \begin{cases} 0 & \zeta\omega_o T_2 \geq 1 \\ 1 & \zeta\omega_o T_2 \leq 1 \end{cases}$$

$$\varepsilon_{max} = \left\{ \cos \sqrt{1 - \zeta^2}\ t_{max} + \frac{\zeta - \omega_o T_2}{\sqrt{1 - \zeta^2}} \sin \sqrt{1 - \zeta^2}\ t_{max} \right\} e^{-\zeta t_{max}} \tag{A-12}$$

Defining the error as $1-y(t)$, the per unit sensitivity of the error to changes in K_1 can be evaluated. Define the per unit sensitivity of the error to changes in K_1 as

$$S^{\varepsilon}_{K_1} = \frac{\frac{\Delta\varepsilon}{\varepsilon}}{\frac{\Delta K_1}{K_1}} \approx \frac{\partial\varepsilon}{\partial K_1} \frac{K_1}{\varepsilon} \tag{A-13}$$

By the chain rule for partial derivatives, this can be expressed as

$$S^{\varepsilon}_{K_1} = \frac{\partial\varepsilon}{\partial\zeta} \frac{\partial\zeta}{\partial K_1} \frac{K_1}{\varepsilon} \tag{A-14}$$

But

$$\frac{\partial\varepsilon}{\partial\zeta} = e^{-\zeta t} \left\{ - \frac{(1 - \zeta\omega_o T_2)}{1 - \zeta^2} t \cos\sqrt{1 - \zeta^2}t + \left[\frac{\omega_o T_2 t}{\sqrt{1 - \zeta^2}} + \frac{1 - \zeta\omega_o T_2}{(1 - \zeta^2)^{3/2}} \right] \cdot \sin\sqrt{1 - \zeta^2}t \right\} \tag{A-15}$$

so that

$$S^{\varepsilon}_{K_1} = - \frac{2\zeta - \omega_o T_2}{2} \frac{\frac{-(1 - \zeta\omega_o T_2)}{1 - \zeta^2} t \cos\sqrt{1 - \zeta^2}t + \left[\frac{\omega_o T_2 t}{\sqrt{1 - \zeta^2}} + \frac{1 - \zeta\omega_o T_2}{(1 - \zeta^2)^{3/2}} \right] \sin\sqrt{1 - \zeta^2}t}{\cos\sqrt{1 - \zeta^2}t + \frac{\zeta - \omega_o T_2}{\sqrt{1 - \zeta^2}} \sin\sqrt{1 - \zeta^2}t} \tag{A-16}$$

Notch Filter Analysis

Consider a filter with transfer function

$$H(s) = \frac{s^2 + \omega_o^2}{s^2 + 2\zeta\omega_o s + \omega_o^2} \tag{A-17}$$

After making the substitution $s = j\omega$, this transfer function can be put in the following form:

$$H(f) = \frac{1}{1 + j\dfrac{2\zeta(f/f_o)}{1 - (f/f_o)^2}} \tag{A-18}$$

The half-power points for this function occur when

$$\frac{2\zeta(f/f_o)}{1 - (f/f_o)^2} = \pm 1 \tag{A-19}$$

so that for positive frequencies, the half-power points are at the following frequencies:

$$f_2 = f_o\left(\zeta + \sqrt{\zeta^2 + 1}\right)$$

$$f_1 = f_o\left(-\zeta + \sqrt{\zeta^2 + 1}\right) \tag{A-20}$$

the bandwidth of the filter, $BW = f_2 - f_1$, is then

$$BW = 2\zeta f_o \tag{A-21}$$

The response of this filter to a unit step input is

$$y(t) = 1 - \left[\frac{2\zeta}{\sqrt{1 - \zeta^2}} \sin\left(\sqrt{1 - \zeta^2}\ \omega_o t\right)\right] e^{-\zeta\omega_o t} \tag{A-22}$$

for the underdamped case.

Let

$$\varepsilon = \frac{2\zeta}{\sqrt{1 - \zeta^2}} \sin\left(\sqrt{1 - \zeta^2}\, \omega_o t\right) e^{-\zeta\omega_o t} \tag{A-23}$$

be the error. For the underdamped case this error will have a maximum value when

$$t = \frac{1}{\omega_o\sqrt{1 - \zeta^2}} \tan^{-1}\left(\frac{\sqrt{1 - \zeta^2}}{\zeta}\right) \tag{A-24}$$

as indicated in figure A-5a, after which the error will have a series of peaks of alternating sign and decreasing magnitude. Consider the first negative maximum of the error. Because of the exponential factor in the expression for the error, no succeeding maxima or minima will exceed it in magnitude, so it represents the maximum overshoot of the step response, the maximum amount by which the output exceeds the final value of the output, although it is not the largest error. In figure A-5a, the settling time t_1 is the time after which the error never exceeds the maximum overshoot.

For the critically damped and overdamped cases, the response is as indicated in figure A-5b.

PRESENTATION OF RESULTS

$B_N t_s$ Product

In figure A-6, the product of the noise-equivalent bandwidth B_N and the settling time t_s is plotted versus the damping factor ζ for five values of lead time constant. The simple lag network, in which the lead time constant T_2 is zero, appears best from a consideration of just the $B_N t_s$ product, since it not only has the lowest values, but

the values remain relatively constant over a wide range of damping factor. The abrupt decreases in the $B_N t_s$ product that are apparent in the curves for $\omega_o T_2 = 2.0$ and $\omega_o T_2 = 1.5$ occur when

$$\zeta = \frac{1 + (\omega_o T_2)^2}{2\omega_o T_2}$$

Sensitivity of Damping Factor to K_L Changes

The sensitivity of damping factor to changes in the loop gain is plotted as a function of damping factor for five values of lead time constant in figure A-7.

Sensitivity of Error to K_1 Changes

Figure A-8 is a plot of the sensitivity of the error to changes in the forward gain plotted as a function of time for three lead time constants and for a damping factor of 0.95, the value at which the noise-equivalent bandwidth and settling time product is minimum when the lead time constant is zero.

Damping Factor and Settling Time versus Maximum Overshoot

Figures A-9, A-10, A-11, A-12, and A-13 are plots of damping factor and $\omega_o t_s$ versus maximum overshoot for the underdamped loop, each figure for a different lead time constant. A comparison of the effect of lead time constant on overshoot and the resultant settling time can be obtained from these curves.

Notch Filter Damping Factor and Settling Time

Figure A-14 presents damping factor and settling time as a function of maximum overshoot for the notch filter.

SUMMARY

Loop Analysis

Figures A-6, A-7, and A-8 indicate that as long as loop gain variations are not encountered, the simple lag network provides superior performance as long as damping factors above approximately 0.8 are used. For damping factors in the vicinity of critical damping, which appears to be the logical area of damping factor to operate, $\omega_o T_2 = 1.0$ minimizes the sensitivity of the damping factor to changes in loop gain. Although figure A-8 indicates that the error is still very sensitive to changes in K_1 at most times, this is probably not as serious as it appears at first.

For example, considering the curve of figure A-8 for $\omega_o T_2 = 1.0$, it can be seen that the error is insensitive to changes in K_1 in the vicinity of $\omega_o t = 10.5$. From figure A-11 it can be seen that the maximum overshoot corresponding to a settling time of this value is less than 10^{-6}. Since ω_o can be expected to be on the order of 100 rad/s, this operation would require allowing times on the order of 0.1 s for settling, which is not unreasonable.

Although figure A-6, which is plotted for an error of 10^{-4}, indicates that the simple lag network produces the minimum bandwidth-time product for any damping factor, the sensitivity of the error to changes of loop gain will likely preclude operating the system at minimum settling times. Allowing additional time for settling before taking a measurement will reduce the magnitude of the error. However, so much time may be required that lead compensation may be preferable, even though its minimum bandwidth-time product is higher than that of the simple lag network.

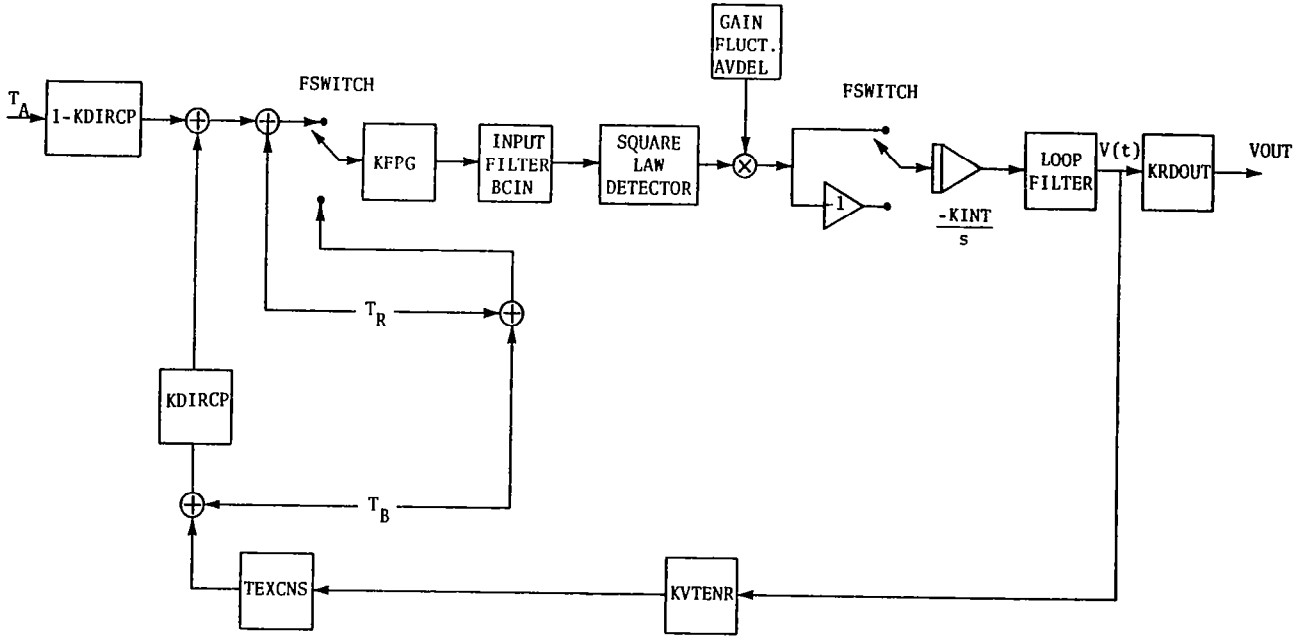

Figure A-1. Block diagram of closed-loop, noise-injection, feedback deterministic radiometer models.

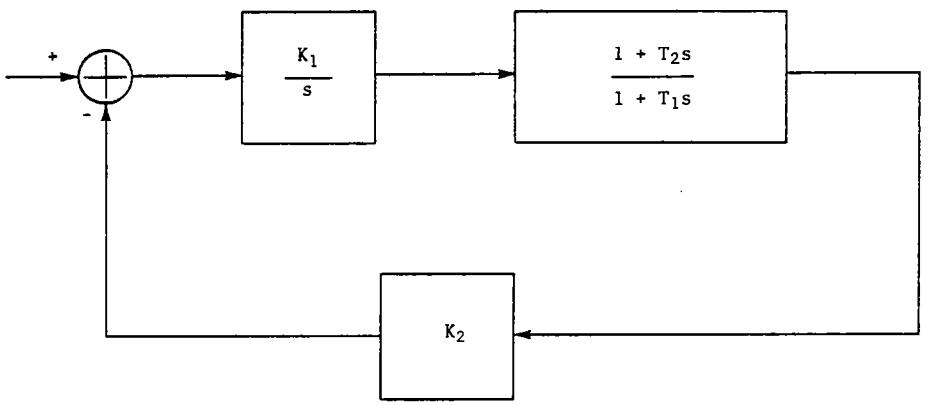

Figure A-2. Block diagram of system analyzed.

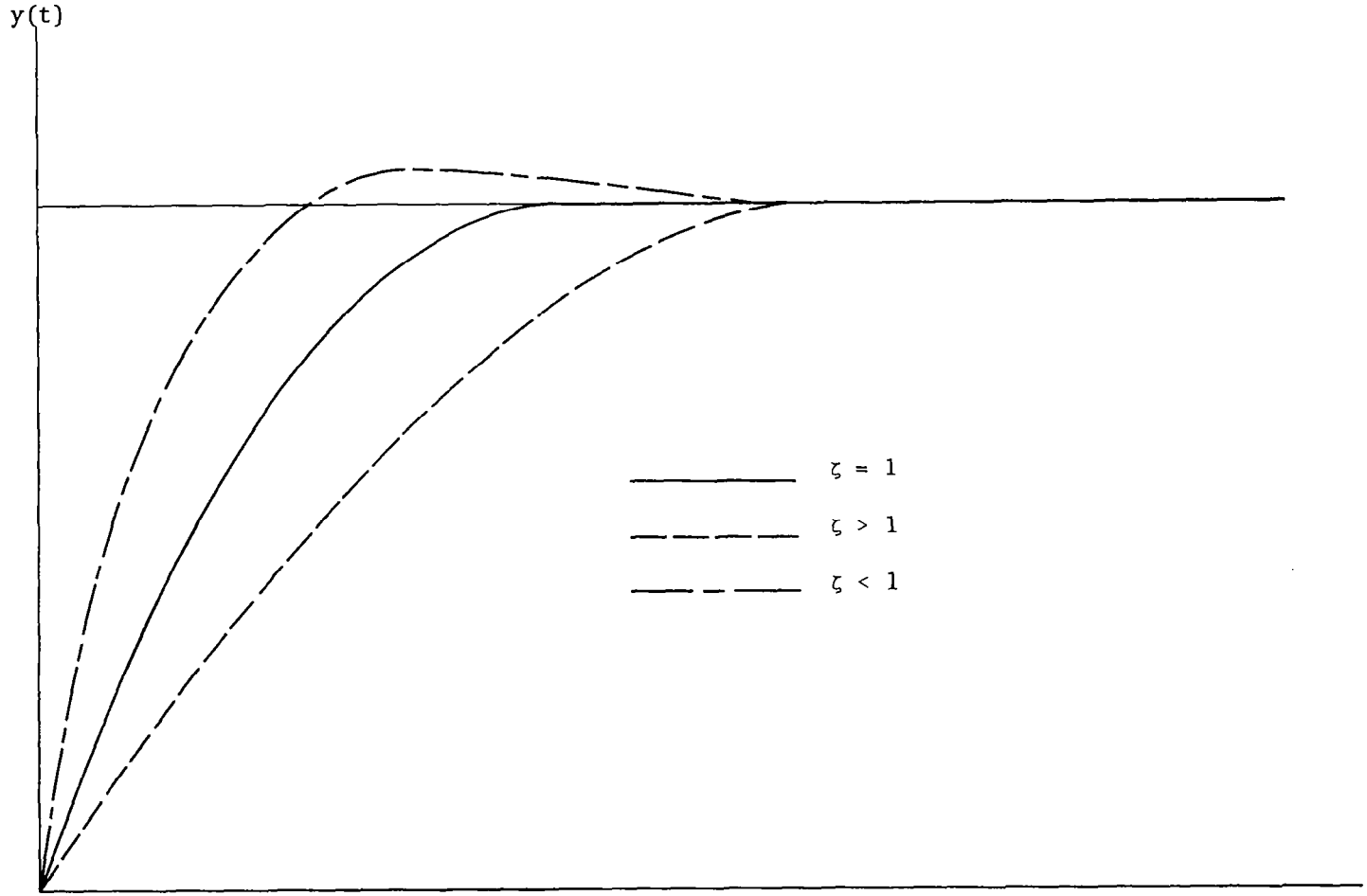

Figure A-3. System step responses.

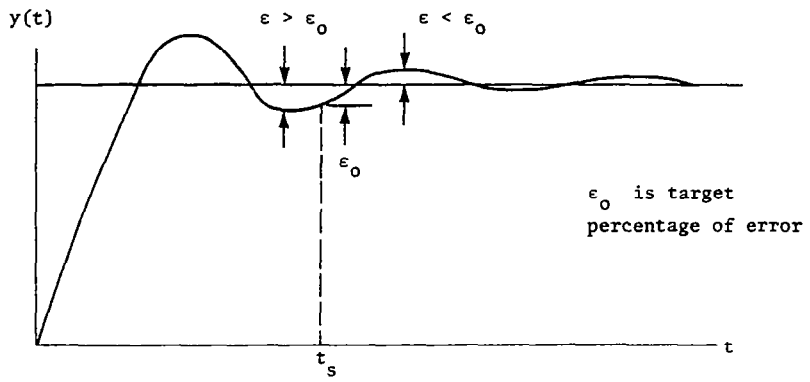

(a) Underdamped: overshoot exceeds target error

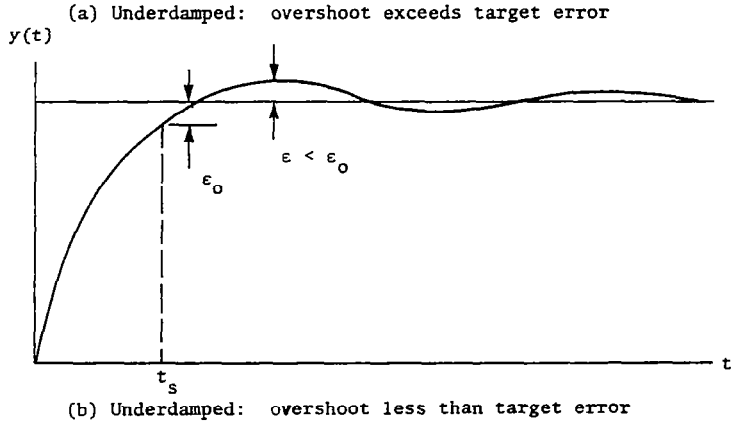

(b) Underdamped: overshoot less than target error

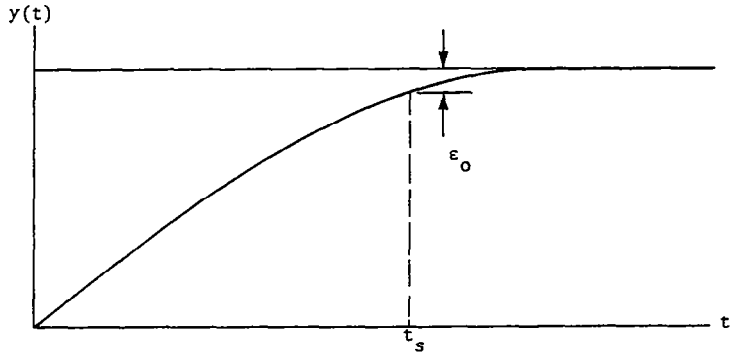

(c) Critically damped and overdamped

Figure A-4. Examples of settling time determination.

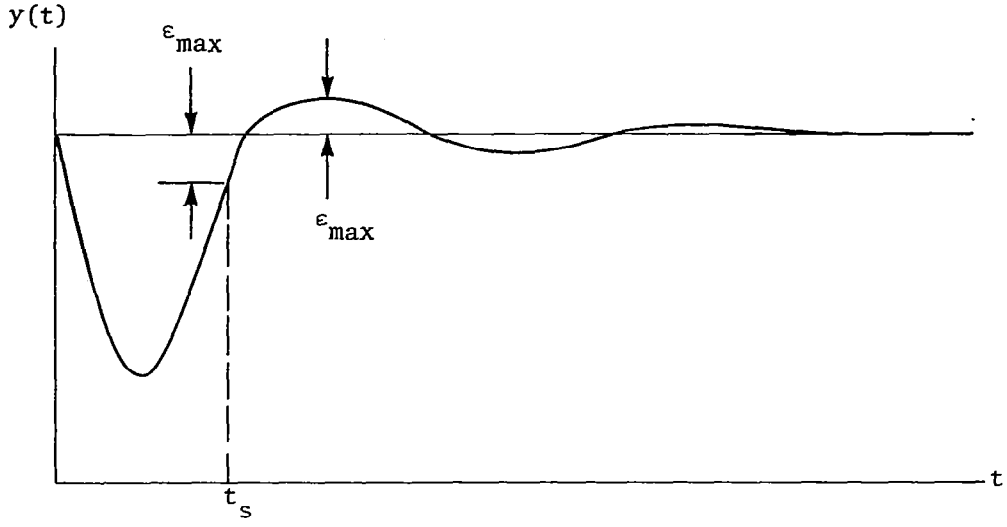

(a) Settling time determination for maximum error curve—underdamped notch filter response.

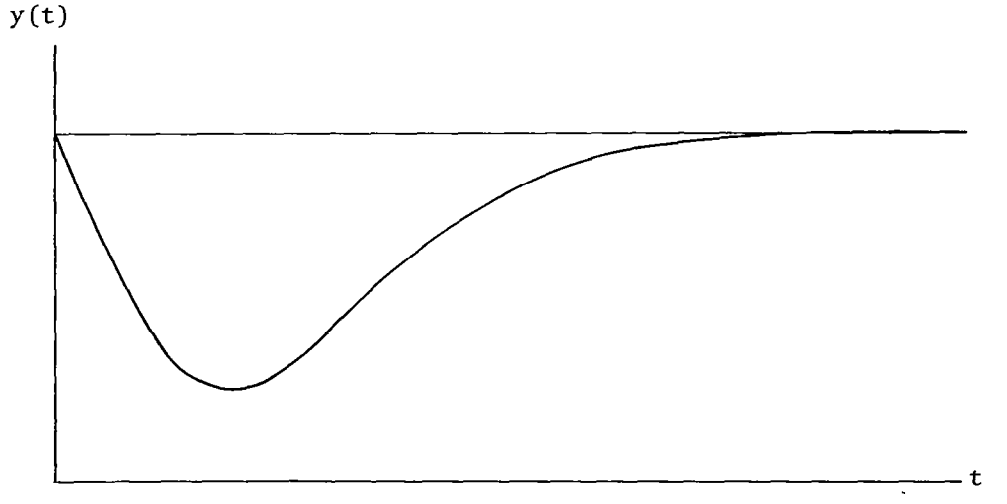

(b) Notch filter response: critically damped and overdamped.

Figure A-5. Notch filter responses.

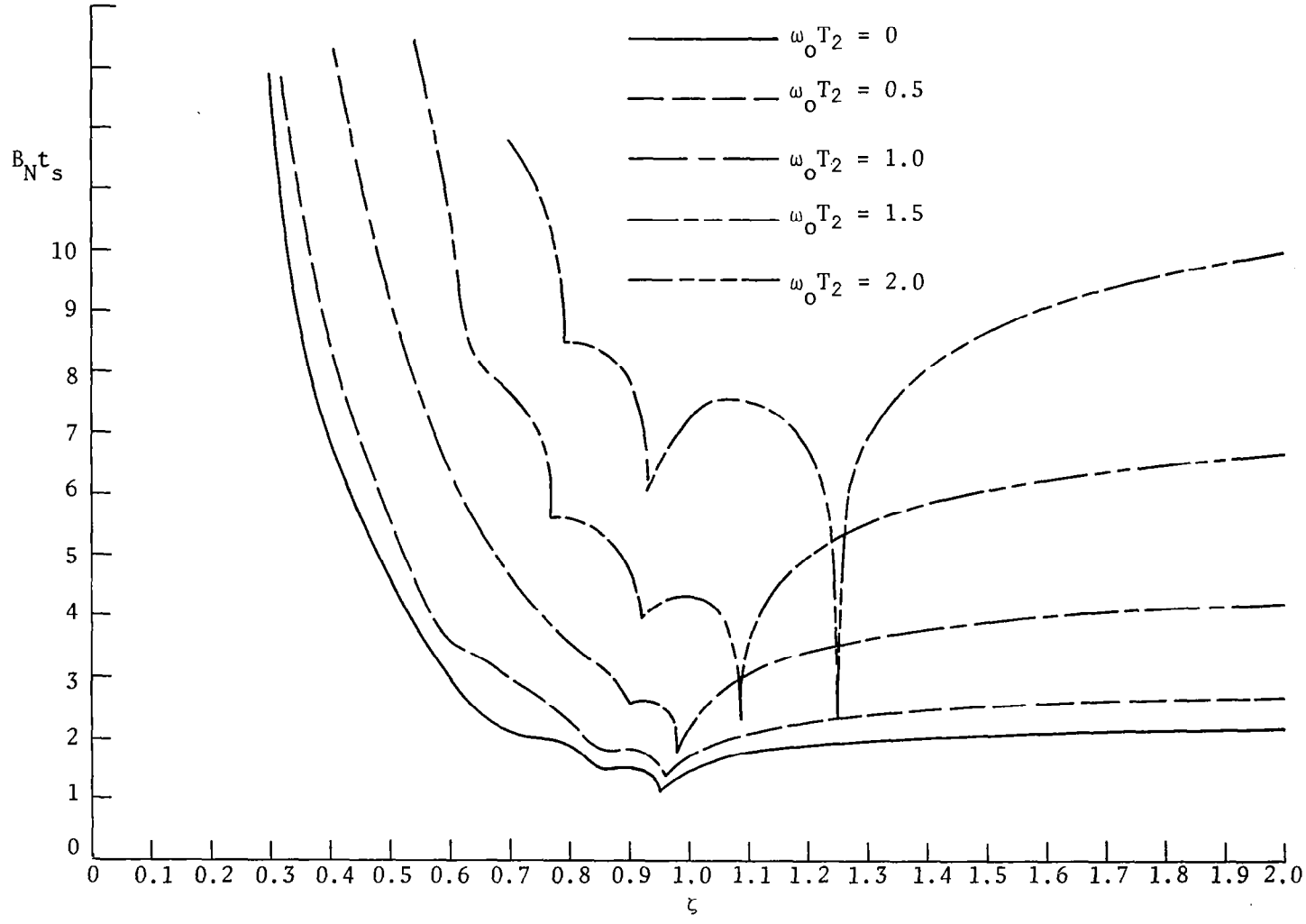

Figure A-6. Product of noise-equivalent bandwidth and settling time plotted versus damping factor and lead time constant.

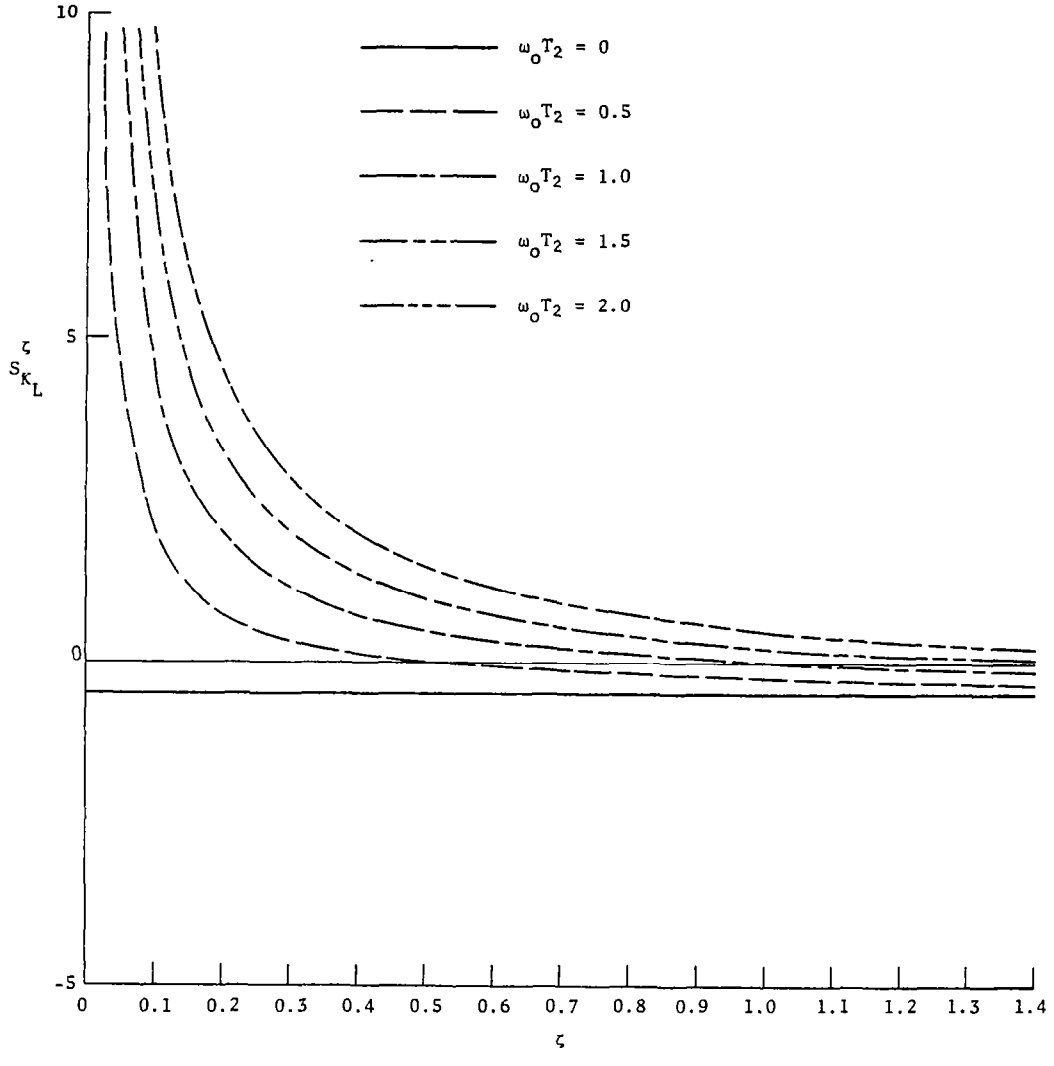

Figure A-7. Sensitivity of damping factor to changes in loop gain as function of damping factor and lead time constant.

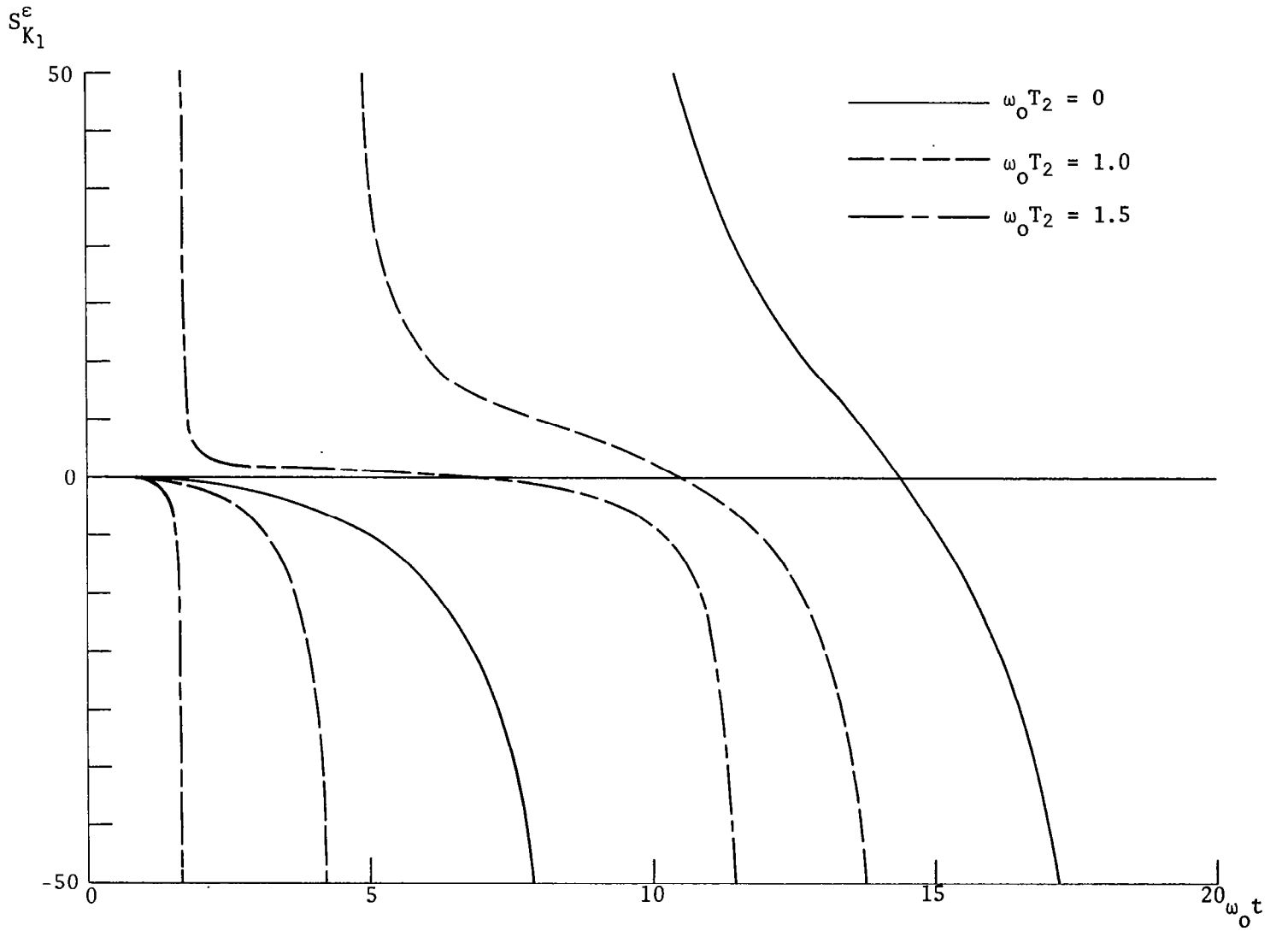

Figure A-8. Sensitivity of error to changes in forward gain as function of lead time constant and time.

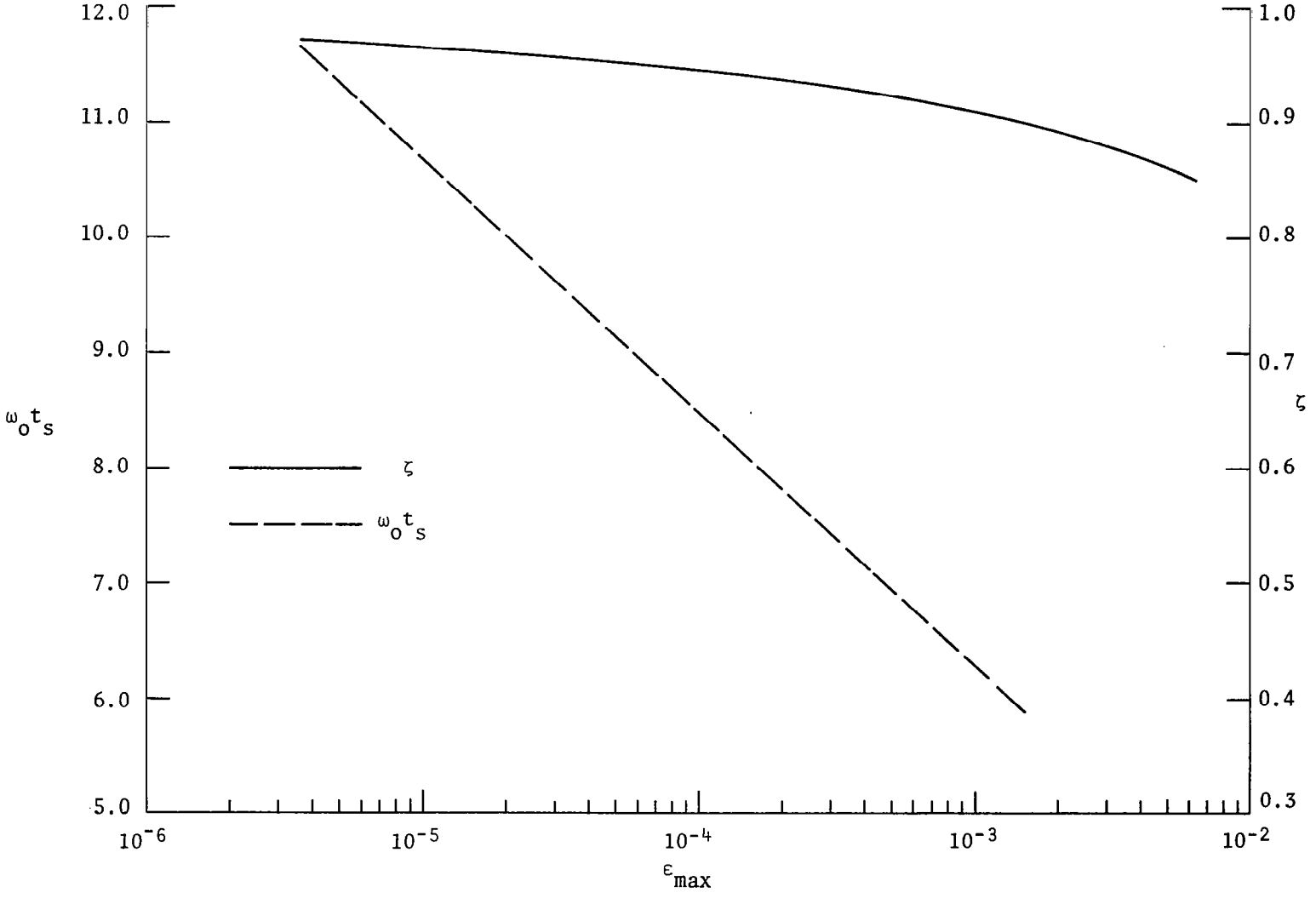

Figure A-9. Damping factor and settling time versus maximum overshoot for $\omega_o T_2 = 0$.

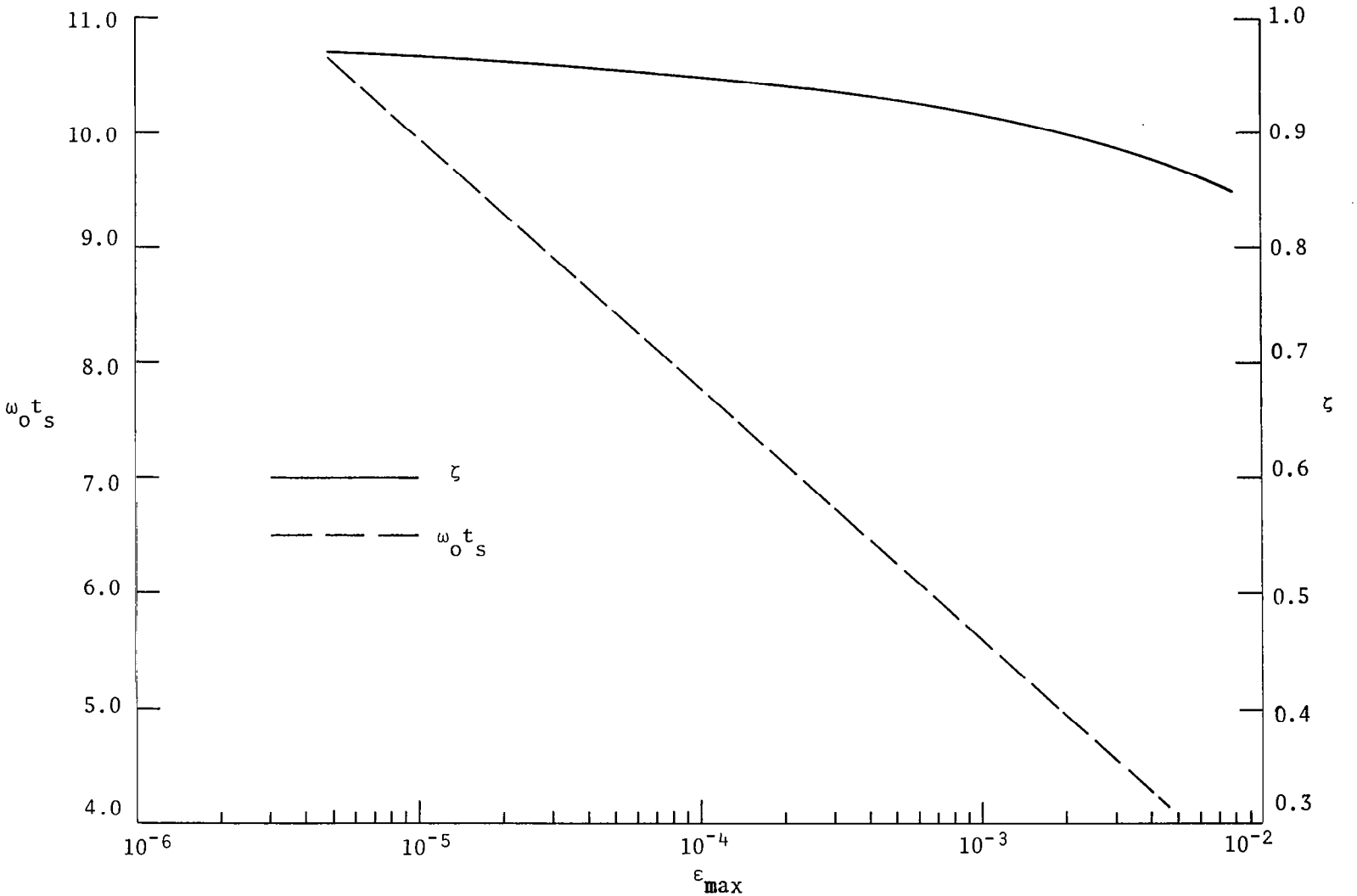

Figure A-10. Damping factor and settling time versus maximum overshoot for $\omega_o T_2 = 0.5$.

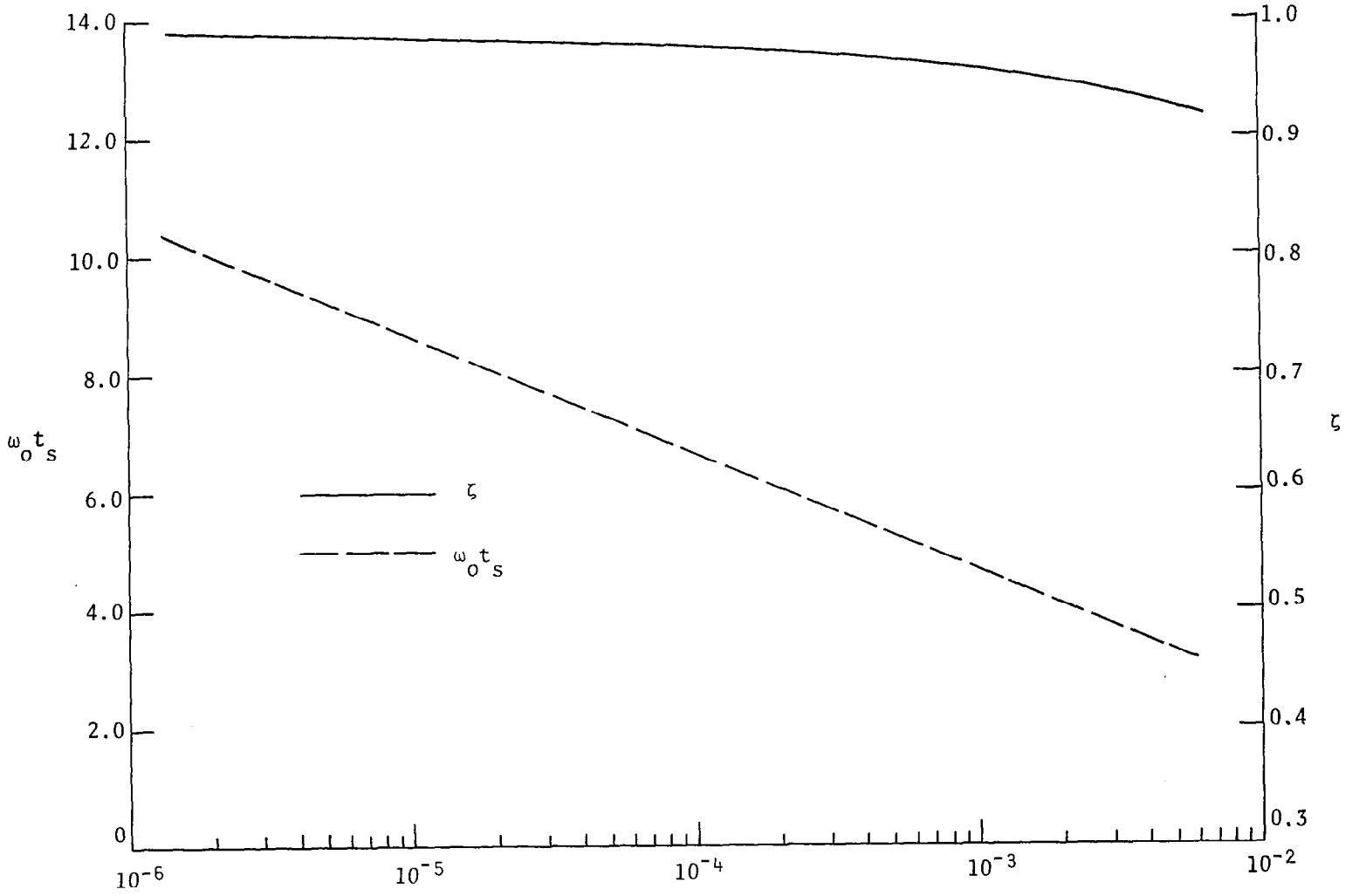

Figure A-11. Damping factor and settling time versus maximum overshoot for $\omega_o T_2 = 1.0$.

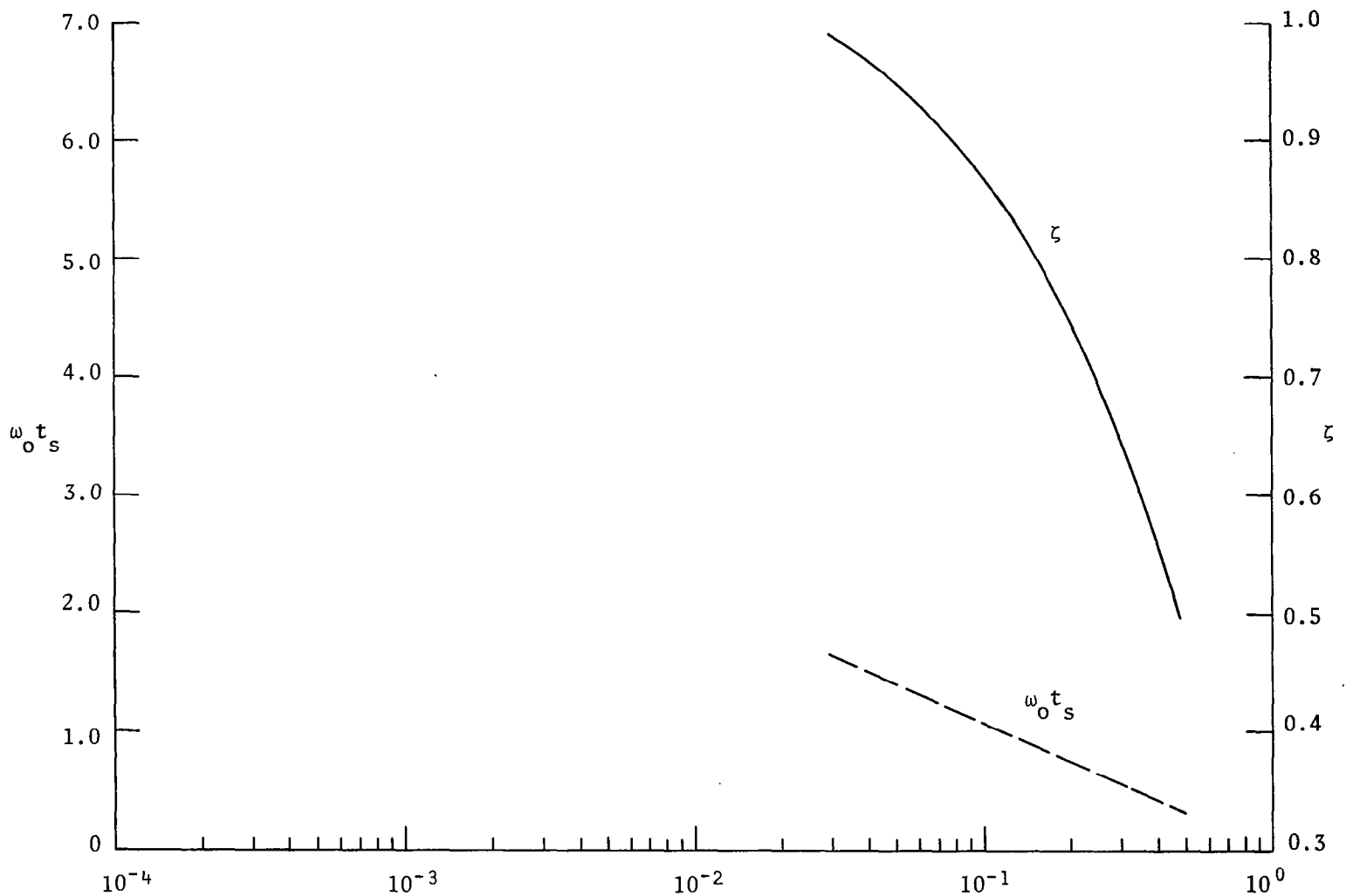

Figure A-12. Damping factor and settling time versus maximum overshoot for $\omega_o T_2 = 1.5$.

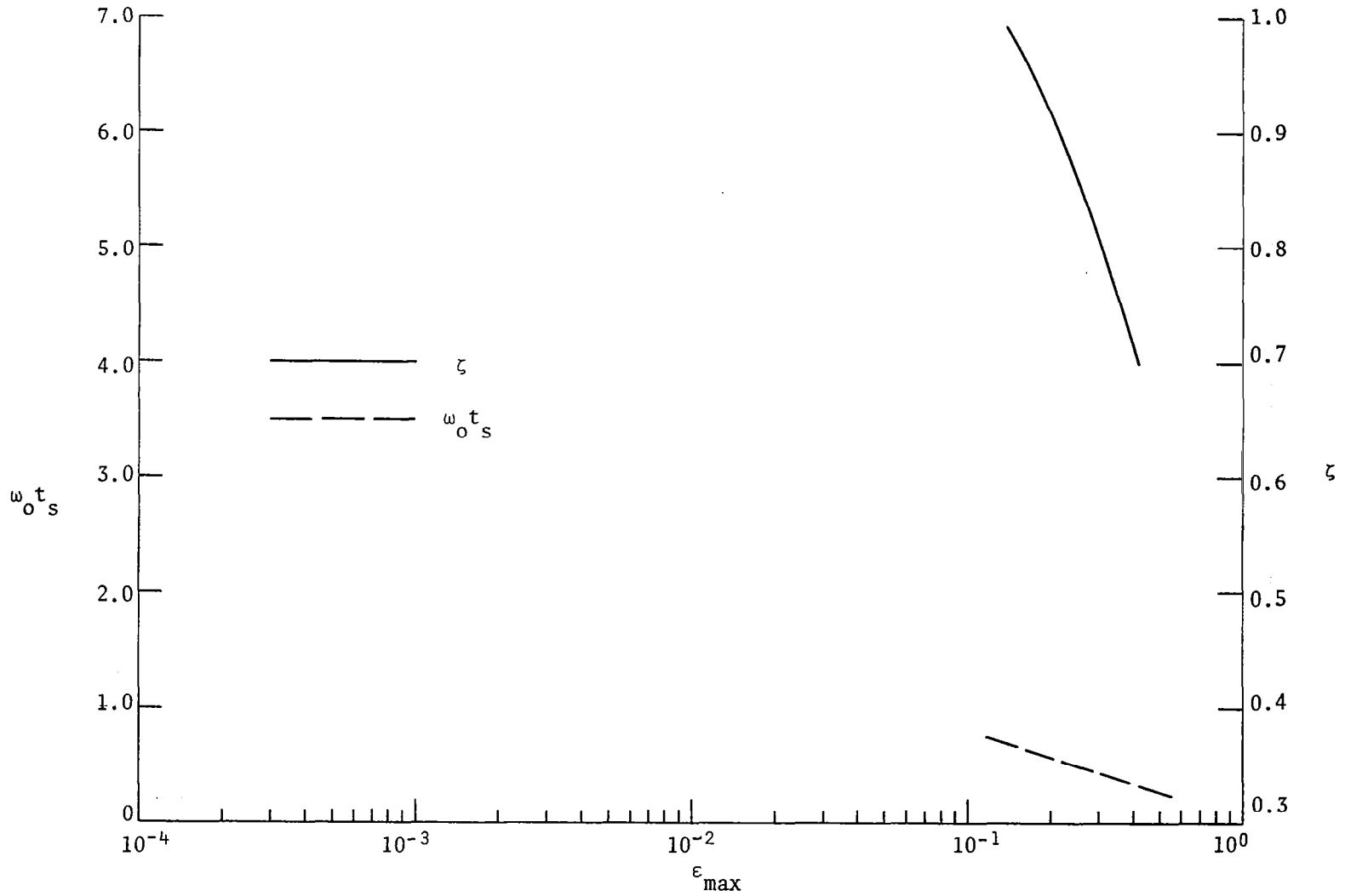

Figure A-13. Damping factor and settling time versus maximum overshoot for $\omega_o T_2 = 2.0$.

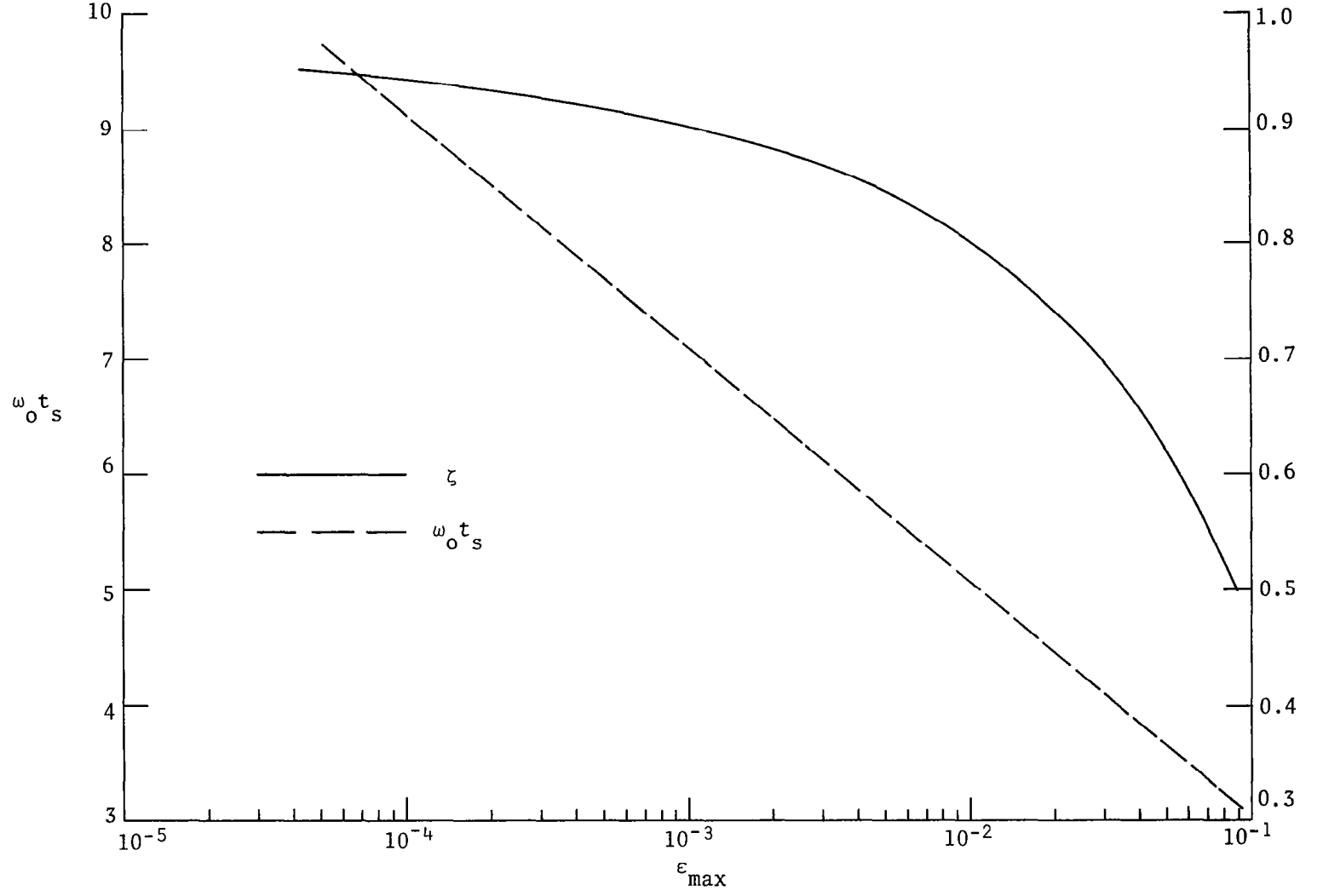

Figure A-14. Damping factor and settling time versus maximum overshoot for the notch filter.

REFERENCES

1. Stanley, W.D.: Digital Simulation of Dynamic Processes in Radiometer Systems. Final Report on NAS1-14193, Task Authorization No. 46. NASA CR-159266, 1980.

2. Stanley, W.D.; Harrington, R.F.; and Lawrence, R.W.: Dynamic Simulation of Random Processes in Radiometers Using CSMP and ACSL. Presented at IEEE SOUTHEASCON Conference (Roanoke, VA), April 1979; also published in Conference Proceedings.

3. Harrington, R.F.; Couch, R.H.; and Fedors, J.C.: An Airborne Remote Sensing 4.5 to 7.2 Gigahertz Stepped Frequency Microwave Radiometer. Presented at the 1979 International Microwave Symposium (Orlando, FL), April-May, 1979; also published in Conference Proceedings.

4. Stanley, W.D.; and Peterson, S.J.: Equivalent Statistical Bandwidths of Conventional Filters. IEEE Trans. Comm., Vol. COM-27, Oct. 1979.

5. Bendat, J.S.; and Piersol, A.G.: Random Data: Analysis and Measurement Procedures, John Wiley and Sons, Inc., 1971.

6. Tiuri, M.E.: Radio Astronomy Receivers. IEEE Trans. Antennas Prop., Vol. AP-12, Dec. 1964, pp. 930-938.

7. Evans, G.; and McLeish, C.W.: RF Radiometer Handbook. Artech House (Dedham, MA), 1977.

8. Dicke, R.H.: The Measurement of Thermal Radiation at Microwave Frequencies. Rev. Sci. Instr., Vol. 17, July 1946, pp. 268-275.

9. Hardy, W.N.; Gray, K.W.; and Love, A.W.: An S-Band Radiometer Design with High Absolute Prevision. IEEE Trans. Microwave Theory and Technique, Vol. MTT-22, Apr. 1974, pp. 382-390.

10. Tretter, S.A.: Introduction to Discrete-Time Signal Processing. John Wiley & Sons, Inc. (NY), 1976.

11. Stanley, W.D.: Digital Signal Processing. Reston Publishing Co. (Reston, VA), 1975.

TABLE 1.- PREDICTED SENSITIVITIES BASED ON NOISE FLUCTUATIONS AND MEASUREMENT TIMES (INCLUDING BOTH PROCESSING AND SETTLING TIMES) FOR PROPOSED DIGITAL SYSTEM.

		N=1	2	4	8	16	32	64
B_{SI} = 20 MHz	τ	26.75 ms	53.5 ms	107 ms	214 ms	428 ms	856 ms	1.712 s
	ΔT	2.096 K	1.504 K	1.168 K	0.866 K	0.626 K	0.447 K	0.318 K
	τ_S	146 ms	153 ms	158 ms	164 ms	170 ms	177 ms	184 ms
	τ_M	173 ms	206.5 ms	265 ms	378 ms	598 ms	1.033 s	1.896 s
B_{SI} = 100 MHz	ΔT	0.938 K	0.672 K	0.523 K	0.387 K	0.280 K	0.200 K	0.142 K
	τ_S	162 ms	168 ms	174 ms	180 ms	186 ms	193 ms	200 ms
	τ_M	189 ms	221.5 ms	281 ms	394 ms	614 ms	1.049 s	1.912 s
B_{SI} = 500 MHz	ΔT	0.419 K	0.301 K	0.234 K	0.173 K	0.125 K	0.0894 K	0.0636 K
	τ_S	178 ms	185 ms	190 ms	196 ms	202 ms	209 ms	216 ms
	τ_M	205 ms	238.5 ms	297 ms	410 ms	630 ms	1.065 s	1.928 s
B_{SI} = 2 GHz	ΔT	0.210 K	0.150 K	0.117 K	0.0866 K	0.0626 K	0.0447 K	0.0318 K
	τ_S	192 ms	199 ms	204 ms	210 ms	216 ms	223 ms	230 ms
	τ_M	219 ms	252.5 ms	311 ms	424 ms	644 ms	1.079 s	1.942 s

TABLE 2.- COMPUTER SIMULATION OF PROPOSED DESIGN WITH TWO POST-LOOP SAMPLES IN AVERAGE. (ALL UNITS EXCEPT TIME ARE EXPRESSED IN KELVIN.)

y_2 SIMULATION							
	Temperature Estimates						
TIME(s)	Run 1	Run 2	Run 3	Run 4	$\bar{y}_2$	s_{y_2}	σ_{y_2}
0.213	216.54	188.11	188.29	248.71	210.41	28.82	24.06
0.320	193.82	180.90	243.18	190.79	202.17	27.89	24.06
0.427	203.17	221.00	196.04	172.97	198.30	19.88	24.06
0.533	166.72	218.59	213.69	177.51	194.13	25.87	24.06
0.640	162.72	201.21	210.12	200.32	193.59	21.05	24.06
0.747	212.08	177.42	207.01	185.71	195.56	16.63	24.06
0.853	196.40	225.45	236.77	147.30	201.48	39.92	24.06
0.960	257.53	222.15	212.35	223.05	228.77	19.78	24.06
1.067	245.77	222.87	186.42	229.46	221.13	25.06	24.06
1.173	158.80	197.65	238.19	190.61	196.31	32.64	24.06
1.280	202.10	213.07	188.74	201.84	201.44	9.95	24.06
1.387	202.28	195.78	219.39	224.02	210.37	13.49	24.06
1.493	196.76	269.65	216.54	197.65	220.15	34.24	24.06
1.600	212.08	178.22	216.90	213.33	205.13	18.06	24.06
1.707	212.80	169.85	170.65	209.95	190.81	23.77	24.06
1.813	198.18	212.00	180.45	161.74	188.09	21.80	24.06
1.920	184.01	239.98	177.06	214.31	203.84	29.02	24.06
					203.63	23.99	
					$\hat{\bar{y}}_2$	$\hat{s}_{y_2}$	

TABLE 3.- COMPUTER SIMULATION OF PROPOSED DESIGN WITH FOUR POST-LOOP SAMPLES IN AVERAGE. (ALL UNITS EXCEPT TIME ARE EXPRESSED IN KELVIN.)

y_4 SIMULATION							
	Temperature Estimates						
TIME(s)	Run 1	Run 2	Run 3	Run 4	$\bar{y}_4$	s_{y_4}	σ_{y_4}
0.213	202.59	211.73	208.70	228.44	212.87	11.06	18.69
0.320	196.85	179.48	240.51	171.67	197.13	30.78	18.69
0.427	198.09	241.05	194.89	184.59	204.66	24.94	18.69
0.533	171.00	222.24	206.20	174.57	194.00	25.62	18.69
0.640	184.59	195.02	188.20	206.83	193.50	24.85	18.69
0.747	211.10	186.15	205.45	180.54	195.81	14.76	18.69
0.853	200.37	205.67	217.48	169.31	198.21	20.55	18.69
0.960	229.19	216.50	205.67	204.15	213.88	11.60	18.69
1.067	231.69	224.20	192.26	224.74	218.22	17.64	18.69
1.173	153.94	211.19	234.36	194.80	198.57	33.89	18.69
1.280	199.70	208.21	208.34	186.33	200.65	10.36	18.69
1.387	203.80	199.74	216.81	201.93	205.57	7.67	18.69
1.493	214.71	217.48	204.91	207.01	211.03	6.02	18.69
1.600	191.23	217.83	217.43	217.83	211.08	13.23	18.69
1.707	190.83	174.44	188.07	211.64	191.25	15.37	18.69
1.813	195.24	211.42	203.93	192.84	200.86	8.50	18.69
1.920	188.96	235.52	178.62	207.90	202.75	24.99	18.69
					202.94	17.75	
					$\hat{\bar{y}}_4$	$\hat{s}_{y_4}$	

TABLE 4.- COMPUTER SIMULATION OF PROPOSED DESIGN WITH EIGHT POST-LOOP SAMPLES IN AVERAGE. (ALL UNITS EXCEPT TIME ARE EXPRESSED IN KELVIN.)

y_8 SIMULATION							
	Temperature Estimates						
TIME(s)	Run 1	Run 2	Run 3	Run 4	$\bar{y}_8$	s_{y_8}	σ_{y_8}
0.320	199.72	195.60	224.61	200.05	205.00	13.23	13.86
0.427	197.47	210.26	217.70	178.13	200.89	17.32	13.86
0.533	184.55	231.64	200.54	179.58	199.08	23.48	13.86
0.640	177.80	208.63	197.20	190.70	193.58	12.87	13.86
0.747	197.85	190.59	196.82	193.68	194.74	3.28	13.86
0.853	205.74	195.91	211.46	174.93	197.01	16.06	13.86
0.960	214.78	211.08	211.57	186.73	206.04	12.98	13.86
1.067	230.44	220.35	198.96	214.45	216.05	13.17	13.86
1.173	192.81	217.70	213.31	209.77	208.40	10.89	13.86
1.280	176.82	209.70	221.35	190.56	199.64	19.80	13.86
1.387	201.75	203.98	212.58	194.13	203.11	7.59	13.86
1.493	209.26	208.61	210.86	204.47	208.30	2.72	13.86
1.600	202.97	217.65	211.17	212.42	211.05	6.08	13.86
1.707	191.03	196.13	202.75	214.74	201.16	10.24	13.86
1.813	193.04	192.93	196.00	202.24	196.05	4.36	13.86
1.920	192.10	223.47	191.28	200.37	201.81	15.02	13.86
					202.62 $\hat{\bar{y}}_8$	11.86 $\hat{s}_{y_8}$	

TABLE 5.- COMPUTER SIMULATION OF PROPOSED DESIGN WITH 16 POST-LOOP SAMPLES IN AVERAGE. (ALL UNITS EXCEPT TIME ARE EXPRESSED IN KELVIN.)

y_{16} SIMULATION							
	Temperature Estimates						
TIME(s)	Run 1	Run 2	Run 3	Run 4	$\bar{y}_{16}$	$s_{y_{16}}$	$\sigma_{y_{16}}$
0.533	192.14	213.62	212.58	189.82	202.04	12.81	10.02
0.640	187.64	209.44	207.45	184.42	197.24	13.03	10.02
0.747	191.20	211.12	198.68	186.63	196.91	10.70	10.02
0.853	191.77	202.27	204.33	182.81	195.30	9.98	10.02
0.960	206.32	200.83	204.20	190.21	200.39	7.15	10.02
1.067	218.09	208.13	205.21	194.69	206.53	9.63	10.02
1.173	203.80	214.39	212.44	198.25	207.22	7.55	10.02
1.280	203.63	215.03	210.16	202.51	207.83	5.87	10.02
1.387	197.28	210.84	212.94	201.95	205.75	7.39	10.02
1.493	193.04	209.16	216.11	197.52	203.96	10.57	10.02
1.600	202.36	210.82	211.87	203.27	207.08	4.96	10.02
1.707	200.14	202.37	206.81	209.60	204.73	4.27	10.02
1.813	198.01	205.29	203.59	207.33	203.56	4.00	10.02
1.920	191.57	209.80	197.01	207.55	201.48	8.65	10.02
					202.86	8.33	
					$\hat{\bar{y}}_{16}$	$\hat{s}_{y_{16}}$	

TABLE 6.- COMPUTER SIMULATION OF PROPOSED DESIGN WITH 32 POST-LOOP SAMPLES IN AVERAGE. (ALL UNITS EXCEPT TIME ARE EXPRESSED IN KELVIN.)

y_{32} SIMULATION							
	Temperature Estimates						
TIME(s)	Run 1	Run 2	Run 3	Run 4	$\bar{y}_{32}$	$s_{y_{32}}$	$\sigma_{y_{32}}$
0.960	199.23	207.23	208.39	190.01	201.22	8.51	7.15
1.067	202.86	208.79	206.33	189.55	201.88	8.57	7.15
1.173	197.50	212.75	205.56	192.44	202.06	8.94	7.15
1.280	197.70	208.65	207.25	192.66	201.57	7.68	7.15
1.387	201.80	205.83	208.57	196.08	203.07	5.43	7.15
1.493	205.56	208.64	210.66	196.10	205.24	6.44	7.15
1.600	203.68	212.60	212.16	200.76	207.30	5.99	7.15
1.707	201.89	208.70	208.48	206.05	206.28	3.16	7.15
1.813	197.64	208.06	208.26	204.64	204.65	4.96	7.15
1.920	192.30	209.48	206.56	202.53	202.72	7.51	7.15
					203.60	6.72	
					$\hat{\bar{y}}_{32}$	$\hat{s}_{y_{32}}$	

TABLE 7.- COMPUTER SIMULATION OF PROPOSED DESIGN WITH 64 POST-LOOP SAMPLES IN AVERAGE. (ALL UNITS EXCEPT TIME ARE EXPRESSED IN KELVIN.)

y_{64} SIMULATION							
	Temperature Estimates						
TIME(s)	Run 1	Run 2	Run 3	Run 4	$\bar{y}_{64}$	$s_{y_{64}}$	$\sigma_{y_{64}}$
1.813	198.43	207.65	208.33	196.04	202.61	6.29	5.09
1.920	197.58	209.13	206.45	197.32	202.62	6.07	5.09
					202.62 $\hat{\bar{y}}_{64}$	6.18 $\hat{s}_{y_{64}}$	

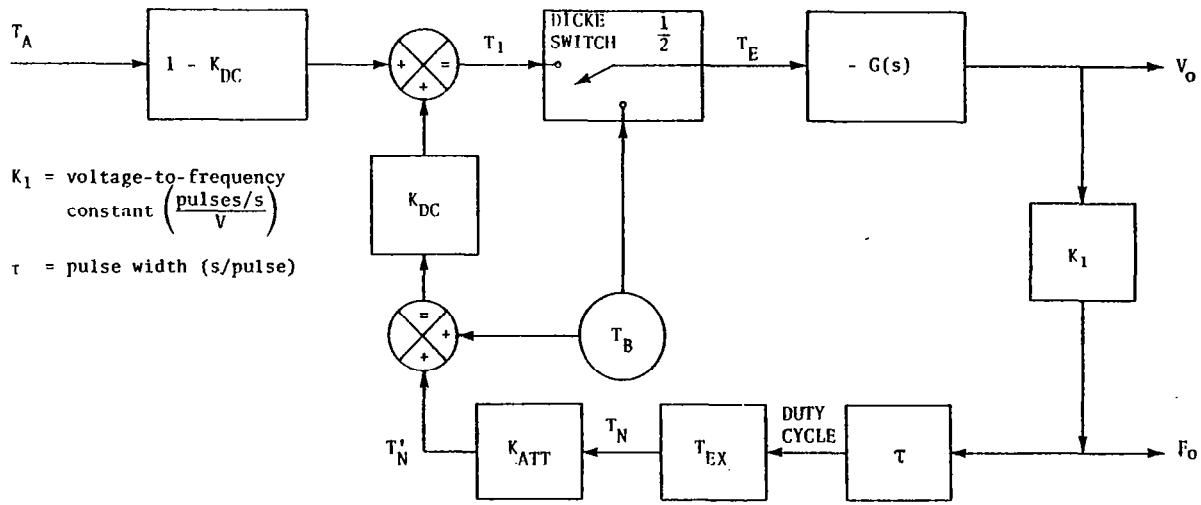

K_1 = voltage-to-frequency constant $\left(\frac{\text{pulses/s}}{\text{V}}\right)$

τ = pulse width (s/pulse)

K_1 = voltage-to-frequency constant $\frac{\text{pulses/s}}{\text{V}}$

τ = pulse width (s/pulse)

$T_1 = (1 - K_{DC})T_A + K_{DC}(T_B + T_N')$

$T_E = \frac{1}{2}(T_1 - T_B)$, $V_o = -GT_E$

$T_N' = K_{ATT}T_{EX}\tau K_1 V_o = \frac{\beta V_o}{K_{DC}}$

$\beta = K_{DC}K_{ATT}T_{EX}\tau K_1$

$$\frac{V_o}{T_B - T_A} = \frac{(1-K_{DC})G/2}{1+G\beta/2}$$

$$\frac{F_o}{T_B - T_A} = \frac{(1-K_{DC})GK_1/2}{1 + G\beta/2}$$

$$\frac{T_E}{T_A - T_B} = \frac{(1-K_{DC})/2}{1 + G\beta/2}$$

Figure 1. Block diagram of control mechanism in feedback noise-injection radiometer.

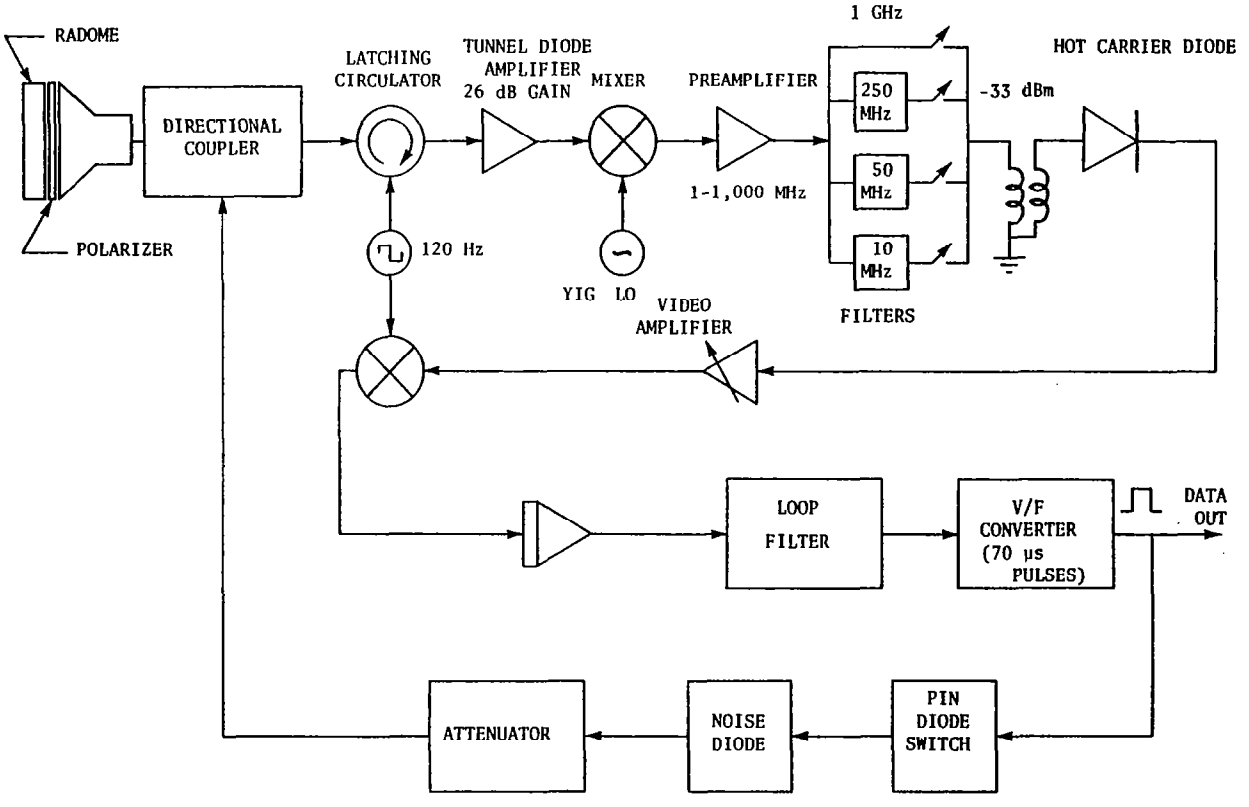

Figure 2. Block diagram of radiometer system used as a reference in this study.

(a)

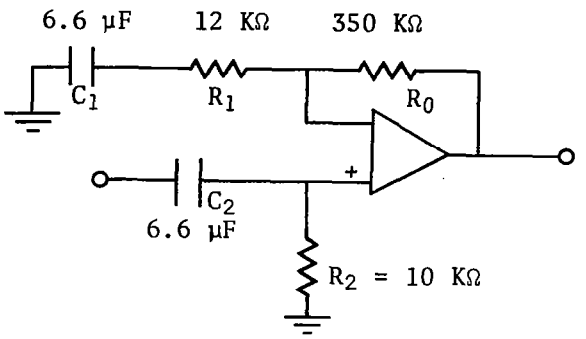

(b)

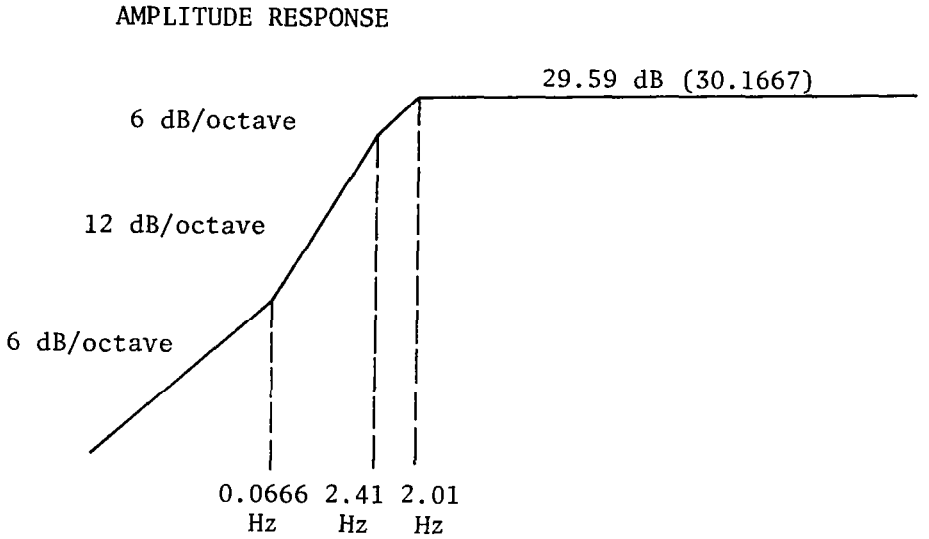

Figure 3. Circuit used for stages IC1 and IC2 and its Bode plot.

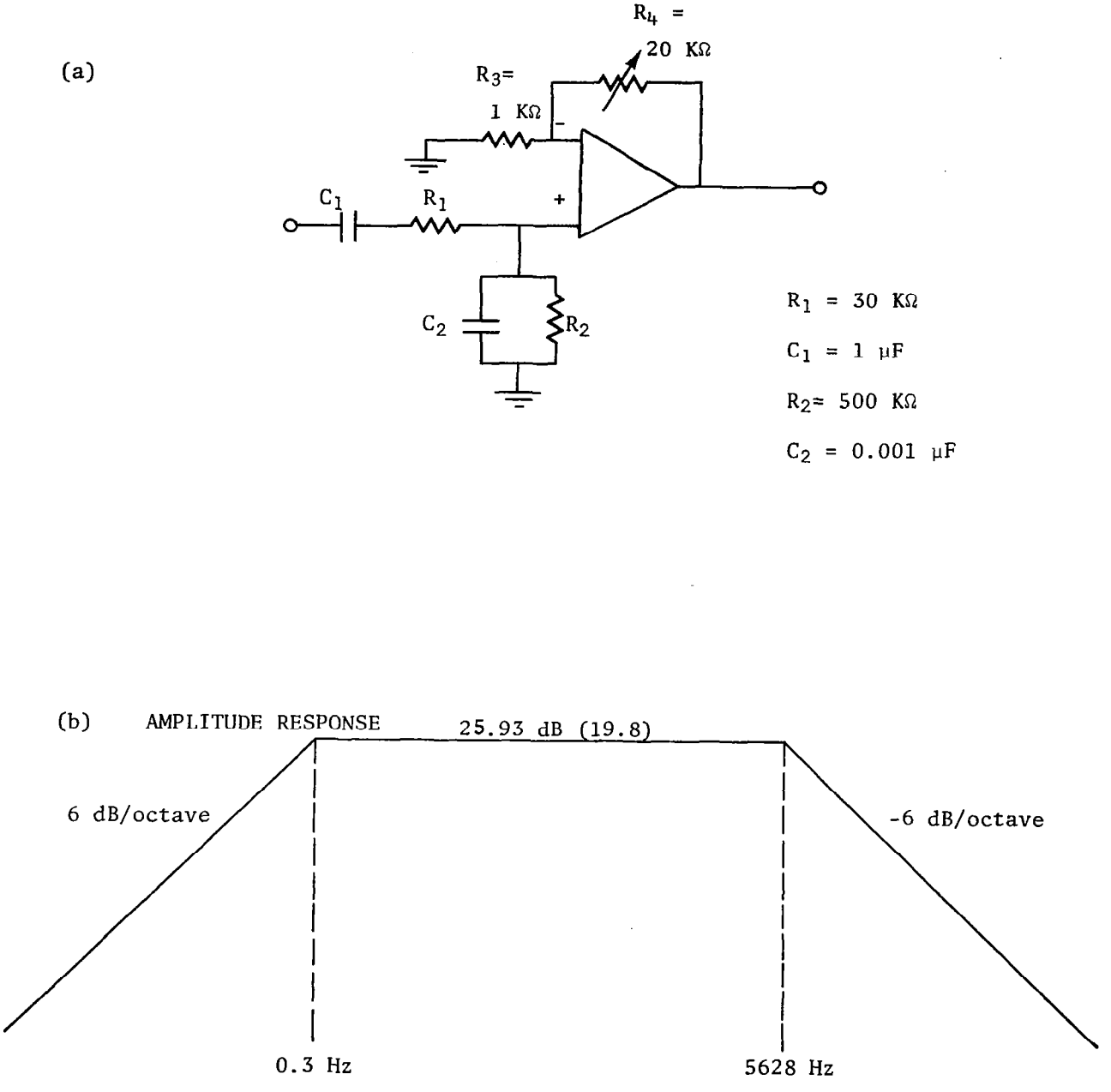

Figure 4. Circuit used for stage IC3 and its Bode plot.

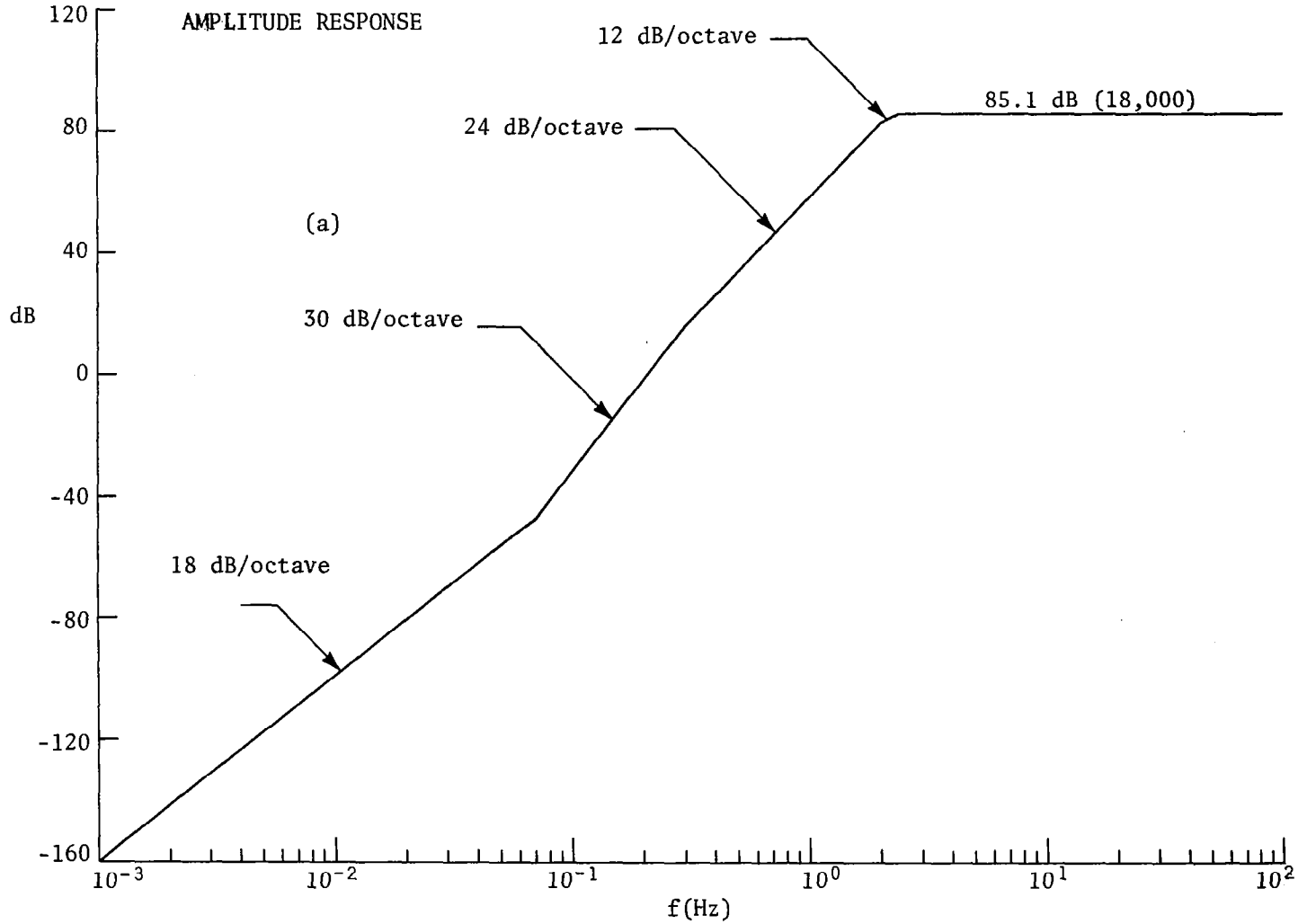

Figure 5. Bode plot of video amplifier (continued on p. 111).

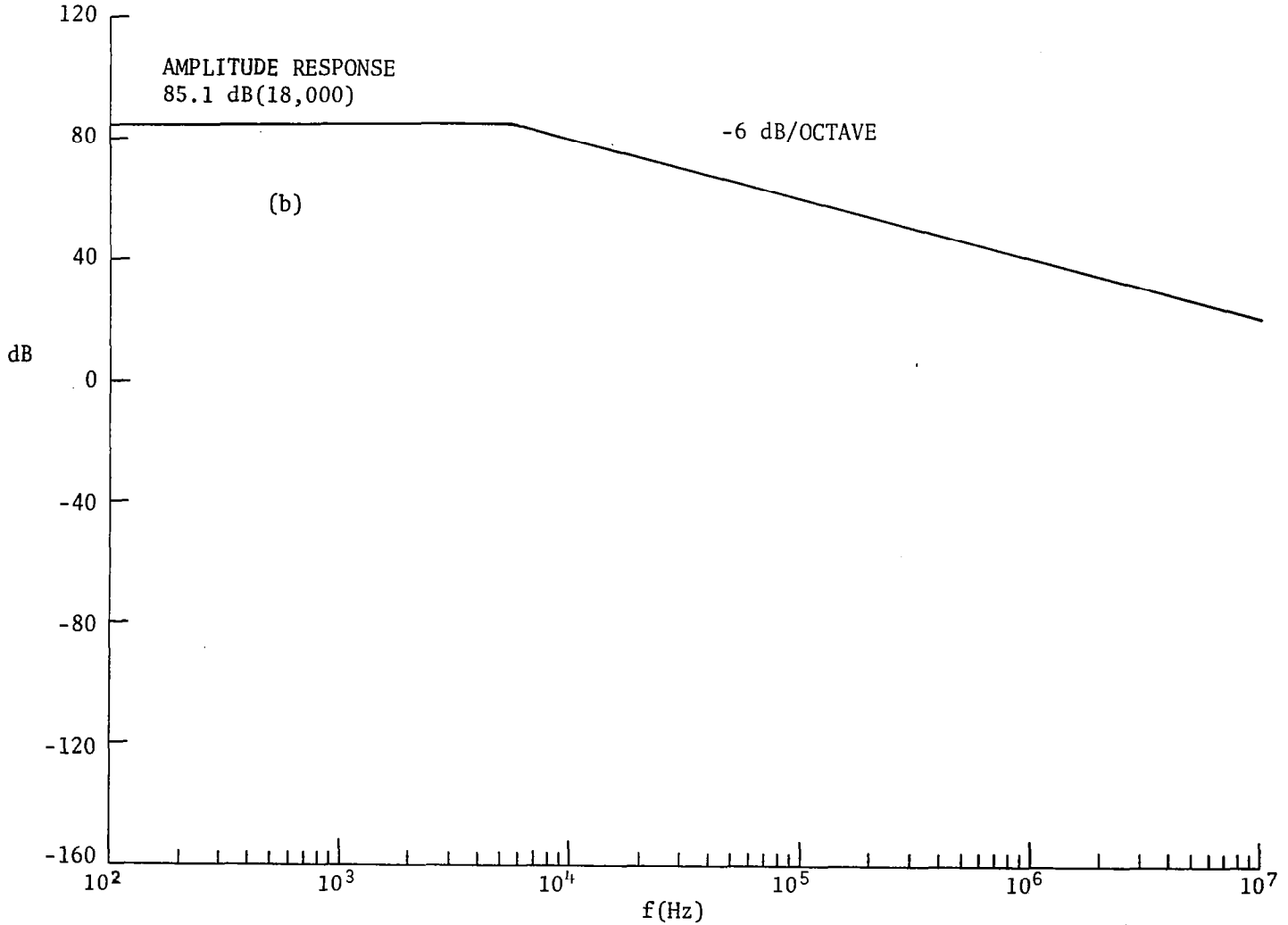

Figure 5. (Concluded).

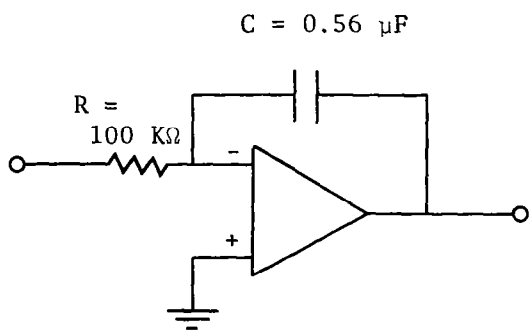

Figure 6. Integrator circuit used in estimation circuit.

(a)

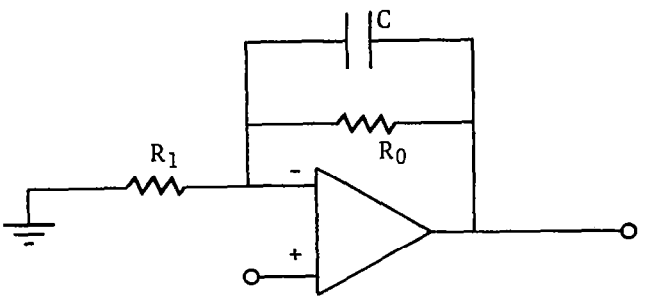

R_0 = 50 KΩ

R_1 = 5 KΩ

C = 0.56 μF

(b)

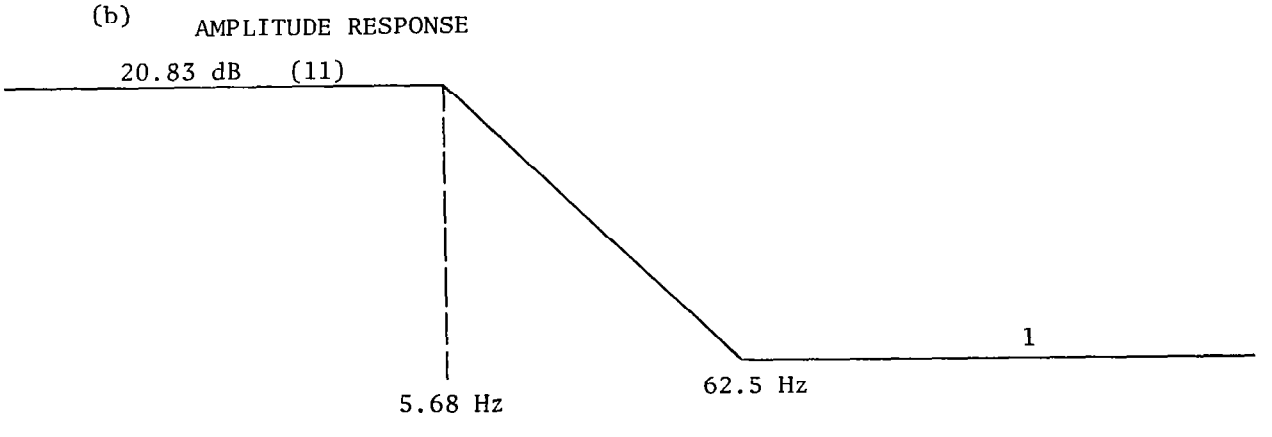

Figure 7. Original loop filter (lag-lead network) and its Bode plot.

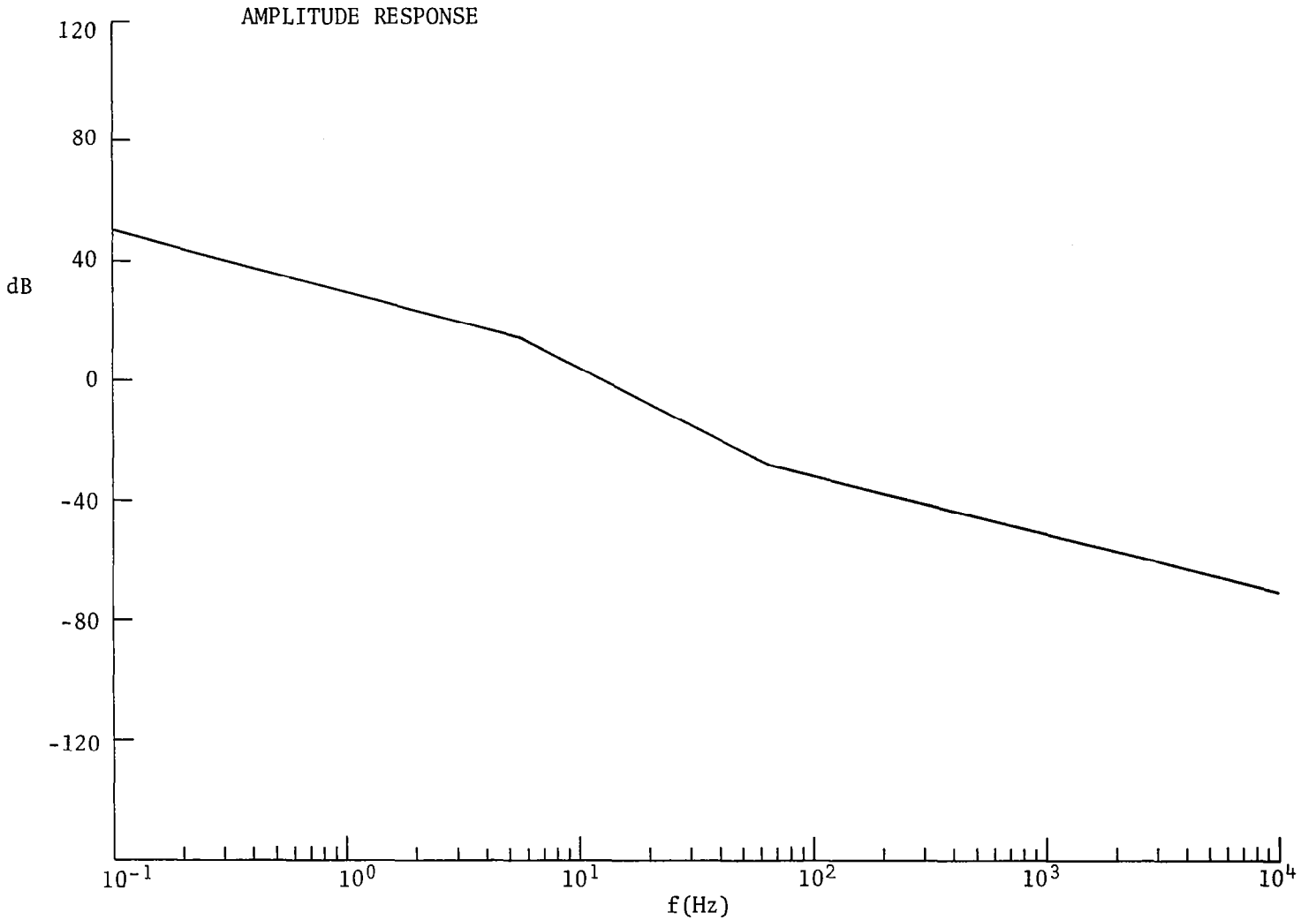

Figure 8. Bode plot of estimation circuit.

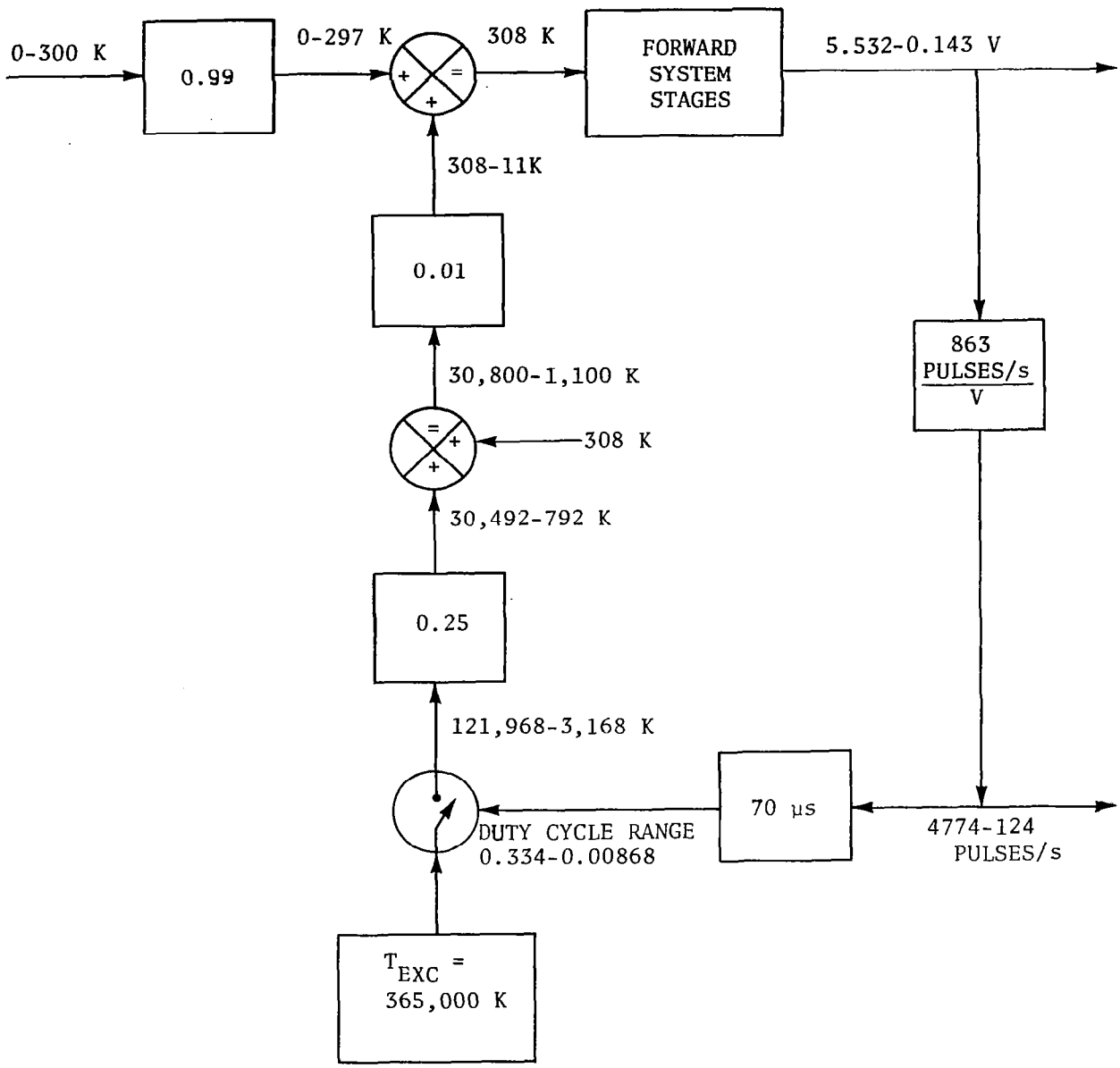

Figure 9. Illustration of noise addition in loop and range of values.

(a)

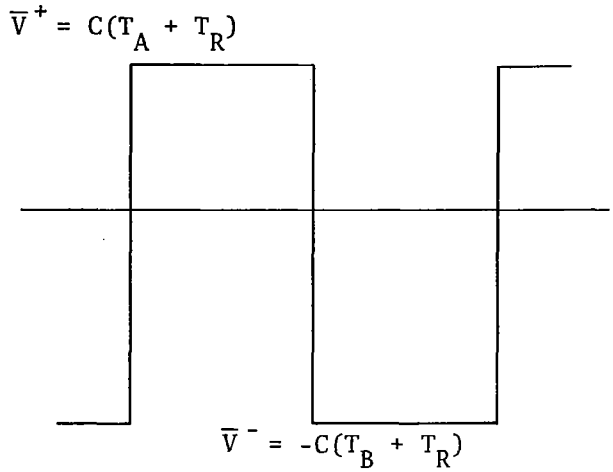

T_A	0	100 K	200 K	300 K
$\overline{V}^+$	3.58 V	4.15 V	4.72 V	5.29 V
$\overline{V}^-$	-5.33 V	-5.33 V	-5.33 V	-5.33 V

$C = 5.705 \times 10^{-3}$

$T_R = 627$ K

(b)

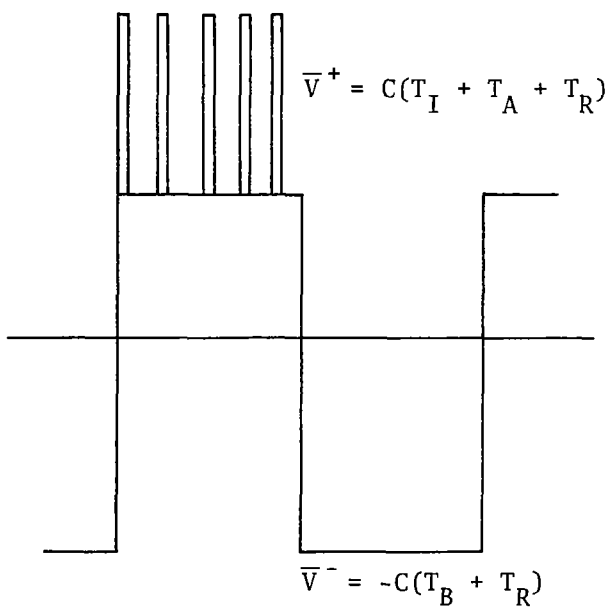

T_A	0	100 K	200 K
$\overline{V}^+$	5.33 V	5.33 V	5.33 V
$\overline{V}^-$	-5.33 V	-5.33 V	-5.33 V

Figure 10. Manner in which noise pulses add to signal to force net error temperature to zero.

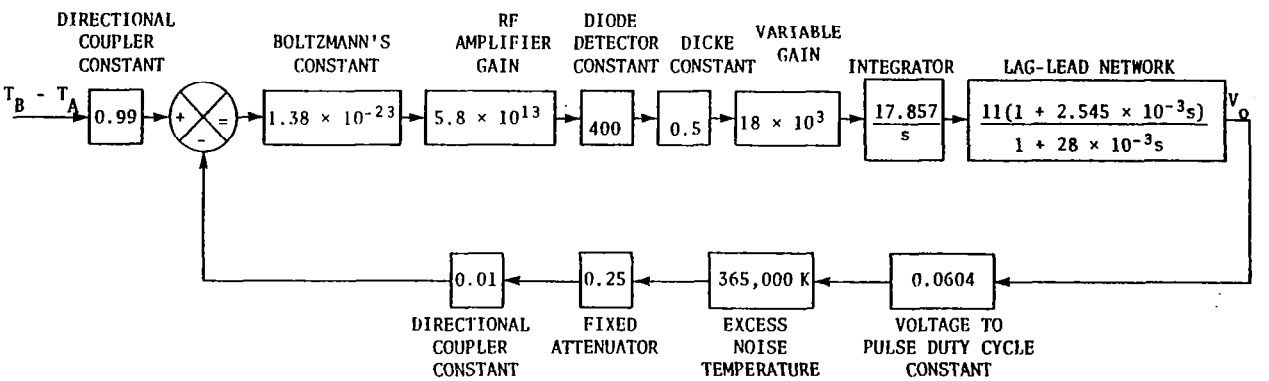

Figure 11. Control loop model for stepped frequency radiometer.

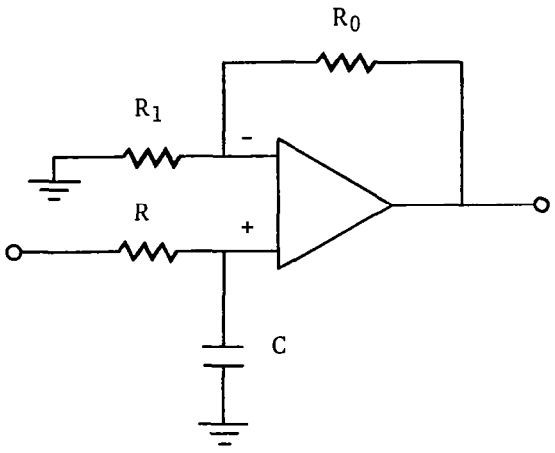

Figure 12. Form of lag network used to replace lag-lead network.

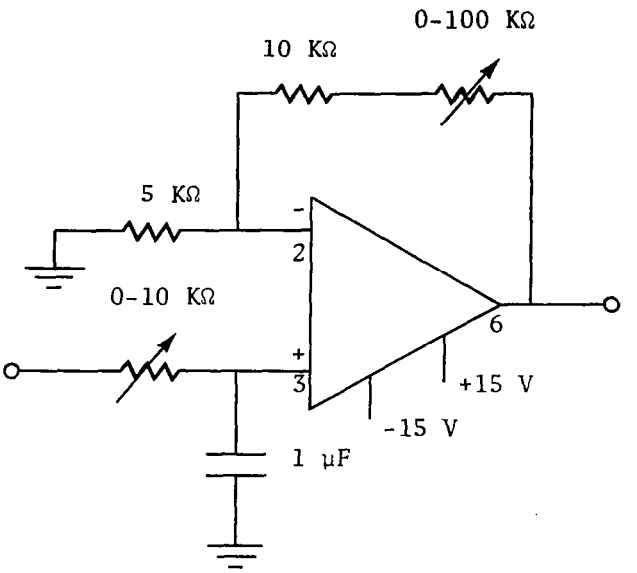

Figure 13. Test circuit used to optimize the loop response.

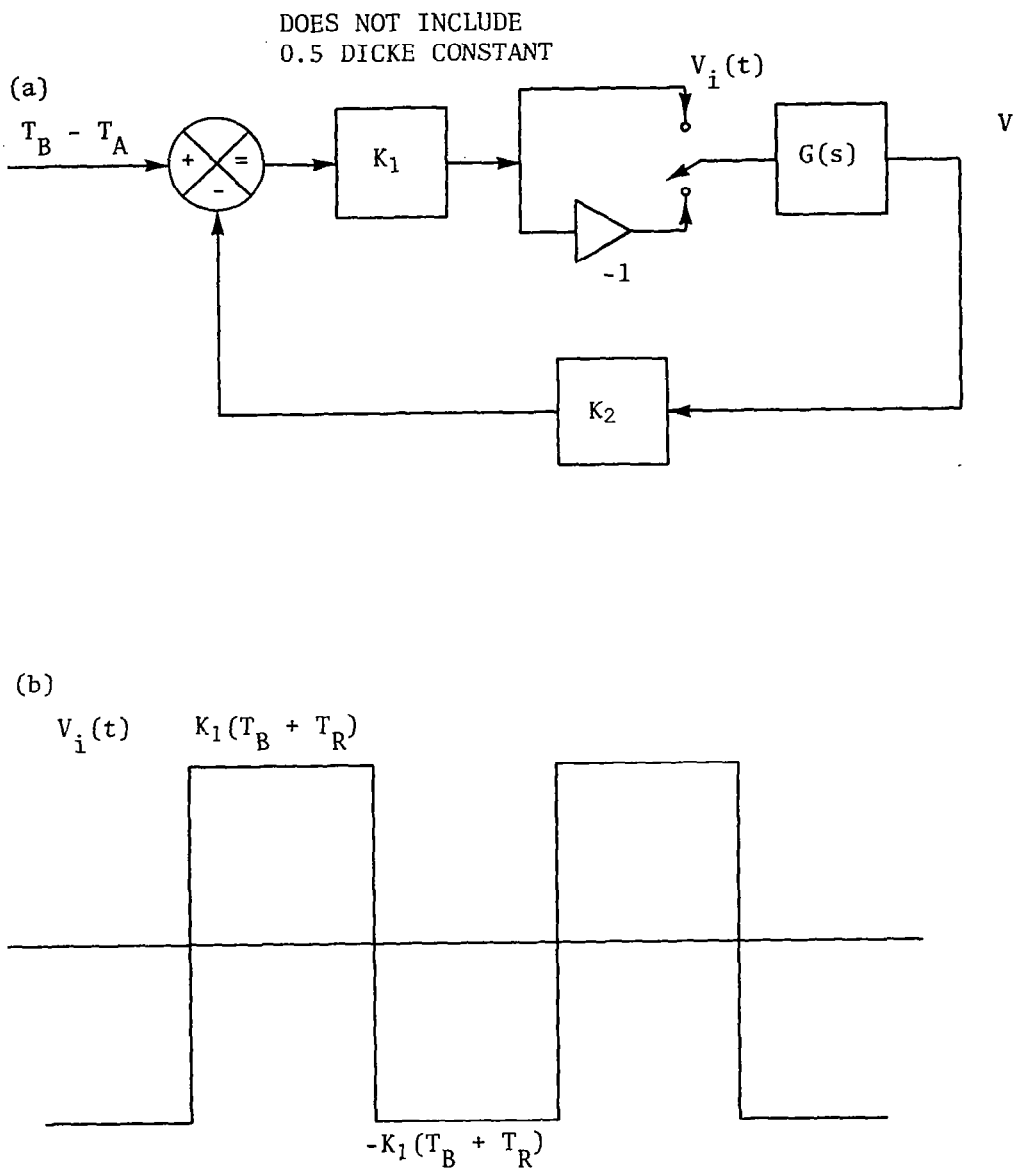

Figure 14. System model and waveform used in Dicke ripple analysis.

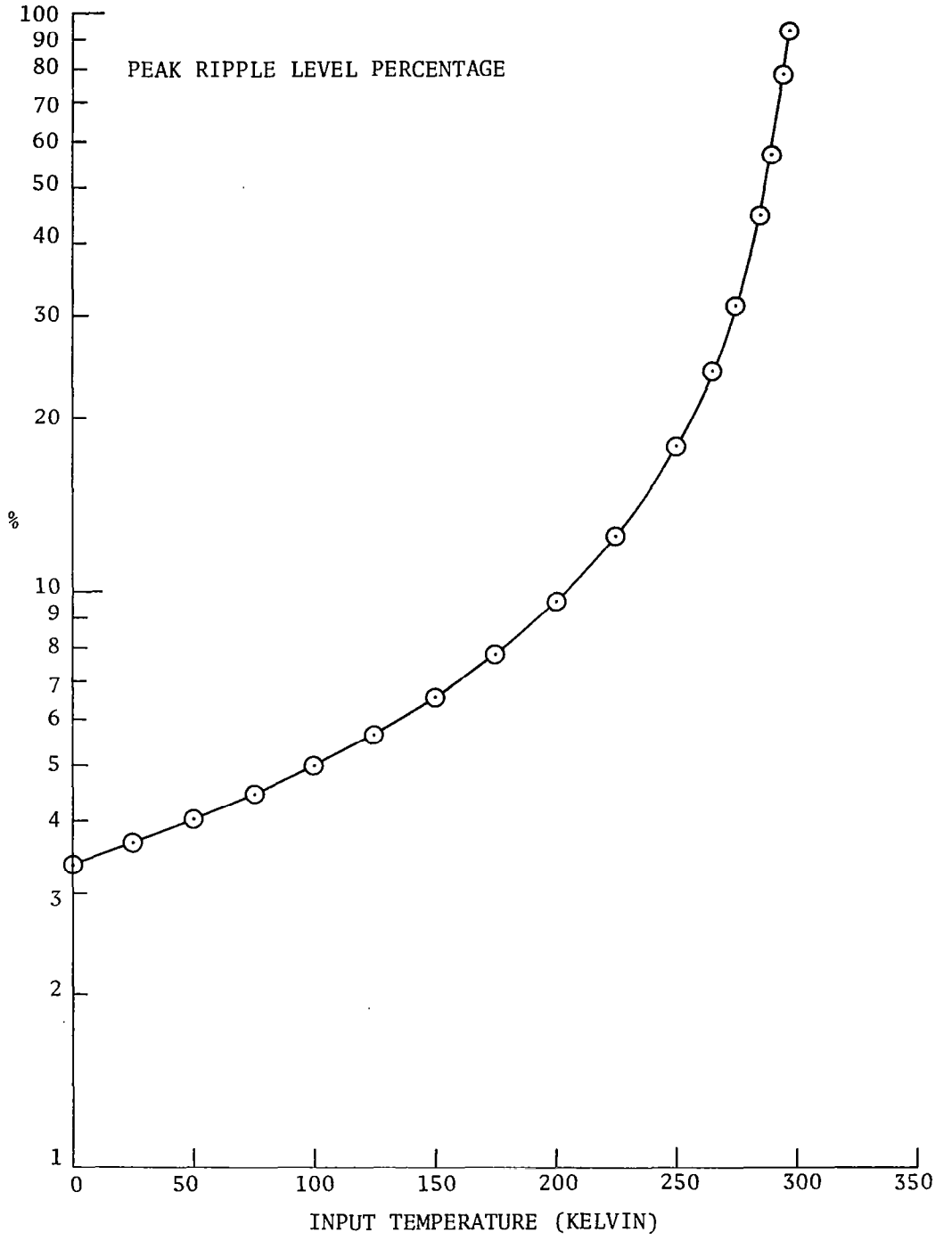

Figure 15. Ripple level output percentage versus input temperature.

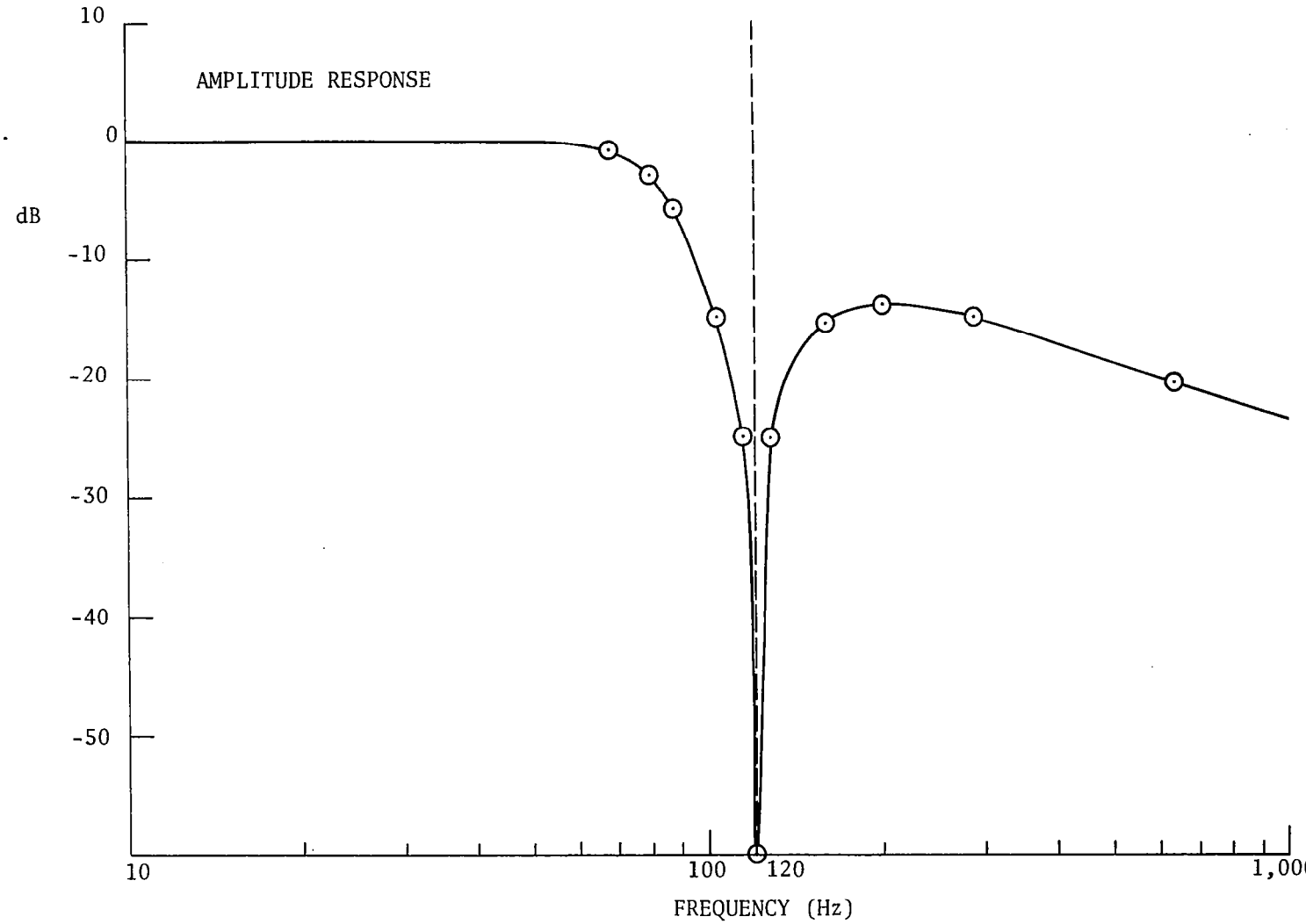

Figure 16. Amplitude response of possible analog loop notch filter.

(a)

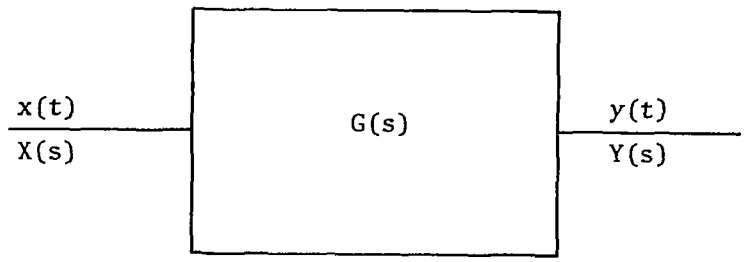

(b)

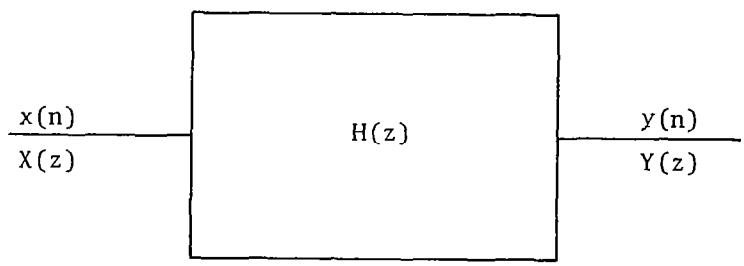

Figure 17. System forms used in digital discussions.

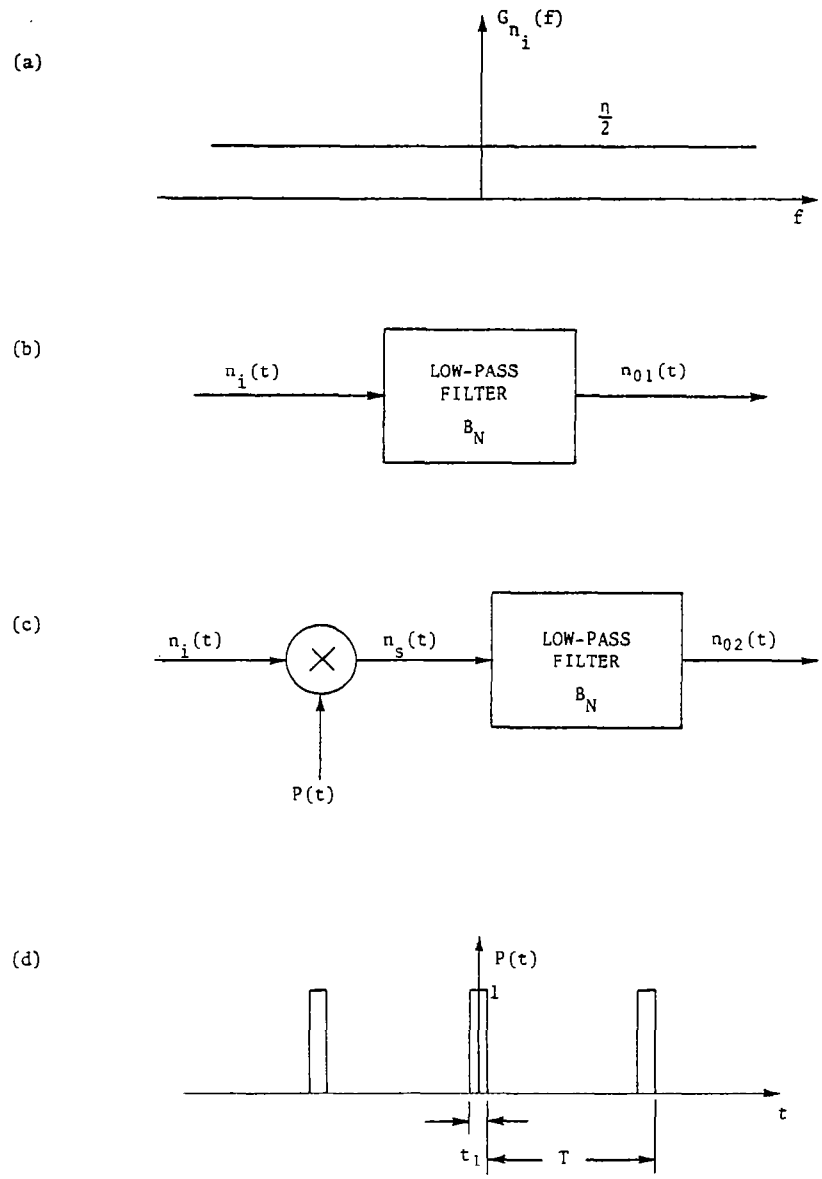

Figure 18. Noise and system forms used in developing the concept of noise sampling.

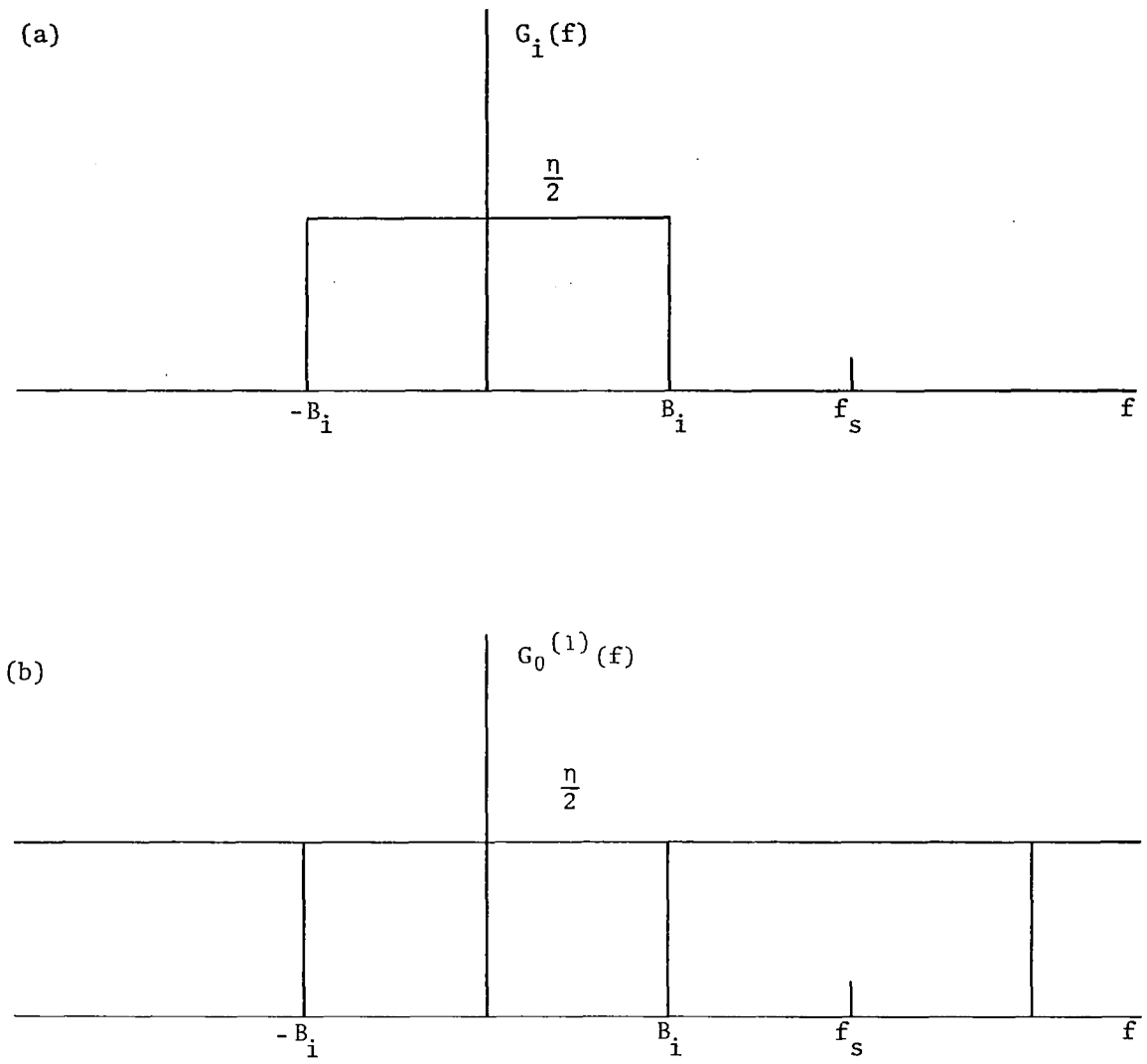

Figure 19. Sampling of bandwidth-limited signal exactly at Nyquist rate ($f_s = 2B_i$).

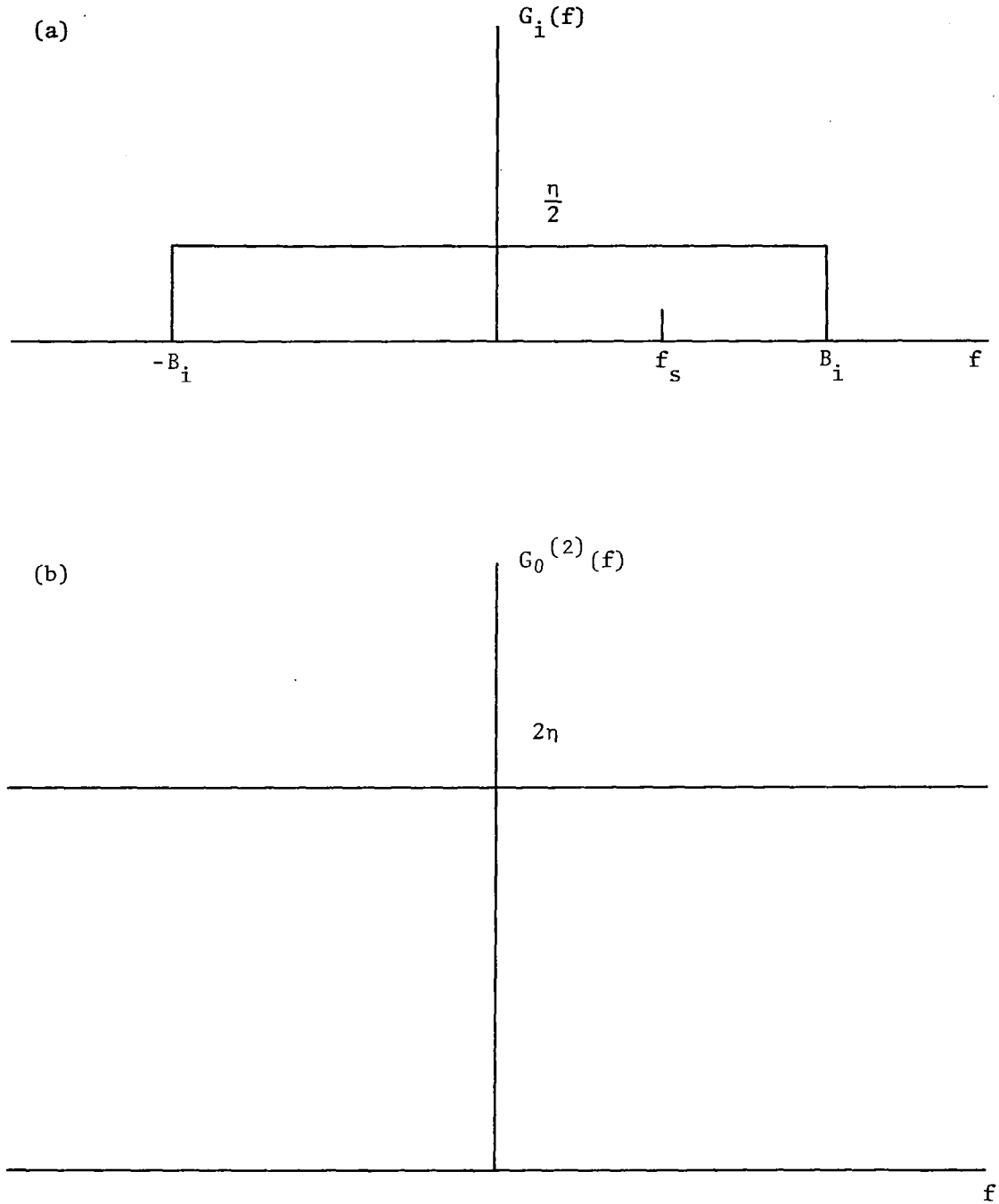

Figure 20. Sampling of bandwidth-limited signal at one-fourth the Nyquist rate.

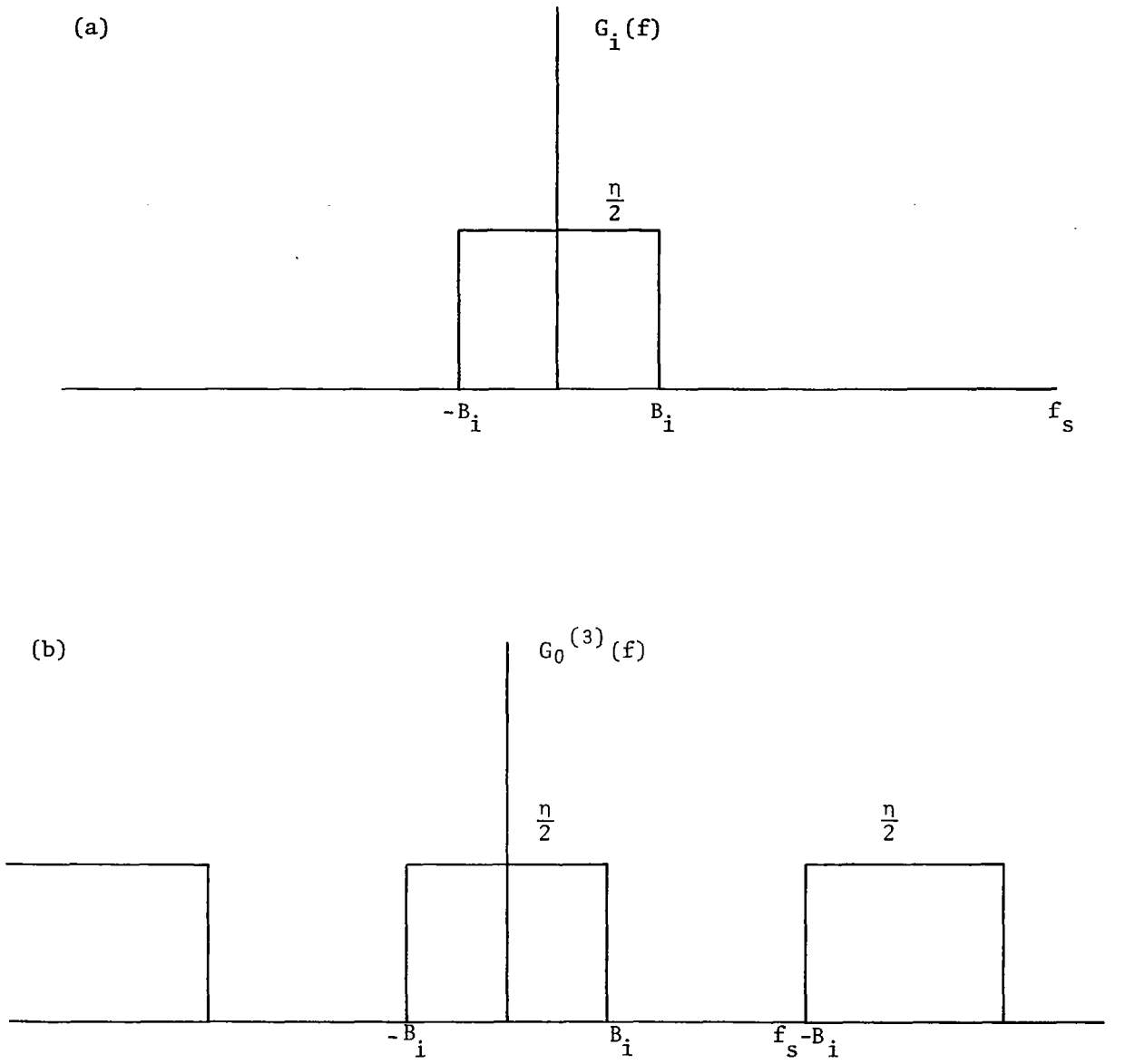

Figure 21. Sampling of bandwidth-limited signal at twice the Nyquist rate.

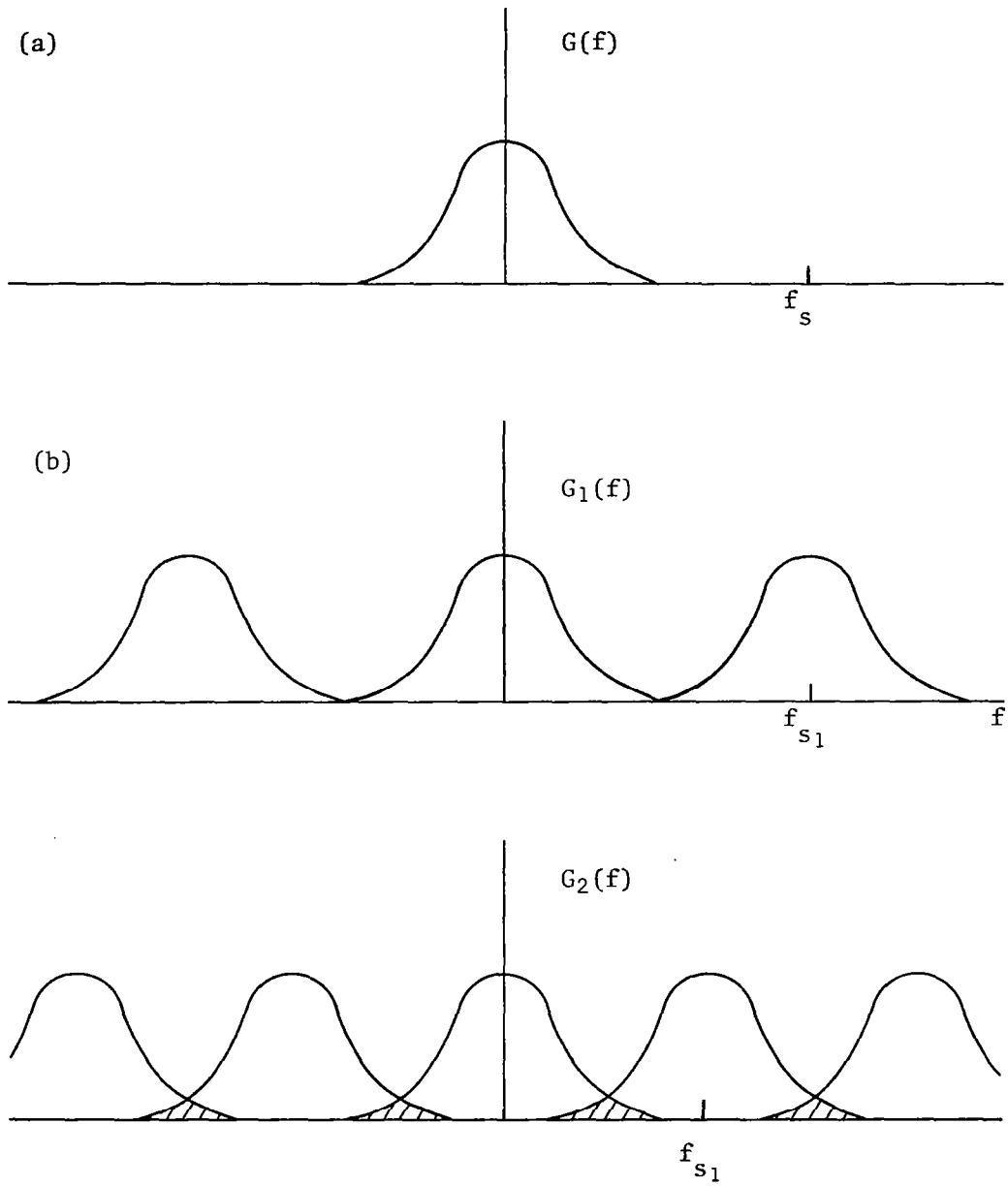

Figure 22. Sampling at different rates of signal whose spectrum has gradual rolloff.

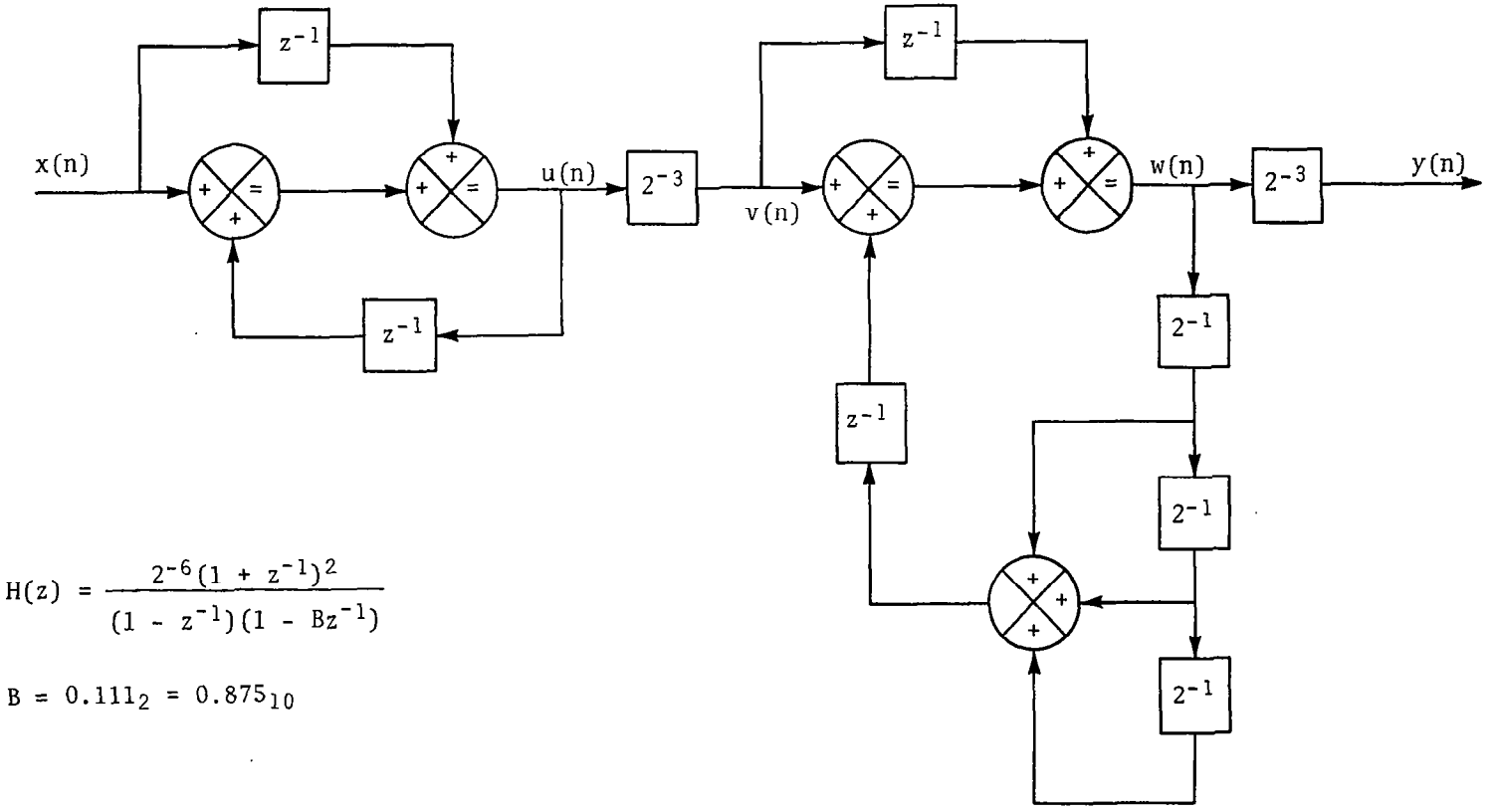

Figure 23. The first second-order digital estimating circuit investigated.

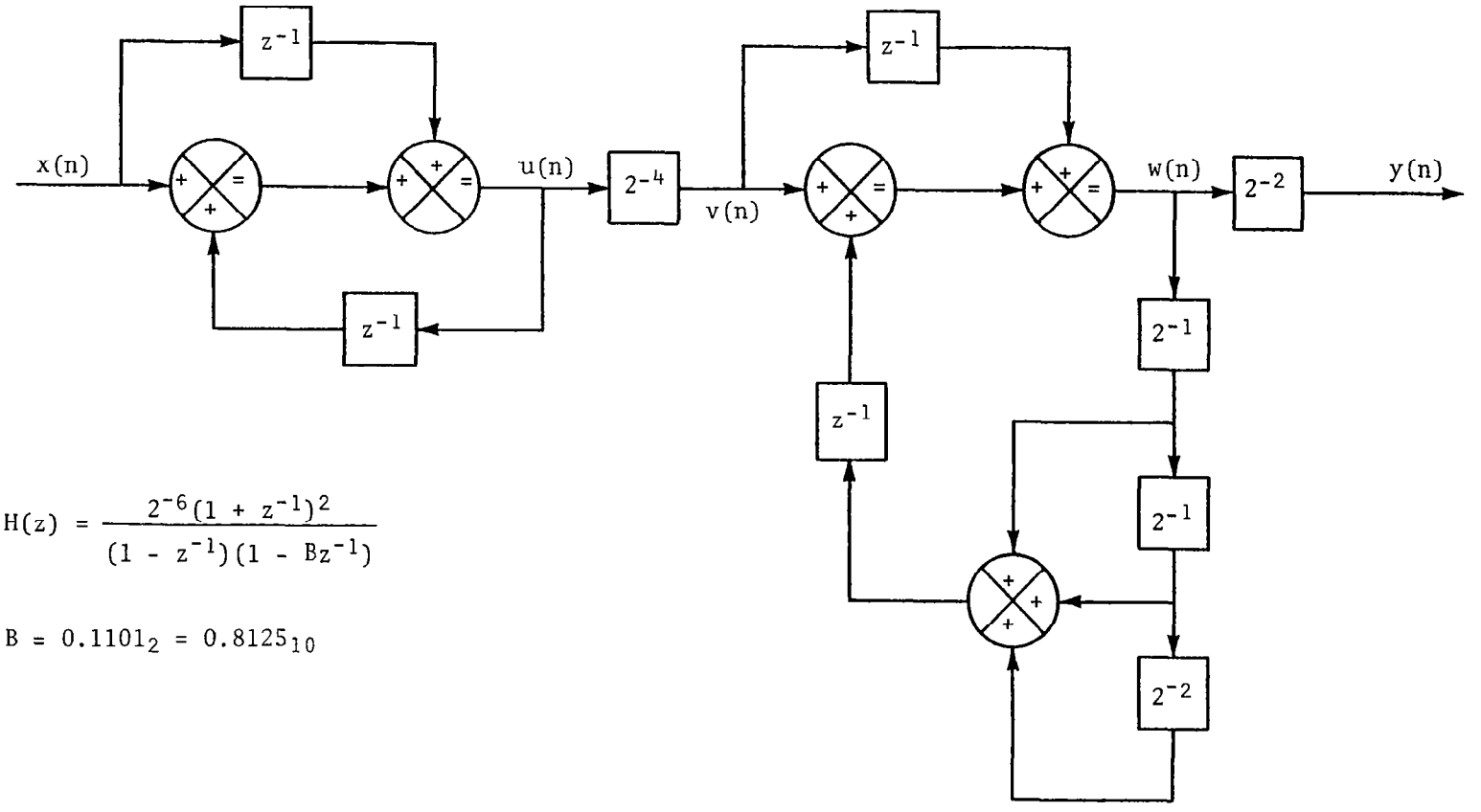

$$H(z) = \frac{2^{-6}(1 + z^{-1})^2}{(1 - z^{-1})(1 - Bz^{-1})}$$

$$B = 0.1101_2 = 0.8125_{10}$$

Figure 24. Mode A of the second second-order digital estimating circuit investigated.

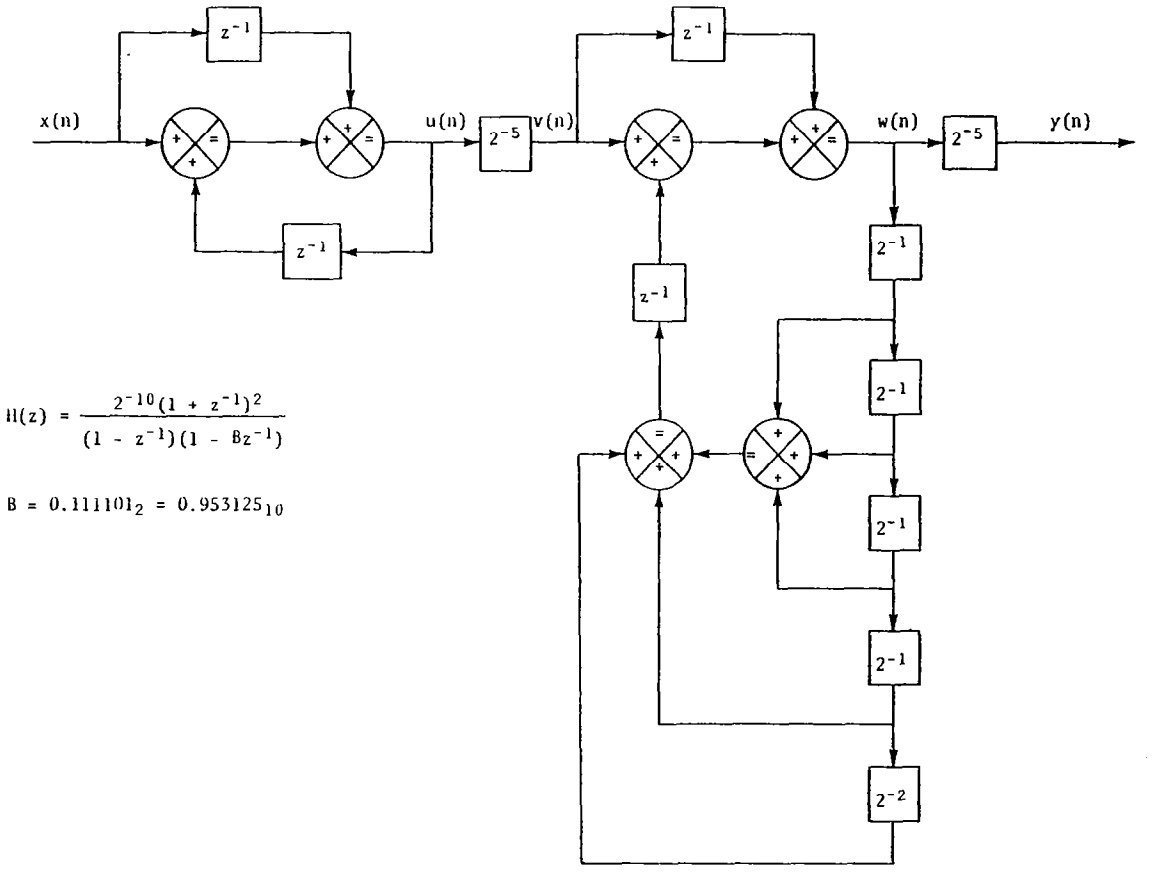

Figure 25. Mode B of the second second-order digital estimating circuit investigated.

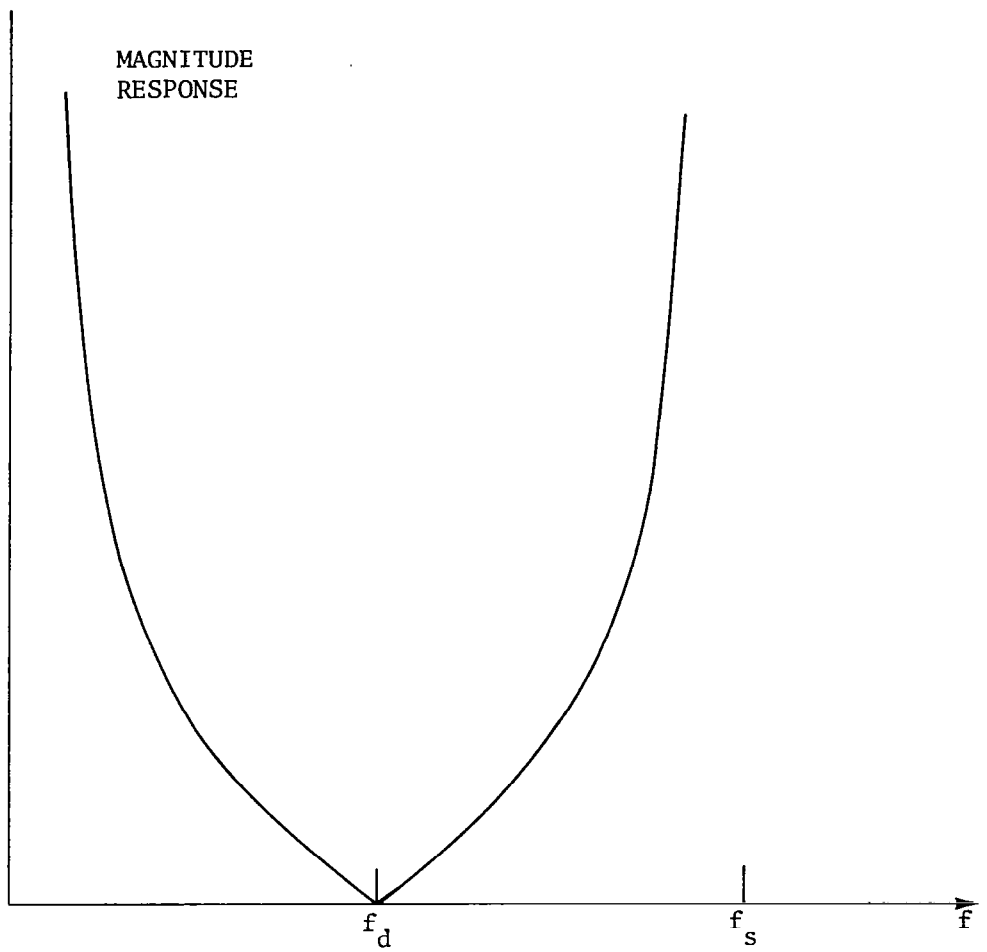

Figure 26. Magnitude response of integration algorithm with Dicke frequency equal to the folding frequency.

DIGITAL LOOP FILTER

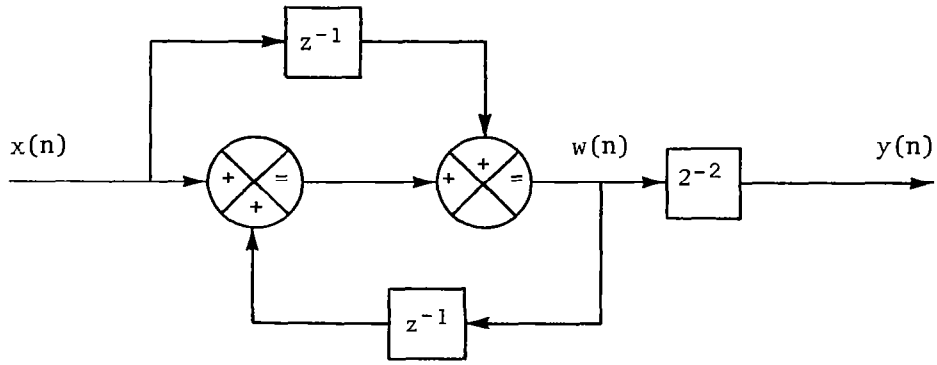

Figure 27. Proposed first-order control loop filter.

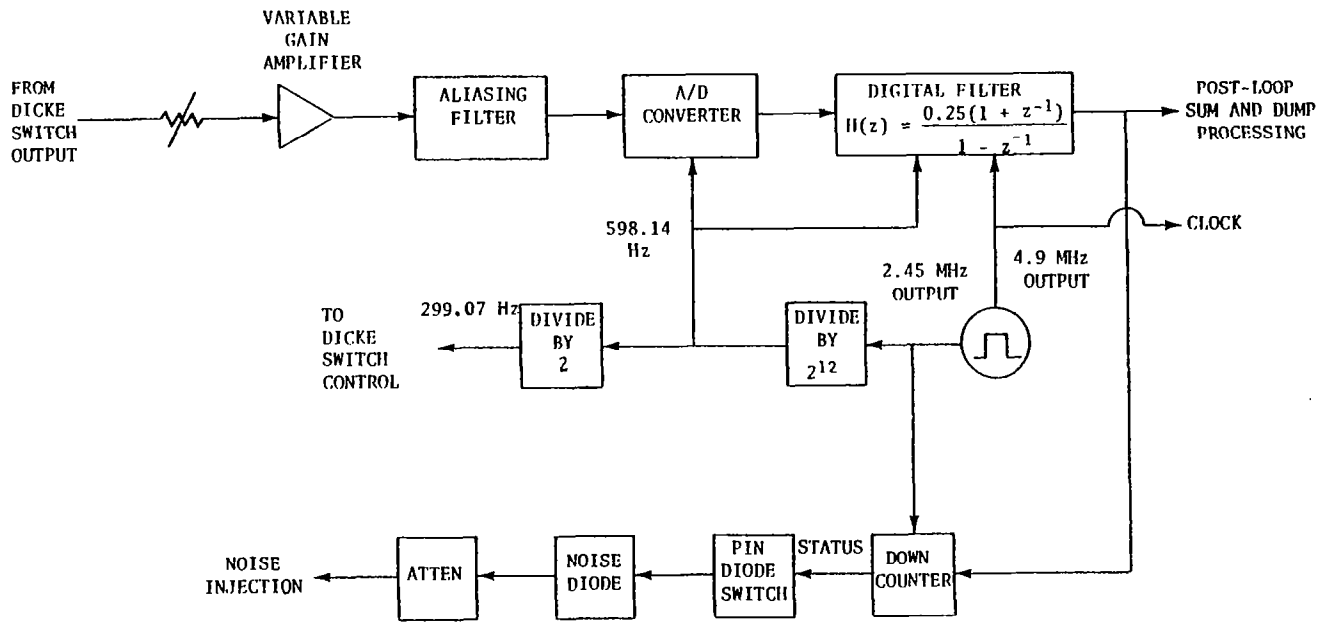

Figure 28. Proposed loop estimation and feedback system.

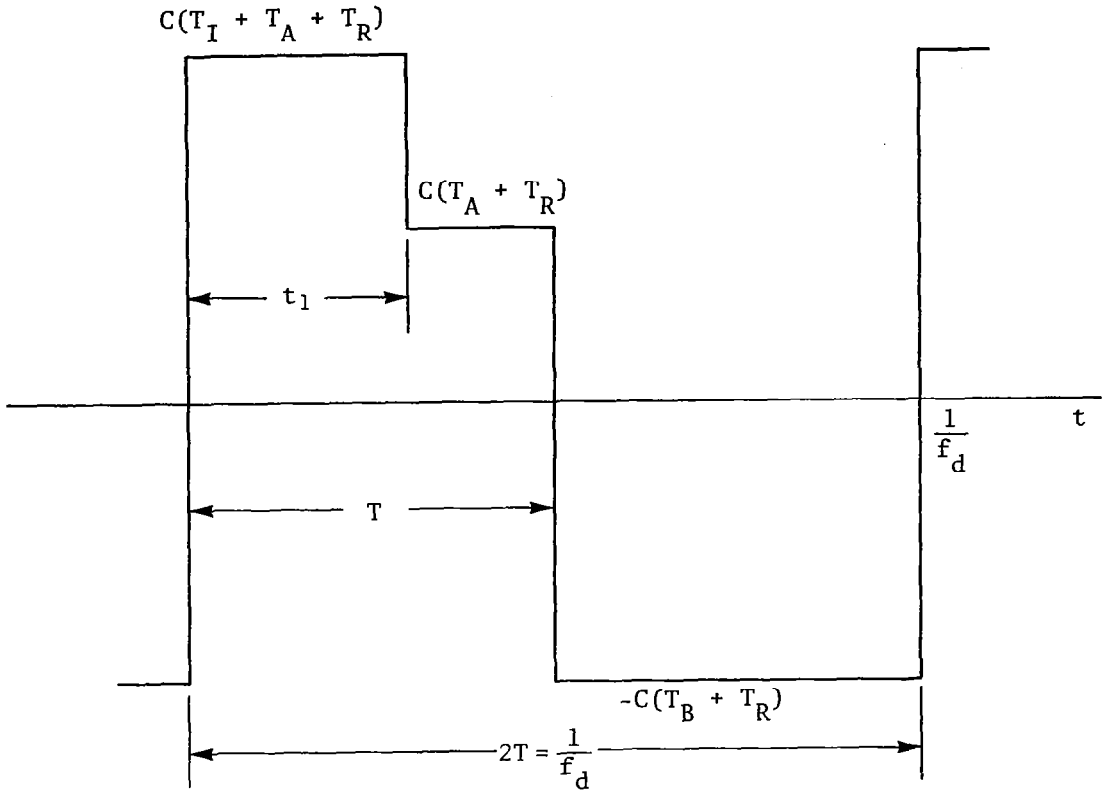

Figure 29. Noise-injection cycle in proposed design.

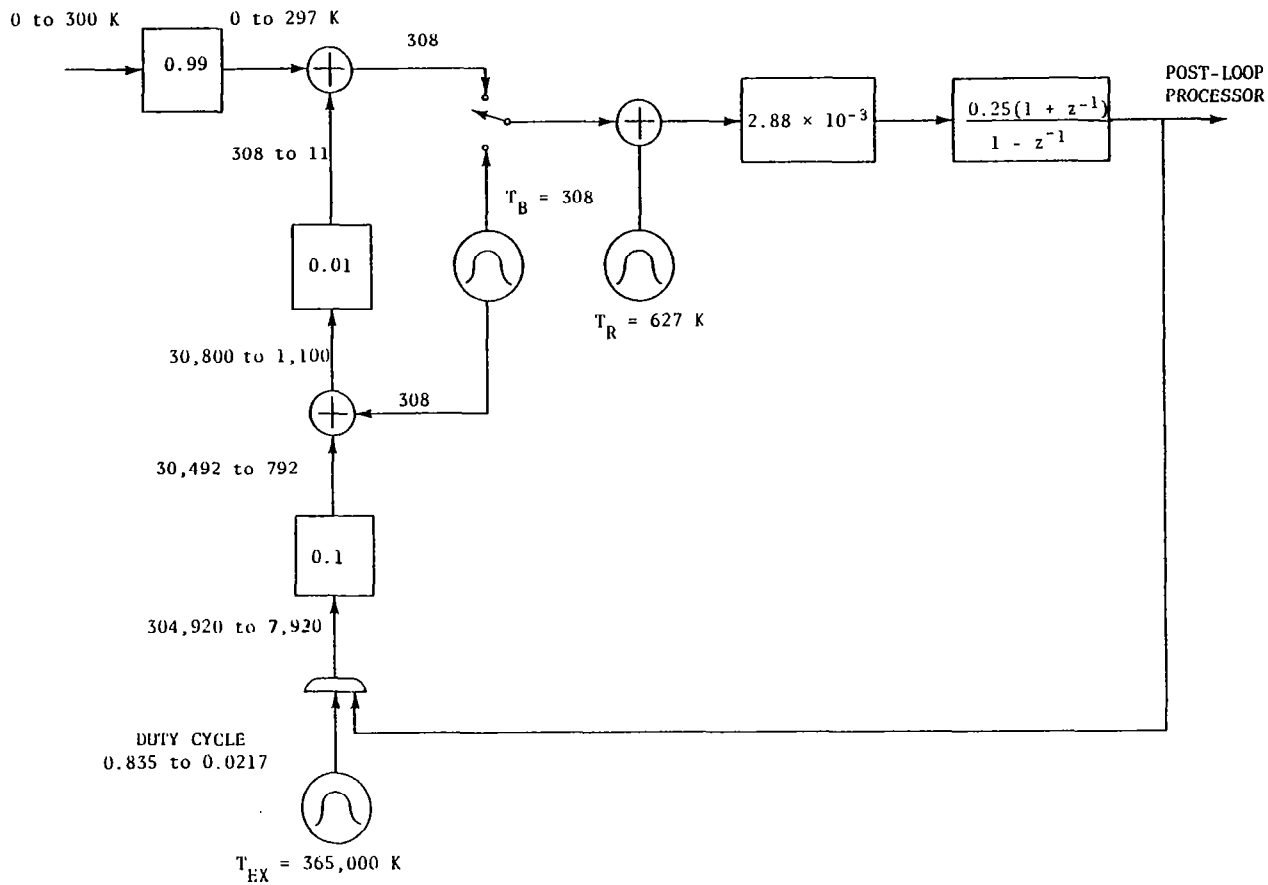

Figure 30. Ranges of temperatures and duty cycle of proposed design.

(a)

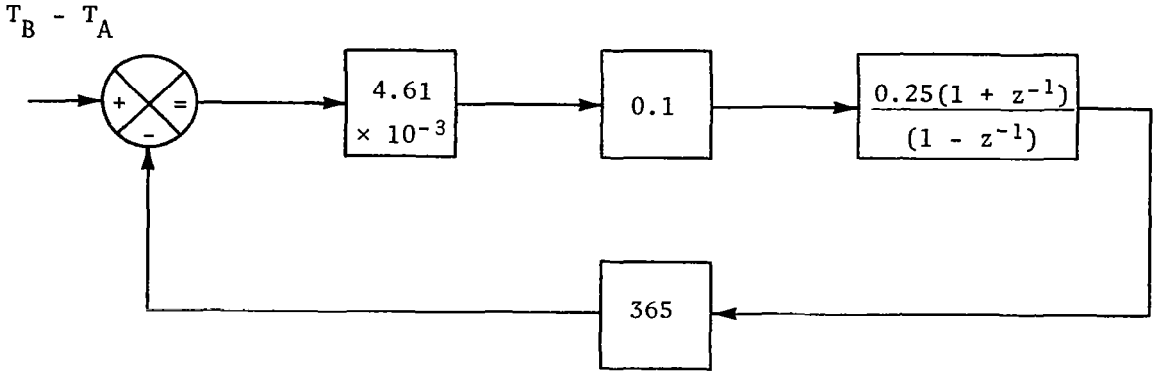

(b)

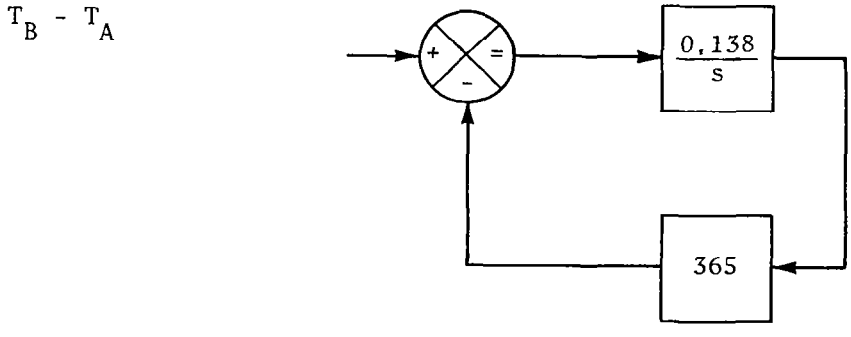

Figure 31. Control model for discrete-time loop and its approximate continuous-time equivalent model.

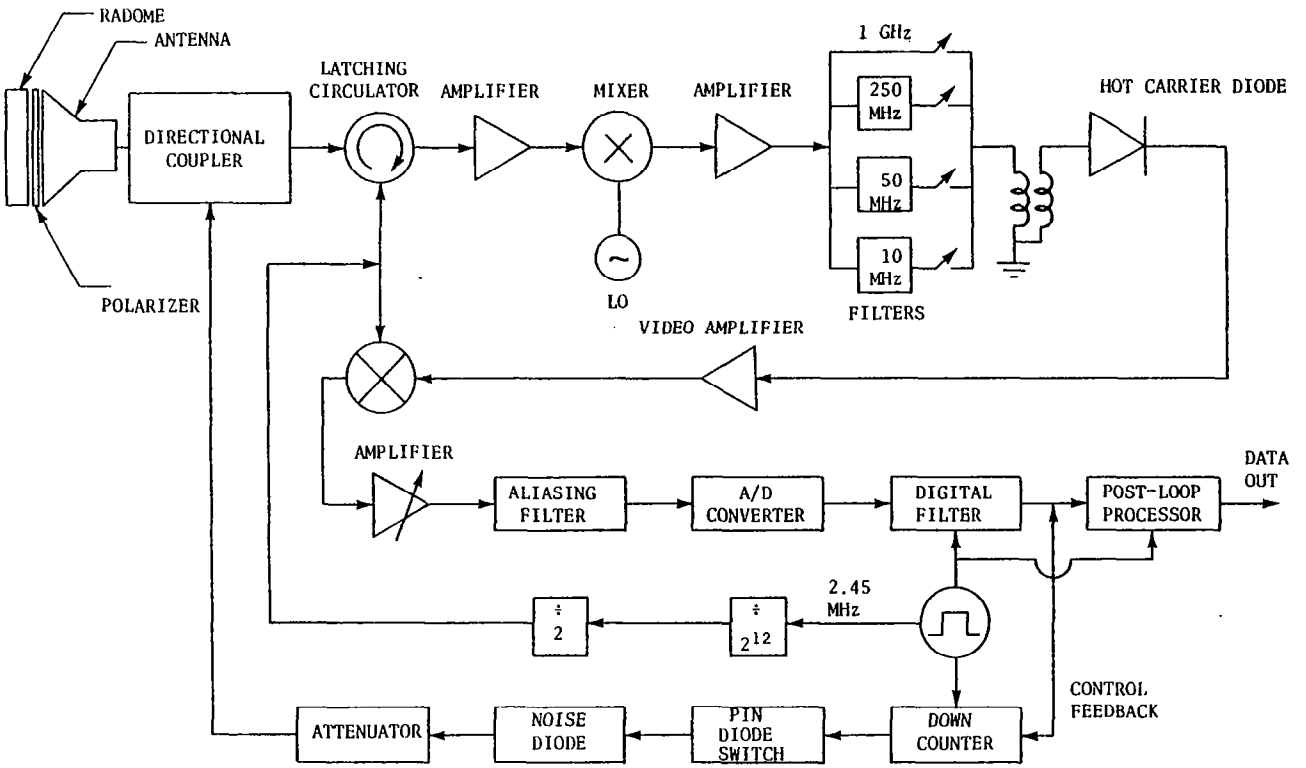

Figure 32. Block diagram of proposed system.

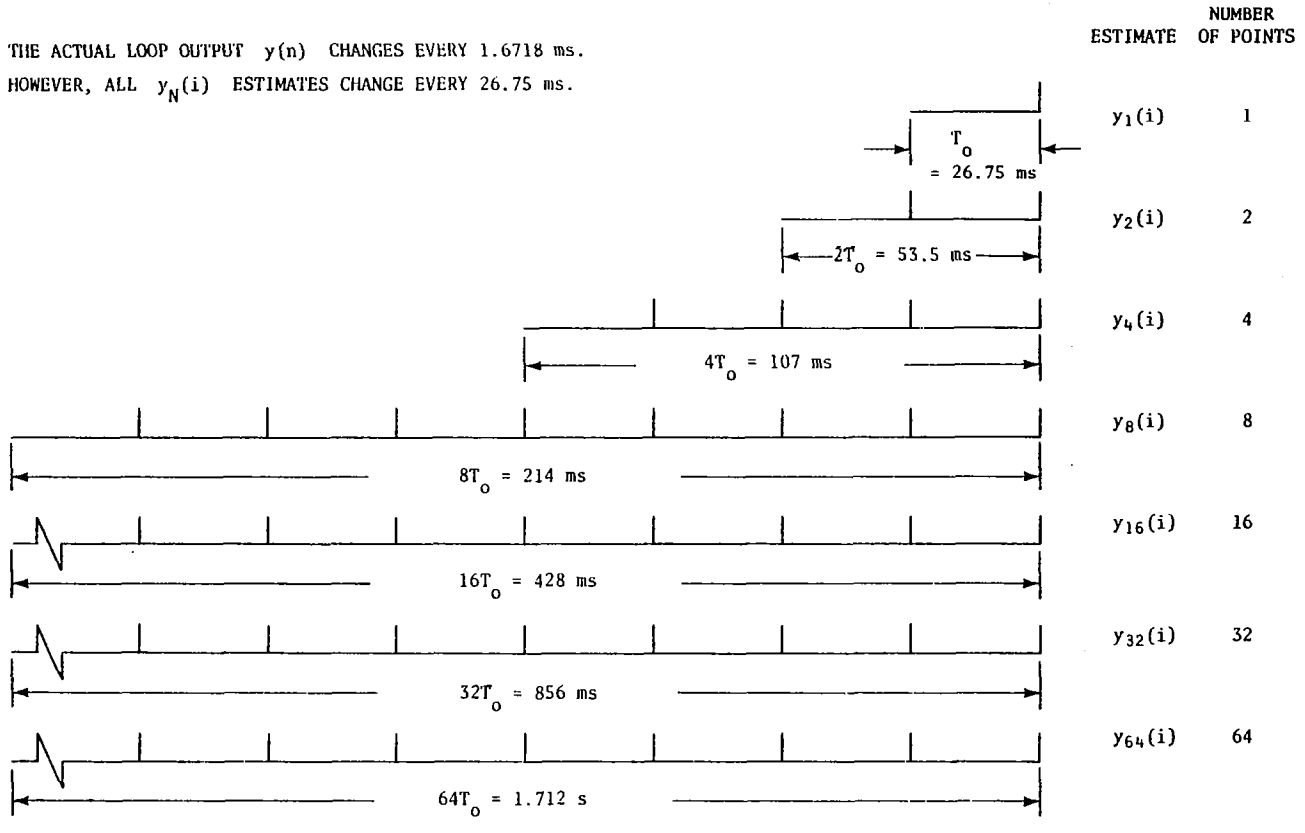

Figure 33. Sum-and-dump algorithms proposed for post-loop processor.

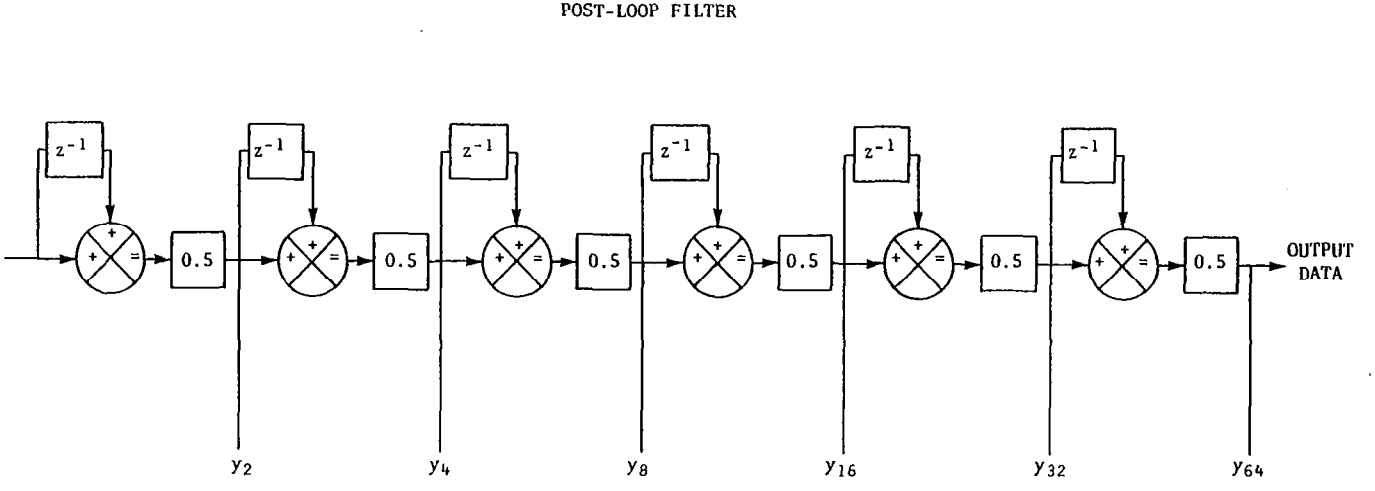

Figure 34. Digital filter format for sum-and-dump algorithms.

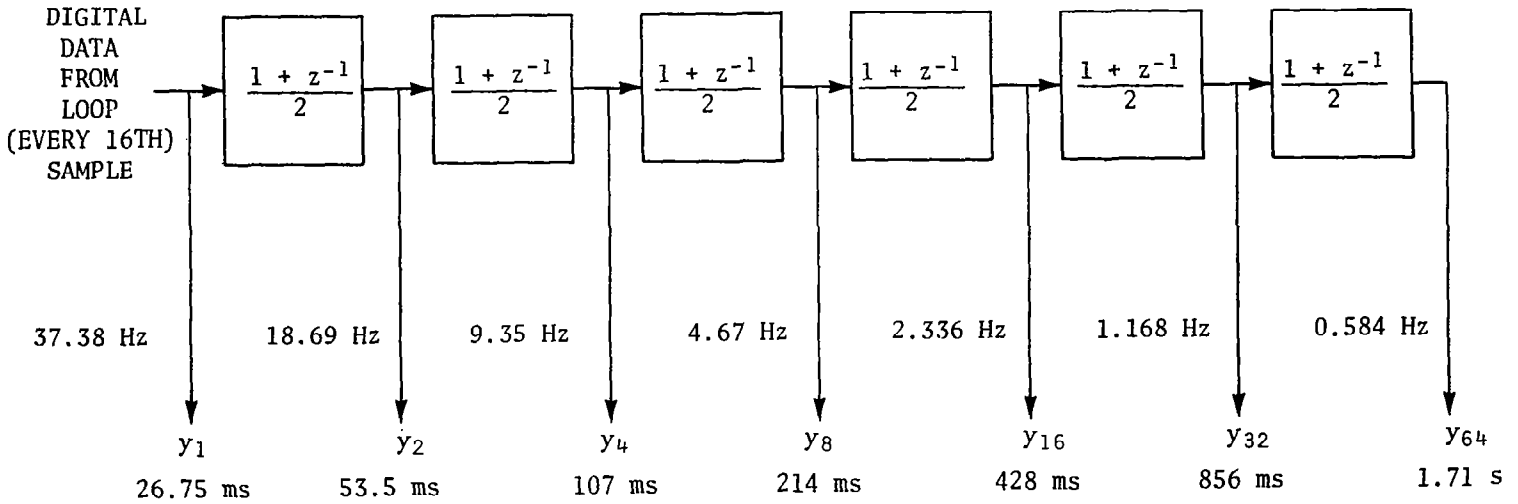

Figure 35. Sum-and-dump algorithms from a z-transform point of view.

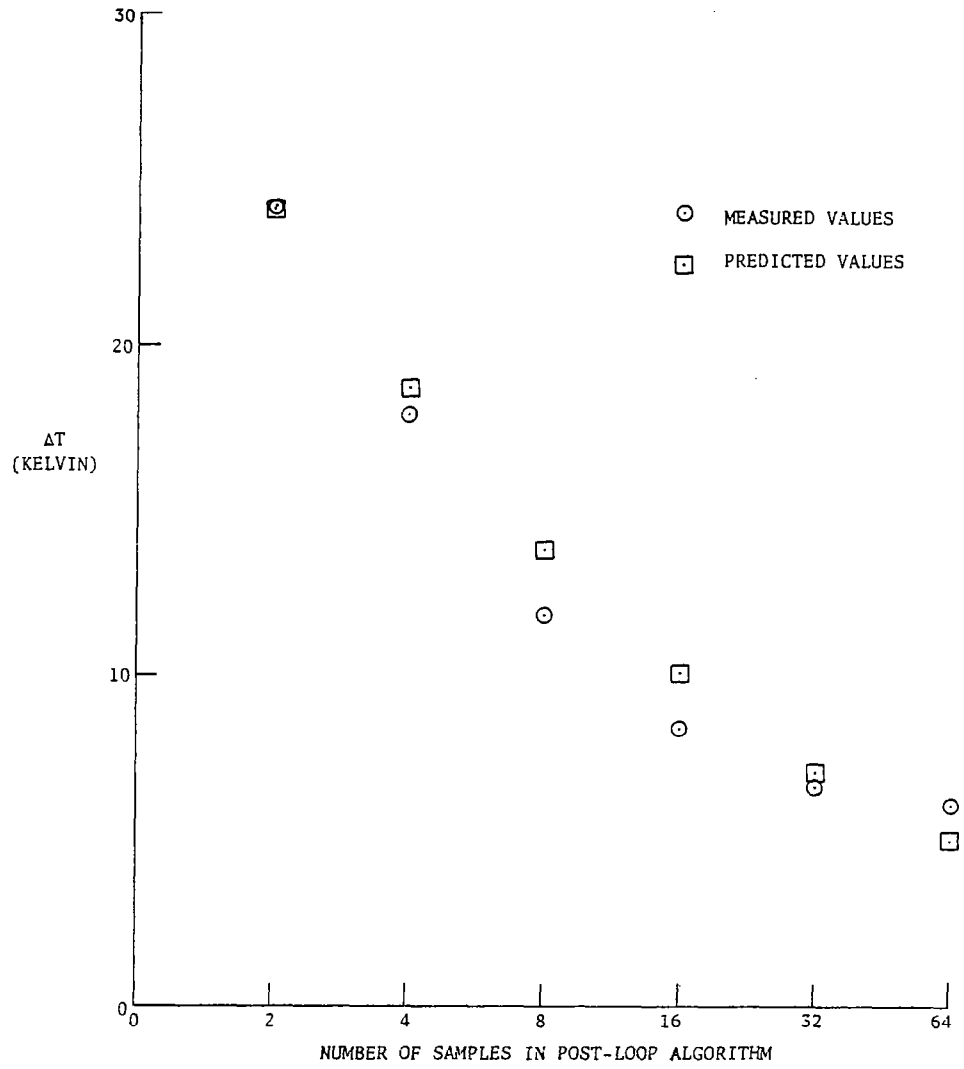

Figure 36. Sensitivities of proposed design resulting from dynamic simulation (78.125-kHz bandwidth).

1. Report No.	2. Government Accession No.	3. Recipient's Catalog No.
NASA CR-3327		

4. Title and Subtitle	5. Report Date
PRELIMINARY DEVELOPMENT OF DIGITAL SIGNAL PROCESSING IN MICROWAVE RADIOMETERS	September 1980
	6. Performing Organization Code
7. Author(s)	8. Performing Organization Report No.
William D. Stanley	
	10. Work Unit No.
9. Performing Organization Name and Address	
Old Dominion University Research Foundation P. O. Box 6369 Norfolk, Virginia 23508	11. Contract or Grant No. NAS1-15676
	13. Type of Report and Period Covered Final Report Jan. 1 - Dec. 31, 1979
12. Sponsoring Agency Name and Address	14. Sponsoring Agency Code
National Aeronautics and Space Administration Washington, DC 20546	

15. Supplementary Notes

Langley Technical Monitor: William F. Croswell

Appendix by John M. Jeffords

16. Abstract

The contract covered by the report involved a number of closely related tasks including: the development of several control-loop and dynamic noise model computer programs for simulating microwave radiometer measurements; computer modeling of an existing stepped frequency radiometer in an effort to determine its optimum operational characteristics; investigation of the classical second-order analog control loop to determine its ability to reduce the estimation error in a microwave radiometer; investigation of several digital signal-processing unit designs; initiation of efforts to develop required hardware and software for implementation of the digital signal-processing unit; investigation of the general characteristics and peculiarities of digital processing noiselike microwave radiometer signals; and computer data reduction of results obtained from actual ice missions.

17. Key Words (Suggested by Author(s))	18. Distribution Statement
Radiometer Signal processing Digital signal processing	Unclassified - Unlimited Subject Category 33

19. Security Classif. (of this report)	20. Security Classif. (of this page)	21. No. of Pages	22. Price
Unclassified	Unclassified	142	A07

For sale by the National Technical Information Service, Springfield, Virginia 22161

NASA-Langley, 1980